

University of Massachusetts Medical School

eScholarship@UMMS

---

GSBS Dissertations and Theses

Graduate School of Biomedical Sciences

---

2008-09-09

## Structural and Functional Studies of the KCNQ1-KCNE K<sup>+</sup> Channel Complex: A Dissertation

Steven D. Gage

*University of Massachusetts Medical School*

Let us know how access to this document benefits you.

Follow this and additional works at: [https://escholarship.umassmed.edu/gsbs\\_diss](https://escholarship.umassmed.edu/gsbs_diss)



Part of the [Amino Acids, Peptides, and Proteins Commons](#), [Genetic Phenomena Commons](#), and the [Inorganic Chemicals Commons](#)

---

### Repository Citation

Gage SD. (2008). Structural and Functional Studies of the KCNQ1-KCNE K<sup>+</sup> Channel Complex: A Dissertation. GSBS Dissertations and Theses. <https://doi.org/10.13028/5p7x-nx02>. Retrieved from [https://escholarship.umassmed.edu/gsbs\\_diss/409](https://escholarship.umassmed.edu/gsbs_diss/409)

This material is brought to you by eScholarship@UMMS. It has been accepted for inclusion in GSBS Dissertations and Theses by an authorized administrator of eScholarship@UMMS. For more information, please contact [Lisa.Palmer@umassmed.edu](mailto:Lisa.Palmer@umassmed.edu).

STRUCTURAL AND FUNCTIONAL STUDIES OF THE KCNQ1-KCNE K<sup>+</sup>  
CHANNEL COMPLEX

A Dissertation Presented

By

Steven D. Gage

Submitted to the Faculty of the  
University of Massachusetts Graduate School of Biomedical Sciences, Worcester  
in partial fulfillment of the requirements for the degree of

Doctor of Philosophy

September 9, 2008

Biochemistry and Molecular Pharmacology

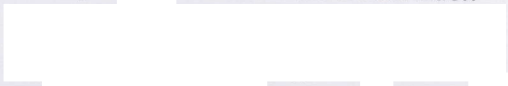
STRUCTURAL AND FUNCTIONAL STUDIES OF THE KCNQ1-KCNE K<sup>+</sup> CHANNEL  
COMPLEX

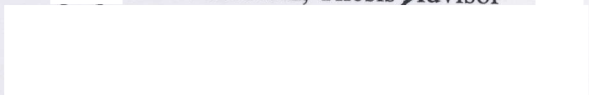
A Dissertation Presented

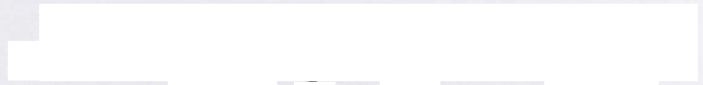
By

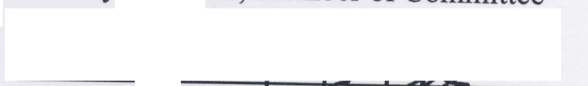
Steven D. Gage

*The signatures of the Dissertation Defense Committee signifies completion and approval as to  
style and content of the Dissertation*


  
William R. Kobertz, Thesis Advisor

  
Ann Rittenhouse, Member of Committee


  
Haley Melikian, Member of Committee

  
Dan Cox, Member of Committee

*The signature of the Chair of the Committee signifies that the written dissertation meets the  
requirements of the Dissertation Committee*

  
Anthony Carruthers, Chair of Committee

*The signature of the Dean of the Graduate School of Biomedical Sciences signifies that the  
student has met all graduation requirements of the school.*

  
Anthony Carruthers, Ph.D.,

Dean of the Graduate School of Biomedical Sciences

Program in Biochemistry & Molecular Pharmacology

Tuesday, September 9, 2008

## DEDICATIONS

I wanted to start out by thanking my two cats, Cleo and Zoe. Zoe's constant enthusiasm for anything I wrote and her occasional constructive criticisms were well received. Though Cleo's unbridled enthusiasm may instead be for cat food, her sedentary support for my work made clear her belief that everything would be fine. Along the same vein, I also wanted to thank the laptop Bill gave me to use. It has seen better days, and its apparent demise occurred minutes (literally) after I had saved everything. You did well.

I want to thank my grandparents, Ernst and Gertrude Wolf. Their example, and that of my other relatives in research, engineering and medicine, Ken Gage, Klaus Baron, Walt and Mark Goresky, Walter and Helmut Ruska, Ernst Spannhake and Max Wolf (I hope I have not missed anyone), have provided me with much awe and inspiration (and maybe a little self-doubt?). The size of the shoes I wish to fill has kept me going, and will hopefully never keep me from success.

I wanted to thank my oldest friends Greg and Peter Sirokman, John Karakashian and John Sidiropoulos. Early in my life, when my inspiration was great but my self-doubt greater, I really relied on you to give me the motivation to prove myself to everyone. I especially wanted to thank my oldest friend, Ted Hallock, and his family. Though you may be a little rough around the edges, I'll never pause to give you a hug.

I (definitely) get by with a little help from my friends. I wanted to thank Dan Paulsen, Tuba Bař and Volkan Çetin for providing encouragement and keeping me sane. I especially want to thank my friend Sam Gow; whether we are getting a bite to eat,

taking in a Sox game or spending the evening discussing neural network theory, it has always been fun. I love you all, and I do not know what I would do without you.

I wanted to thank the nurses and doctors who treated me at UMass and Tufts. I am presenting this thesis only by the skill their hands and the grace of G-d.

I loved my research. The techniques, the channel, the lab – my life as a student would have been the perfect career if I just received a higher stipend. Without Bill, I would not have had this opportunity. I've learned so much from you, and I wish I could fully explain my appreciation. I hope I have helped your career as much as you have helped mine.

I want to thank my family, Ursula, Don and my Uncle Tom. I suppose everyone has an eccentric upbringing, but my folks really did their best! I also want to thank my brother Tom. I wanted to beat you to the degree, but it just was not in the cards. I am very proud you.

I wanted to thank everyone who proof-read my thesis – you must be saints.

Finally, I wanted to thank my girlfriend Carol. I love you very much. I really owe my happiness and my success to you; without you, my world would be much less full. You gave me the strength to get better. I hope you are as happy as I am.

## ACKNOWLEDGEMENTS

I would like to thank the members of the Kobertz Lab for providing helpful critique and listening to my ideas, especially Trevor Morin and Tuba Bas. I especially want to thank Virla Berrios, Kshama Chandrasekhar and Caroline Dacwag (from the Imbalzano lab) for their help in learning mammalian tissue culture. I want to thank Jessica Rocheleau for her work in co-authoring Chapter III.

I would like to thank the members of the Rittenhouse lab, especially Tora Mitra-Ganguli for teaching me the whole-cell patch clamp technique. I would also like to thank Liwang Liu for suggestions and helpful advice regarding amphotericin B perforated patch clamp, and John Heneghan, Mandy Roberts-Crowley and Ann Rittenhouse for guidance involving the use of the patch clamp technique.

I would like to thank the Rhind, Zamore and Rittenhouse labs for letting me use their equipment, and Geoffrey Abbott for providing me with the HA-tagged KCNE3 clone used in Chapter II.

Lastly, I would like to thank my mentor. He taught me nearly every scientific technique I possess, from the use of two-electrode voltage clamp to SDS-PAGE. Through his mentorship, I have also improved my presentation and writing skills. Lastly, he has given me an opportunity to pursue electrophysiology.

## THESIS ABSTRACT

KCNQ1 is a homotetrameric voltage-gated potassium channel expressed in cardiomyocytes and epithelial tissues. However, currents arising from KCNQ1 have never been physiologically observed. KCNQ1 is able to provide the diverse potassium conductances required by these distinct cell types through coassembly with and modulation by type I transmembrane  $\beta$ -subunits of the KCNE gene family.

KCNQ1-KCNE  $K^+$  channels play important physiological roles. In cardiac tissues the association of KCNQ1 with KCNE1 gives rise to  $I_{Ks}$ , the slow delayed outwardly rectifying potassium current.  $I_{Ks}$  is in part responsible for repolarizing heart muscle, and is therefore crucial in maintaining normal heart rhythmicity.  $I_{Ks}$  channels help terminate each action potential and provide cardiac repolarization reserve. As such, mutations in either subunit can lead to Romano-Ward Syndrome or Jervell and Lange-Nielsen Syndrome, two forms of Q-T prolongation. In epithelial cells, KCNQ1-KCNE1, KCNQ1-KCNE2 and KCNQ1-KCNE3 give rise to potassium currents required for potassium recycling and secretion. These functions arise because the biophysical properties of KCNQ1 are always dramatically altered by KCNE co-expression.

We wanted to understand how KCNE peptides are able to modulate KCNQ1. In Chapter II, we produce partial truncations of KCNE3 and demonstrate the transmembrane domain is necessary and sufficient for both assembly with and modulation of KCNQ1. Comparing these results with published results obtained from chimeric KCNE peptides and partial deletion mutants of KCNE1, we propose a bipartite modulation residing in

KCNE peptides. Transmembrane modulation is either active (KCNE3) or permissive (KCNE1). Active transmembrane KCNE modulation masks juxtamembranous C-terminal modulation of KCNQ1, while permissive modulation allows C-terminal modulation of KCNQ1 to express. We test our hypothesis, and demonstrate C-terminal Long QT point mutants in KCNE1 can be masked by active transmembrane modulation.

Having confirmed the importance the C-terminus of KCNE1, we continue with two projects designed to elucidate KCNE1 C-terminal structure. In Chapter III we conduct an alanine-perturbation scan within the C-terminus. C-terminal KCNE1 alanine point mutations result in changes in the free energy for the KCNQ1-KCNE1 channel complex. High-impact point mutants cluster in an arrangement consistent with an alpha-helical secondary structure, “kinked” by a single proline residue. In Chapter IV, we use oxidant-mediated disulfide bond formation between non-native cysteine residues to demonstrate amino acid side chains residing within the C-terminal domain of KCNE1 are close and juxtaposed to amino acid side chains on the cytoplasmic face of the KCNQ1 pore domain. Many of the amino acids identified as high impact through alanine perturbation correspond with residues identified as able to form disulfide bonds with KCNQ1. Taken together, we demonstrate that the interaction between the C-terminus of KCNE1 and the pore domain of KCNQ1 is required for the proper modulation of KCNQ1 by KCNE1, and by extension, normal  $I_{Ks}$  function and heart rhythmicity.



## TABLE OF CONTENTS

<b>Title Page</b>	i
<b>Signature Page</b>	ii
<b>Dedications</b>	iii
<b>Acknowledgements</b>	v
<b>Abstract</b>	vi
<b>Table of Contents</b>	viii
<b>List of Tables</b>	xi
<b>List of Figures</b>	xii
<b>Abbreviations</b>	xv
<b>Preface</b>	xviii
<b>Chapter I</b>	
<b>Introduction</b>	
Intrinsic properties of voltage-gated potassium channels	1
<i>KCNQ1</i>	10
KCNE peptides	13
<i>Cardiac I<sub>Ks</sub> current (KCNQ1-KCNE1)</i>	16
<i>Epithelial KCNQ1-KCNE complexes</i>	26
<i>Other KCNQ1-KCNE complexes</i>	33
<i>Promiscuity</i>	35

M-currents	40
------------	----

## **Chapter II**

### **KCNE3 truncation mutants reveal a bipartite modulation of**

#### **KCNQ1 K<sup>+</sup> channels**

Abstract	48
Introduction	49
Results	51
Discussion	76
Materials and methods	85

## **Chapter III**

### **Secondary structure of a KCNE cytoplasmic domain**

Abstract	93
Introduction	94
Results	96
Discussion	114
Materials and methods	121

## **Chapter IV**

### **The intracellular, juxtamembranous domain of KCNE1**

**interacts directly with the cytoplasmic face of the KCNQ1 pore**

#### **domain**

Abstract	126
Introduction	127
Results	130
Discussion	156
Materials and methods	162

## **Chapter V**

### **Conclusions and Future Directions**

General Discussion	171
Future Directions	180
Conclusion	191
<b>References</b>	<b>192</b>

## LIST OF TABLES

<b>Table 2-1</b>	Electrophysiological Properties of KCNE3 Truncation Mutants	62
<b>Table 3-1</b>	Electrophysiological Properties of KCNE1 Mutants	100
<b>Table 3-2</b>	$\alpha$ -helical Characteristics of C-terminal E1 Segments	116
<b>Table 4-1</b>	Oxidant-mediated current inhibition of cysteine mutant $I_{Ks}$	155

## LIST OF FIGURES

<b>Figure 1-1</b>	The structure of <i>Shaker</i> -like voltage-gated potassium channels	4
<b>Figure 1-2</b>	The large intracellular C-terminus of KCNQ1 channel complexes	11
<b>Figure 1-3</b>	KCNE peptides	14
<b>Figure 1-4</b>	Ionic currents involved in the cardiac action potential	18
<b>Figure 1-5</b>	Cochlear Structure	24
<b>Figure 1-6</b>	KCNE-modulated KCNQ1 channels play physiological roles in several types of epithelial cells	27
<b>Figure 1-7</b>	Related KCNQ channel complexes give rise to M-currents, responsible for regulating neuronal excitability	42
<b>Figure 2-1</b>	KCNQ1/KCNE3 channels have a large standing current at negative membrane potentials	52
<b>Figure 2-2</b>	KCNE3 truncation mutants	55
<b>Figure 2-3</b>	KCNE3 N-terminal truncation mutants produce standing currents at negative potentials when co-expressed with Q1	57
<b>Figure 2-4</b>	KCNE3 C-terminal and combined N- and C-terminal truncation mutants also exhibit standing currents at negative potentials when co-expressed with Q1	60

<b>Figure 2-5</b>	A Long QT mutation in the C-terminus of KCNE1 is masked by the KCNE3 transmembrane domain	64
<b>Figure 2-6</b>	KCNE3 C-terminal mutants demonstrate a functional dependence on cRNA injection ratios	66
<b>Figure 2-7</b>	Functional characterization of KCNQ1/KCNE3-HA Complexes	70
<b>Figure 2-8</b>	WT and C-terminal mutant HA-tagged KCNE3 peptides are glycosylated and not proteolytically degraded in oocytes	73
<b>Figure 2-9</b>	A bipartite model for modulation of KCNQ1 by KCNE1 and KCNE3	81
<b>Figure 3-1</b>	KCNE1 alanine mutants show diverse gating properties	97
<b>Figure 3-2</b>	Periodicity of gating perturbations in the KCNE1 C-terminal domain	103
<b>Figure 3-3</b>	Negatively charged side chains produce smaller perturbations than alanine at position S68	106
<b>Figure 3-4</b>	Branched amino acids cause larger perturbations at position S74	109
<b>Figure 3-5</b>	The transmembrane-abutting C-terminal domain is comprised of two helical regions	112

<b>Figure 4-1</b>	Native and “cysless” $I_{Ks}$ subunits give rise to currents which are mutually reminiscent	132
<b>Figure 4-2</b>	The positions of exogenous cysteine mutants scanned in this study	134
<b>Figure 4-3</b>	Q1-cys, H363C is able to form higher molecular mass species with a panel of E1-cys point mutations	138
<b>Figure 4-4</b>	Cysteine point mutations residing in the S6 gate and the S4-5 linker are able to form higher molecular mass species with E1 cysteine point mutants	143
<b>Figure 4-5</b>	The ~ 150 kDa species is a Q1-E1 disulfide-bound heterodimer found on the cell surface	147
<b>Figure 4-6</b>	Whole-cell perforated patch clamp recordings of CHO cells transfected with point mutants of Q1 and E1	152
<b>Figure 4-7</b>	Close contacts within the cytoplasmic face of $I_{Ks}$ channel complexes	157
<b>Figure 5-1</b>	The bipartite model for KCNE modulation of KCNQ1 Channels	173
<b>Figure 5-2</b>	Bipartite KCNE modulation: transmembrane and C-terminal association	178
<b>Figure 5-3</b>	State-dependent crosslink formation	183

## LIST OF ABBREVIATIONS

<b>K<sup>+</sup></b>	potassium (ion)
<b>Kv</b>	voltage-gated potassium channel
<b>KCNQ1, KvLQT1, Kv7.1, Q1</b>	voltage-gated potassium channel, KQT-like subfamily, member 1
<b>KCNQ2-5, Kv7.2-5</b>	potassium voltage-gated channel, KQT-like subfamily, member 2-5
<b>Kv1.x</b>	potassium voltage-gated channel, <i>Shaker</i> -related subfamily, member x
<b>Kv2.x</b>	potassium voltage gated channel, <i>Shab</i> -related subfamily, member x
<b>Kv3.x</b>	potassium voltage gated channel, <i>Shaw</i> -related subfamily, member x
<b>Kv4.x</b>	potassium voltage-gated channel, <i>Shal</i> -related subfamily, member x
<b>hERG</b>	potassium voltage-gated channel, subfamily H (eag-related), member 2
<b>BK, KCNMA1</b>	potassium large conductance calcium-activated channel, subfamily M, alpha member 1
<b>Kir</b>	potassium inwardly-rectifying channel
<b>HCN1-4</b>	hyperpolarization activated cyclic nucleotide-gated potassium channel 1-4
<b>SCN5A</b>	sodium channel, voltage-gated, type V, alpha subunit
<b>CFTR</b>	cystic fibrosis transmembrane conductance regulator
<b>α-subunit</b>	pore-forming channel complex subunit



<b><math>\beta</math>-subunit</b>	modulatory channel complex subunit
<b>KCNE1, MinK, IsK, E1</b>	potassium voltage-gated channel subfamily E member 1
<b>KCNE2-5, MiRP1-4, E2-5</b>	potassium voltage-gated channel subfamily E member 2-5
<b>KCNMB1-4</b>	potassium large conductance calcium- activated channel, subfamily M, beta member 1-4
<b>KChIP</b>	Kv channel-interacting protein
<b>Kv<math>\beta</math></b>	voltage-gated potassium channel subunit beta
<b>S1-6</b>	voltage-gated potassium channel transmembrane helix 1-6
<b>TM Domain</b>	transmembrane domain
<b>NKCC1</b>	solute carrier family 12 (sodium/potassium/ chloride transporters), member 2
<b>Nedd4-2</b>	E3 ubiquitin-protein ligase, member 2
<b>AKAP</b>	A-kinase anchor protein
<b>PKA</b>	cAMP-dependent protein kinase
<b>PKC</b>	protein kinase C
<b>PP1</b>	protein phosphatase 1
<b>LQT(S)</b>	Long QT Syndrome
<b>RWS</b>	Romano-Ward Syndrome
<b>JLNS</b>	Jervell and Lange-Nielsen Syndrome
<b>I<sub>Ks</sub></b>	cardiac potassium current, slow delayed outwardly-rectifying

<b>I<sub>M</sub>, M-current, M-channel</b>	potassium current, muscarine-sensitive
<b>N-terminal, N-terminus</b>	amino-terminal, amino-terminus
<b>C-terminal, C-terminus</b>	carboxy-terminal, carboxy-terminus
<b>N-linked glycosylation</b>	glycosylation mediated through modified asparagine
<b>EKG</b>	electrocardiogram
<b>TEVC</b>	two-electrode voltage clamp
<b>IC<sub>50</sub></b>	concentration resulting in 50% inhibition
<b>Chromanol 293B, 293B</b>	<i>trans</i> -6-Cyano-4-( <i>N</i> -ethylphonyl- <i>N</i> - methylamino)-3-hydroxy-2,2-dimethyl- chromane
<b>PIPn</b>	phosphoinositol n-phosphate
<b>cAMP</b>	adenosine 3',5'-cyclic monophosphate
<b>HA</b>	hemagglutinin A
<b>WT</b>	wild type

## PREFACE

Two of my three data chapters are collaborations between my lab mates and me. Chapters II and III presented in this thesis have been published in peer-reviewed journals. In addition, I have made contributions to other projects and produced preliminary data published in grant proposals; these projects will not be presented within this thesis.

Chapter III is collaboration between Jessica Rocheleau and me. I began the chapter in September of 2003, and relinquished first-authorship to her in January of 2005 upon her decision to join the Kobertz lab and my decision to pursue Chapter IV. My contribution to Chapter III includes the mutagenesis for many of the mutant KCNE1 constructs, as well as TEVC recordings for wild type  $I_{Ks}$  and some of the mutants. Data analysis, including  $\alpha$ -periodicity indices, was performed by Jessica. It is my understanding that Jessica intends to present this work within her thesis.

The preliminary experiments of Chapter IV were conducted by my co-author, Virla Berrios, however none of these results are included in the chapter; her results were inconclusive (see Chapter IV). I was responsible for optimization of the crosslinking protocol as well as production of all biochemical and electrophysiological results presented in this thesis. In my absence, Anatoli Lvov has continued with planned experiments involving whole-cell perforated patch clamp. None of Dr. Lvov's work is presented in this thesis. Mutagenesis of KCNQ1 and KCNE1 was a collaborative effort between Virla and me.

*References*

**Chapter II** - Gage, S.D. and W.R. Kobertz, *KCNE3 truncation mutants reveal a bipartite modulation of KCNQ1 K<sup>+</sup> channels*. J Gen Physiol, 2004. **124**(6): 759-71.

**Chapter III** - Rocheleau, J.M., S.D. Gage, and W.R. Kobertz, *Secondary structure of a KCNE cytoplasmic domain*. J Gen Physiol, 2006. **128**(6): 721-9

# CHAPTER I

## INTRODUCTION

### **INTRINSIC PROPERTIES OF VOLTAGE-GATED POTASSIUM CHANNELS**

Voltage-gated ion channels are proteinaceous membrane-embedded pores. When activated (open), voltage-gated ion channels allow the passive diffusion of ions down their electrochemical gradient. Potassium selective voltage-gated ion channels are a subset of ion conducting complexes that under normal physiological conditions allow outward potassium current, which drives membrane potential negative towards the Nernst-predicted reversal potential of potassium. Hyperpolarization of the plasma membrane is required for several functions (Hille, 1992).

Cells utilize the electrochemical gradients existing across their plasma membrane to establish transmembrane electromotive force required for cellular excitability among other functions. This transmembrane voltage occurs because membranes rest at the voltage at which net influx and efflux for each ionic species is minimized, referred to as the reversal potential for a particular ion. For most resting cells, plasma membrane voltages are sufficiently negative, reducing the net current through the dominant resting ion channel type, potassium. As conduction of other ions changes, membrane voltage subsequently changes and approaches the reversal potential for the new dominant conductance. For example, a large increase in sodium conductance leads to a transient increase in the sodium influx and a concomitant increase in membrane potential towards

the reversal potential for sodium ions. The reversal potential for any ion can be calculated as a function of the resting concentration gradient:

$$(1) E_{ion} = \frac{RT}{FZ} \log \frac{[ion]_{out}}{[ion]_{in}} = \frac{+60\text{mV}}{Z} * \log \frac{[ion]_{out}}{[ion]_{in}} ,$$

where  $R$  is the gas constant,  $T$  is temperature,  $F$  is Faraday's constant,  $Z$  is the valence charge of the ion, and  $[ion]$  is the ionic concentration on one side of the membrane. The reversal potential modifies Ohm's Law, and provides a function describing current of a specific ionic species in an electrochemical gradient:

$$(2) V = IR \text{ or } gV = I .$$

In an electrochemical gradient,

$$(3) g_{ion}(V_m - E_{ion}) = I_{ion} ,$$

where  $V_m$  is transmembrane potential (intracellular relative to extracellular),  $I$  is current (positive current is an efflux of positive ions),  $R$  is resistance, and  $g$  is conductance.

Macroscopic conductance describes the entire population of functional channels on the cell surface,  $N$ , but is dependent not only on the conductance of a single open channel

complex,  $\gamma$ , but also on the percentage of functioning channels open on the cell surface,  $P_o$ . Considering these properties of conductance, equation 3 can be rewritten

$$(4) I_{ion}(t) = (V_m - E_{ion})(N_{ion}P_o(t)\gamma_{ion}) .$$

In other words, the magnitude and direction (influx or efflux) of any ionic current at a given time can be described as a function of electrochemical driving force for that particular ion, the number of functioning ion-permissive channels on the cell surface and the single-channel conductance and open probability of each channel.

Among other roles, voltage-gated potassium channels terminate the action potential. In response to membrane depolarization due to quick sodium influx, a delayed potassium efflux activates. This potassium conductance, combined with diminished sodium influx (due to sodium channel inactivation), reestablishes a negative membrane potential. If the kinetics of this potassium efflux are sufficiently slow, potassium channels which have not deactivated allow excitable membranes to become refractory to future action potentials and can prevent tonic stimulation. Because any positive shift in membrane potential is able to activate potassium channels, voltage-gated potassium channels lacking inactivation can also be involved in potassium recycling in non-excitable cells (Snyders, 1999; Cooper & Jan, 2003; Warth, 2003).

As typified by the *Drosophila melanogaster* potassium channel, *Shaker* (Figure 1-1), voltage-gated potassium channels are tetrameric assemblies usually possessing six transmembrane helices and a pore-loop-helix motif between the fifth and sixth

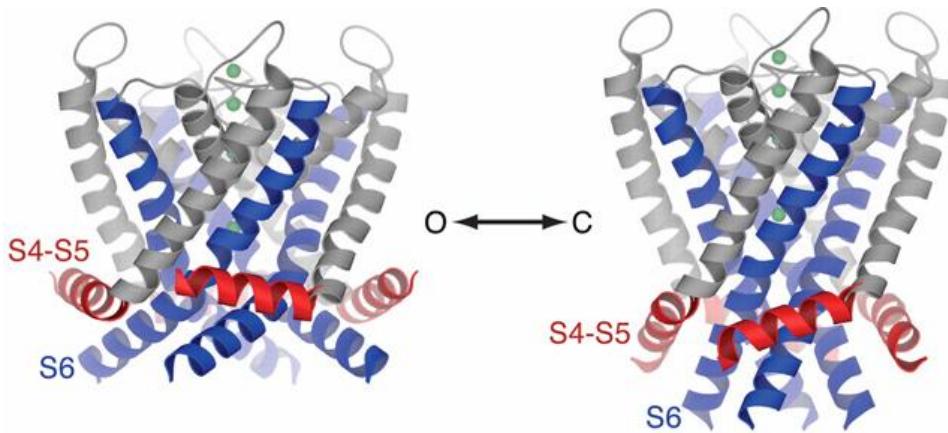
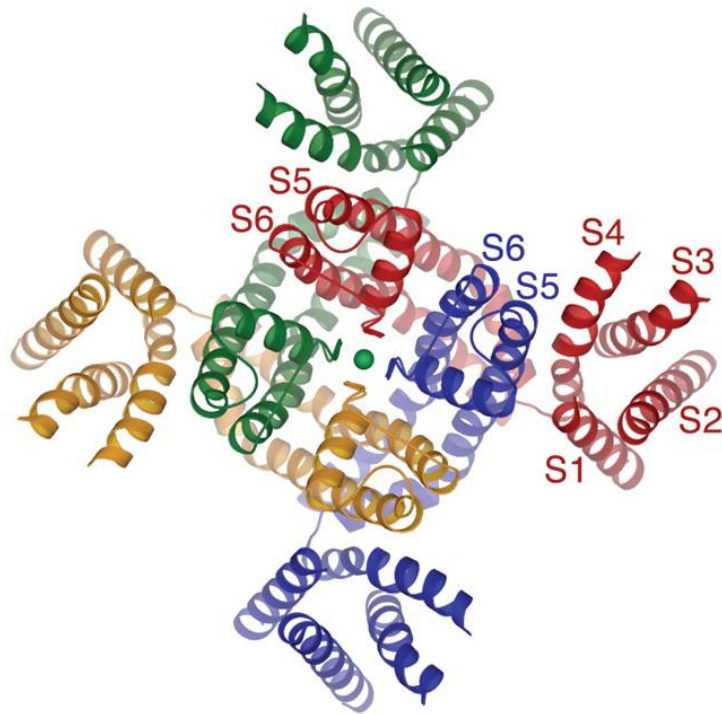
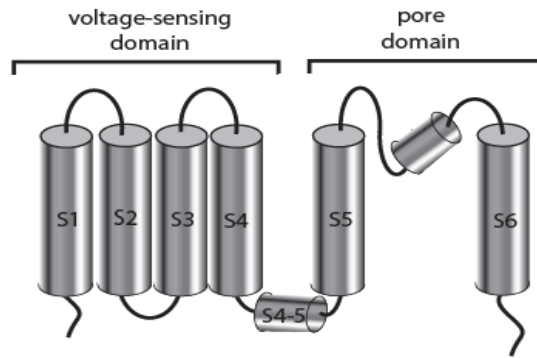




**Figure 1-1.** The structure of *Shaker*-like voltage-gated potassium channels. **Above**, schematic diagram of the canonical transmembrane structure of a single *Shaker*-like pore-forming subunit viewed from within the plane of the plasma membrane. The top of this diagram faces the extracellular side of the plasma membrane; the bottom of this diagram faces the intracellular side of the plasma membrane. *Shaker*-like voltage-gated potassium channel subunits contain six transmembrane helices and a pore-loop-helix between the fifth and sixth transmembrane helices. The structure also contains a small cytoplasmically exposed helix between the fourth and fifth transmembrane helices. Helices clustering to form the pore-domain or the voltage sensing domain are labeled. **Center**, crystal structure of a rat *Shaker* homologue, Kv1.2, viewed from the extracellular side. A potassium ion (colored green) resides in the pore of this structure. The voltage sensing domain is composed of the first four transmembrane helices (labeled for one of the four pore-forming subunits, right). The pore domain and the selectivity filter are formed through the coordination of the fifth and six transmembrane helices and the pore-loop-helix. Each subunit is painted in a different color for clarity. Notice the voltage sensors of each subunit associate with pore domain of an adjacent subunit. **Below**, model of Kv1.2 gating motion, observed from within the plane of the membrane. The S4-5 linker helix (red), S5 and pore-loop-helix (gray) and the S6 gate (blue) are shown, while the voltage sensing domain has been omitted for clarity. The top of the channel complex faces the extracellular milieu; the bottom of the channel complex faces the cytosol. On the left, a computer model in which the S4-5 linker helix is in the hyperpolarized state, based in part on the closed gate conformation observed in the crystal structure of KcsA.

The closed state transitions to the X-ray crystal structure on the right in response to membrane depolarization. Domain swapping of the voltage sensing domain positions the S4-5 linker helix adjacent to the S6 gate within the same subunit and allows movements of the voltage sensor to be transduced into gating motions.

Diagram (*above*) produced by S. Gage. Crystal structures and computer models adapted from Long, S.B., E.B. Campbell, and R. Mackinnon, *Voltage sensor of Kv1.2: structural basis of electromechanical coupling*. *Science*, 2005. **309**(5736): p. 903-8.

transmembrane helix. Most of the functional properties of the potassium channel are intrinsically accomplished by the tetramer formed from this core potassium channel motif (Robbins, 2001).

All voltage-gated channels must form a tight seal with the plasma membrane, providing high resistance to transmembrane ionic conductance in the deactivated, closed state. This function is highlighted by crystal structures in which membrane phospholipids adopting rigid conformations have co-crystalized with the channel (Gonen *et al.*, 2005; Long *et al.*, 2007). Plasma membrane content may play a critical role in establishing channel structure (Jiang *et al.*, 2003a; Lee *et al.*, 2005). Several point mutations have been identified within the voltage sensing domain which decrease the resistance of the membrane to ion permeation (Starace *et al.*, 1997; Starace & Bezanilla, 2001; Tombola *et al.*, 2005). One such example is a histidine mutation in the voltage-sensing domain; this mutant histidine residue is able to adopt multiple conformations, including one that is exposed to the cytosol and another that is exposed to the extracellular lumen. This histidine can accept a proton on one side of the membrane, and release it on the other, allowing a proton current to arise from conduction across the voltage sensor (Starace *et al.*, 1997; Starace & Bezanilla, 2001).

Voltage-gated potassium channels are selectively permeable to potassium. This selective permeability arises from the structure of the potassium channel selectivity filter. The selectivity filter, located on the extracellular face of potassium channels, has been likened visually to the shape of an “inverted teepee”. The backbone amide oxygens from all four pore-forming subunits coordinate, forming the lattice of the selectivity filter.

This lattice mimics the positions of oxygens within the aqueous chelation cage of a potassium ion, and minimizes the energy of potassium ion dissolution from water. The selectivity filter of potassium channels is poorly permissive to conduction of other aqueous ions because the backbone oxygens within the selectivity filter are not able to adequately mimic the aqueous chelation of other ions (Doyle et al., 1998; Morais-Cabral et al., 2001; Zhou et al., 2001).

All voltage-gated ion channels are able to change their conductance as a function of both time and membrane potential. Potassium ion channels sense changes in membrane potential through movement of the voltage sensing domain. The voltage sensor is composed of the first four transmembrane helices of each pore-forming subunit, but is dependent upon the basic positively charged arginines residing in the fourth transmembrane helix (S4). Positive changes in membrane potential (for instance occurring as a result of sodium influx during action potential) repel the positively charged amino acids of the voltage sensor. The nature of the resulting voltage sensor movement is still quite controversial, but either a translational or rotational movement in the voltage sensor (or both) results in tension on the N-terminal side of the S4-5 linker helix (Gandhi & Isacoff, 2002; Jiang *et al.*, 2002b; Starace & Bezanilla, 2004; Posson *et al.*, 2005; Ruta *et al.*, 2005). The fifth transmembrane helix (which constitutes part of the pore domain) acts as a fulcrum for the S4-5 linker helix. As N-terminal side of the linker helix moves, the fifth transmembrane helix remains rigid. The resulting tension and movement of the linker helix is transduced through Van der Waals contacts between the linker helix and the sixth transmembrane domain (the gate), pulling and pushing the gate into open

(activated) or closed (deactivated) conformations. The open gate conformation allows ions to move passively down their electrochemical gradient along the ion conduction pathway of the channel complex, while the closed conformation sterically occludes the ion conduction pathway. Activation is a stochastic event; at any membrane potential there is a dynamic equilibrium between activated and deactivated channel complexes – it is the ratio of these populations ( $P_o$ ) which in part determines macroscopic current (Aldrich et al., 1983; Long et al., 2005a, 2005b).

Many voltage-gated potassium channels cannot stay open during prolonged depolarizations. The magnitude of current can decrease through a mechanism distinct from deactivation, termed inactivation. Potassium channel inactivation is independent of gate movement and generally takes one of two forms. Fast, N-type inactivation (with time constants faster than 500 ms) results from steric occlusion of the ion conduction pathway. In the case of *Shaker*, this results from a covalently tethered ball-peptide on the N-terminus of the  $\alpha$ -subunit plugging the channel and occluding the passage of potassium ions. Removal of the ball peptide eliminates fast inactivation; N-type activation can be restored by application of purified inactivation peptide to the intracellular face of *Shaker* (Zagotta et al., 1990; Murrell-Lagnado & Aldrich, 1993). Mammalian Kv channels also possess N-type inactivation, but this inactivation arises from co-assembly with accessory subunits possessing an inactivation peptide (Robbins, 2001; Long et al., 2005a). C-type inactivation is a slower-onset type of inactivation (with time constants greater than 1000 ms) mediated by pore-collapse. C-type inactivation

occurs at sufficiently positive membrane potentials, but otherwise occurs with little voltage dependence (Hoshi et al., 1991; Morais-Cabral et al., 2001; Zhou et al., 2001).

Though potassium channels intrinsically possess most of their required functions, they are still subject to environmental cues. As alluded to above, Kv channels are able to assemble with and be modulated by several classes of small polypeptides. These include Kv $\beta$ s, KChIPs and KCNE peptides (Robbins, 2001). Gene expression and biosynthetic context are also important for native potassium channel function (Papazian, 1999). The contribution of intracellular signaling proteins complicates potassium channel function even further. These many factors further refine the activity of potassium channels, especially KvLQT1 (hereafter referred to by its gene name, KCNQ1). It is the nature of modulation of KCNQ1 that is the subject of this thesis.

*KCNQ1* - Expressed alone in over-expression systems, the potassium channel pore-forming subunit KCNQ1 gives rise to a delayed, outwardly rectifying potassium current. KCNQ1, as with the other members of the KCNQ family of voltage-gated potassium channels, has six transmembrane helices and a single pore-loop-helix motif; this structure is similar to other *Shaker*-like voltage-gated potassium channels (Robbins, 2001). Unlike *Shaker*-type potassium channels, KCNQ1 has a relatively small N-terminal domain with a small helix-loop-helix motif, a PKA phosphorylation site at S27, and lacks a *bona fide* tetramerization domain (T1). Instead of a large T1 domain, KCNQ1 has a large C-terminal domain which is required for association with several aqueous cell-signaling molecules (Figure 1-2). This C-terminal domain is also required

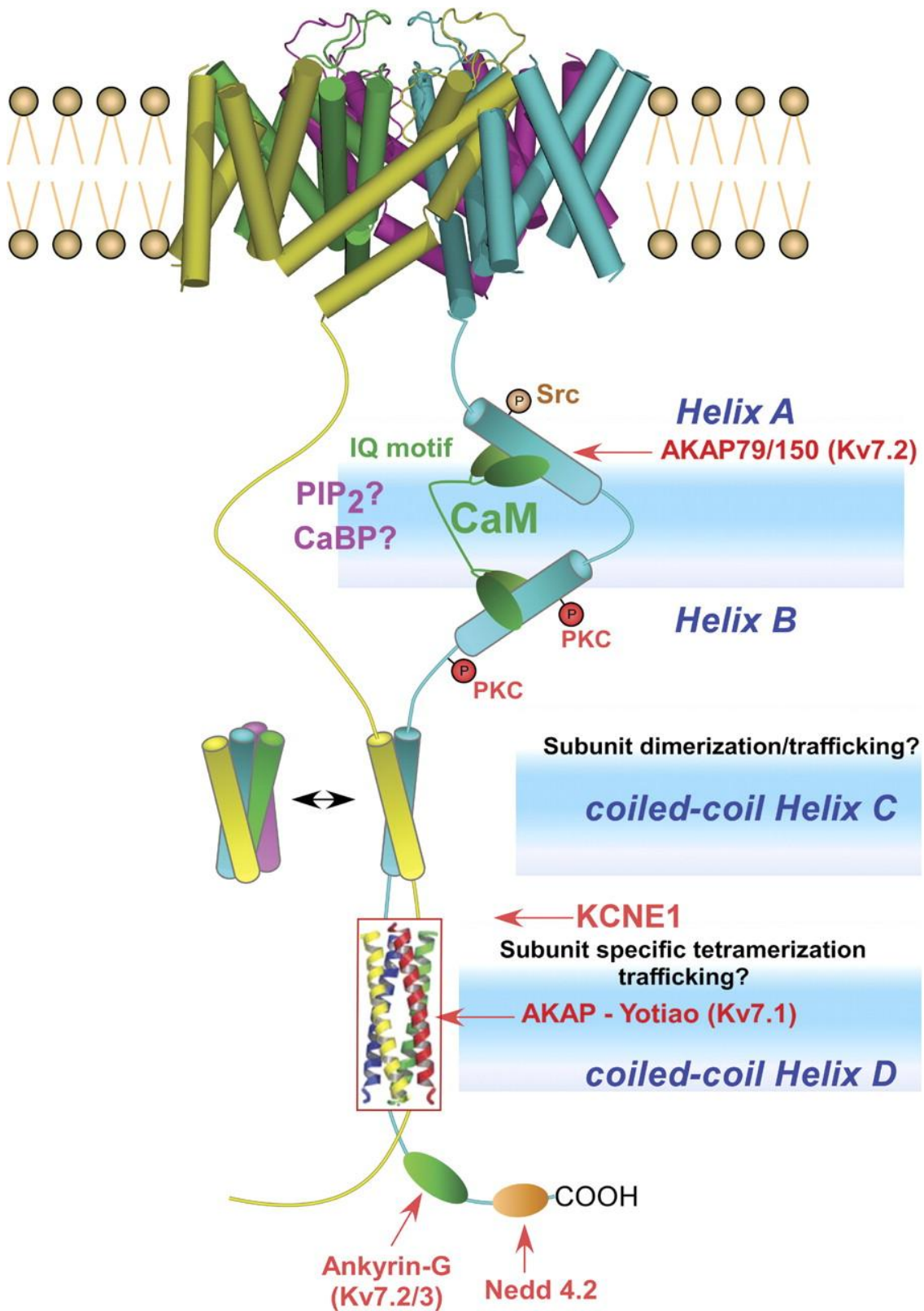


**Figure 1-2.** The large intracellular C-terminus of KCNQ1 channel complexes. Cylinders represent alpha-helices. The C-terminus of all KCNQ subunits contains four  $\alpha$ -helices along with interhelical regions of variable length and as-of-yet undetermined secondary structure. Within the C-terminal domain, the N-terminal pair of  $\alpha$ -helices (helices A & B) is important for interactions with calmodulin, an association which confers calcium sensitivity to these channel complexes. The C-terminal pair of  $\alpha$ -helices is required for dimerization of the preassembled channel complex and tetramerization of the tetrameric channel complex, and confers specificity for heteromeric KCNE and KCNQ subunit association. In KCNQ1, these helices also provide the docking site for Yotiao, an adapter protein involved in anchoring both kinases and phosphatases, and are therefore critical in integrating channel function with extrinsic signaling pathways. The C-terminal end of the KCNQ channel complexes also contains a consensus site for binding with ubiquitin ligases, but the necessity of this binding site is questionable.

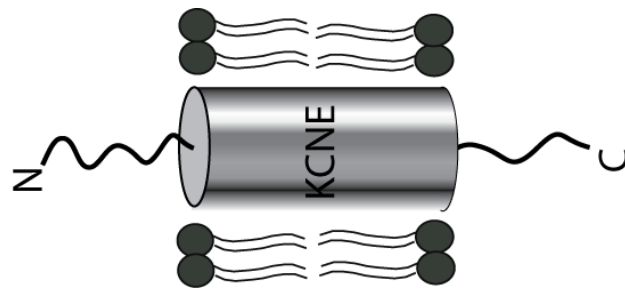
Figure taken from Haitin, Y. and B. Attali, *The C-terminus of Kv7 channels: a multifunctional module*. J Physiol, 2008. **586**(7): p. 1803-10



for proper assembly during biosynthesis and choice of heteromeric association (Li *et al.*, 1992; Marx *et al.*, 2002; Kanki *et al.*, 2004; Dahimene *et al.*, 2006; Howard *et al.*, 2007; Haitin & Attali, 2008). Further, KCNQ1 possesses an unusual type of inactivation. Much like C-type inactivation, the onset of inactivation in KCNQ1 is slow, but transition to the inactivated state is voltage-dependent, whereas classical C-type inactivation is voltage-independent within a positive range of membrane potentials (Hoshi *et al.*, 1991; Pusch *et al.*, 1998). C-type inactivation in KCNQ1 also differs from other potassium channel complexes because the transition to the C-type inactivated state in KCNQ1 reaches equilibrium or is masked by further channel activation. The C-type inactivation observed with KCNQ1 over-expression is mostly a curiosity, considering KCNQ1 currents have not been likened to any physiologically observed potassium current, and inactivation has not been observed with any KCNQ1-KCNE channel complex.

### **KCNE PEPTIDES**

The KCNE gene family (Figure 1-3) encodes MinK (also known as  $I_{sK}$ ) and MiRP1-4 proteins (MiRP4 was originally called Kcne1-1). To avoid any confusion, these proteins will be referred to by their gene names, KCNE1-5. KCNE peptides are type I transmembrane peptides ranging in size between 103 and 170 amino acids, and are found in a variety of tissues (McCrossan & Abbott, 2004). The hallmark of KCNE peptides is that each one is able to co-assemble with and dramatically modulate the gating properties of KCNQ1 potassium conducting complexes



TM domain

KCNE1	-----MILSNITAVTPFLTKLWQETVQQGGMISGLARRSPRSGDGKLEALVFLMVLGFFGFFTLGIMLSYI
KCNE2	-----KSTLSNFTQTLQEDVFRRIFFITYMDNWRQNTTAEQEAQAKVDAENFYVYVILVLMVMIGMFSFIIVAILVSTV
KCNE3	--METTNGTETWYESLHVLKALNATLHSNLLCRPGPLGPDNQTEERRASLPGRDDHSMMYILFVMFLFAVTVGSLILGYT
KCNE4	-----MLKMEPLNSTHPTAAASSSPLSRAAGGSGNGHEVYFYLVMNSFYGIFLIGIMLGYM
KCNE5	MNCSESQRLRTLRLLELHRGNASGLGAGPRPSMGVVPDPFVGREVTSAKGDDAVLYILLINKIFYACLGGGLLAYT
KCNE1	RSKKLEHSNDPTNVIYESDAWQEKDAYVQARVLESYRSCYVVENHLAIEQPINTHLPETKPSF-----
KCNE2	KSKRREHSNDPYHQYIVEDWQEKYKYSQILNLEESKATIHENIGAAQFKNSP-----
KCNE3	RSRKVKRRSDPYHYIKNRVSMI-----
KCNE4	KSKRREKKSSLLLLYKDEERLWGEAMKPLPVVSGLRVQVPLMLMMLQESVAPALSCTLCSMEGDSVSSSSPDVHLTIQ
KCNE5	RSRKLVKAEKDEPSQACAEHEHAPGGALTADAEAAAGSQAEGRRLASEGLPALAQAERY-----
KCNE4	EEGADDELEETSETPLNESSEGSSENIHQNS

**Figure 1-3.** KCNE peptides. *Left*, cartoon depicting the putative transmembrane topology of KCNE peptides. KCNE peptides are short polypeptides containing a single, lipid bilayer-spanning domain (labeled “TM”, *right*). As KCNE proteins are type I transmembrane peptides, the N-termini of KCNEs face the extracellular milieu and the C-termini face the cytosol. *Right*, amino acid alignment of all of the known members of the KCNE family. KCNE peptides are as labeled on the left. Transmembrane domains for KCNE peptides are boxed and labeled “TM domain”.

*Left*, figure produced by S. Gage. *Right*, figure adapted from McCrossan, Z.A. and G.W. Abbott, *The MinK-related peptides*. *Neuropharmacology*, 2004. **47**(6): p. 787-821

(Barhanin et al., 1996; Sanguinetti et al., 1996; Schroeder et al., 2000b; Tinel et al., 2000a; Angelo et al., 2002; Grunnet et al., 2003). In fact, KCNQ1 is completely dependent upon its association with KCNE peptides – currents arising from KCNQ1 homotetramers have not been detected in native tissues (Robbins, 2001). However, the modulatory effects of KCNE peptides are not limited to the KCNQ1 potassium conducting complex; KCNE peptides are able to associate with a variety of potassium channel pore-forming subunits. KCNE peptides each have at least one N-linked glycosylation site on the extracellular N-terminal side (McCrossan & Abbott, 2004). Structurally, KCNE peptides have been shown to be mainly alpha-helical on their juxtamembranous C-terminal domain, and are believed to be alpha-helical in their transmembrane domain (though interpretation of serial perturbation studies in the transmembrane domain is complicated by the presence of many protein contacts within this region, clustering to multiple faces of the alpha-helical face) (Rocheleau *et al.*, 2006; Chen & Goldstein, 2007; Liu *et al.*, 2007). The variety of KCNEs and KCNE modulation reflect tissue-specific potassium conductance requirements and is addressed below.

***Cardiac  $I_{Ks}$  current (KCNQ1-KCNE1)*** - The best studied of the heteromultimeric complexes formed from KCNQ1 is the cardiac  $I_{Ks}$  current.  $I_{Ks}$  is the slow delayed outwardly rectifying potassium heart current. Channels giving rise to  $I_{Ks}$  are formed by the association of KCNQ1 and KCNE1, also known as MinK and  $I_{sK}$ .  $I_{Ks}$  is one of several potassium currents responsible for maintaining action potential duration, and as

such, mutations in either gene can prolong time interval between the Q and T peaks on an EKG. One such mutation, KCNE1-D76N, is notable since KCNE1 is still able to assemble with KCNQ1, but the resultant mutant KCNQ1-KCNE1 is completely non-conductive at the plasma membrane (Splawski et al., 1997; Splawski et al., 2000). The resulting Long QT Syndrome has been associated with *torsade de pointes*, syncope and fibrillations. Autosomal dominant Q-T prolongation is called Romano-Ward Syndrome, while a recessive form of Long QT Syndrome associated with  $I_{Ks}$  is called Jervell and Lange-Nielsen Syndrome. JLNS is also accompanied by complete bilateral deafness (Jervell & Lange-Nielsen, 1957; Ward, 1964; Barhanin *et al.*, 1996; Sanguinetti *et al.*, 1996; Snyders, 1999).

Cardiac potassium currents function in careful syncopation to preserve cardiac rhythmicity (Figure 1-4). If the myocardium is too refractory to action potentials due to excess potassium current (for instance due to over-expression of  $I_{Ks}$ ), myocardial fibers can exhibit wave break leading to arrhythmicity and, potentially, fibrillations (Munoz et al., 2007). Given too much reduction in cardiac potassium currents, myocardial tissues may not be able to repolarize sufficiently, leading to early- afterdepolarizations, another cause of myocardial arrhythmicity (Satoh & Zipes, 1998). Computer modeling also suggests that  $I_{Ks}$  plays a very important role in providing reserve for potassium channels. This model contains at least two closed states for each KCNQ1 subunit, but only one closed to open transition is slow. This single slow gating transition allows  $I_{Ks}$  channels to dwell in a closed state capable of transitioning to the open state in response to heightened need for potassium efflux. In response to sustained action potentials and dysfunction in

# Cardiac ion currents and cloned subunits

Current	Probable clone
sodium current	hH1
L-type calcium current	$\alpha_{1C}$ dihydropyridine receptor
T-type calcium current	$\alpha_{1G}$
Na-Ca exchange	Na-Ca exchanger
$I_{TO1}$ (4-AP-sensitive)	Kv4.2/4.3
$I_{TO2}$ (Ca-activated)	--
$I_{Ks}$	KCNQ1+KCNE1
$I_{Kr}$	HERG + ?
$I_{Kur}$ or $I_{Kq}$	Kv1.5
$I_{Cl}$ or $I_{Kp}$	CFTR // TWIK
$I_{K1}$ (inward rectifier)	Kir2 family
$I_K$ ATP/ACh	GIRK1+4 / Kir6.2+SUR1
$I_f$ (pacemaker)	HCN2

**Figure 1-4.** Ionic currents involved in the cardiac action potential. *Above*, a membrane voltage versus time diagram representing the cardiac action potential. *Below*, current versus time representation of ionic currents involved in the action potential. The name of each current is labeled on the left, while the known molecular identity of each channel complex is labeled on the right. A cartoon depicting both the magnitude and direction (influx or efflux) of each cardiac ionic current is presented in the center. Note that the direction depicts the movement of positive charges, so the depiction for  $I_{Cl}$  actually shows  $Cl^-$  influx, which is electrically equivalent to a positive efflux. The solid midline represents no net current. Of these cardiac conductances,  $I_{Kr}$  (due to inactivation) and  $I_{Ks}$  (due to slow kinetics) dominate the latter parts of the cardiac action potential.

Figure adapted from Snyders, D.J., *Structure and function of cardiac potassium channels*.

Cardiovasc Res, 1999. **42**(2): p. 377-90

other cardiac potassium currents,  $I_{Ks}$  act as a reserve of potassium conductance and prevent excessive Q-T prolongation. A lack of the repolarization reserve from  $I_{Ks}$  leads this computer model to early-afterdepolarizations in response to sudden decreases in heart rate, an effect observed in  $Cs^+$ -induced Long QT (Satoh & Zipes, 1998; Silva & Rudy, 2005).

There is some controversy concerning how KCNE1 is able to modulate KCNQ1 modulation (Tapper & George, 2000; Melman *et al.*, 2001; Melman *et al.*, 2002a; Melman *et al.*, 2002b). One line of research demonstrates KCNE modulation resides within the transmembrane domain of the peptide. Transmembrane chimeras of KCNE1 and KCNE3, upon co-expression with KCNQ1, alter KCNQ1; KCNE peptides containing the KCNE1 transmembrane domain display biophysical properties reminiscent of native KCNE1, while KCNE peptides containing the transmembrane domain of KCNE3 display properties reminiscent of native KCNE3. Transmembrane KCNE modulation was resolved to an amino acid triplet (FTL in KCNE1, TVG in KCNE3). A transmembrane interaction between KCNE peptides and KCNQ1 is supported by results demonstrating mutations within the voltage sensing domain of KCNQ1 recapitulate some of the biophysical properties observed in KCNQ1-KCNE channel complexes (Panaghie & Abbott, 2007; Shamgar *et al.*, 2008). If KCNE peptides do interact within membrane embedded regions of the KCNQ1 channel complex, this interaction does not result in changes in voltage sensor kinetics. The voltage sensor can be chemically modified in response to membrane depolarization in a manner independent of channel gating (Rocheleau & Kobertz, 2008).



Transmembrane modulation does not reconcile data obtained from partial deletions of KCNE1. Partial truncations of KCNE1 clearly modulate KCNQ1 channel complexes, however the slow gating of  $I_{Ks}$  is perturbed as the C-terminus of KCNE1 is progressively truncated. Both groups agree regions not directly involved in KCNE1 modulation are required for assembly with KCNQ1 (Tapper & George, 2000).

Can these observations be further reconciled? It is noteworthy both KCNE1 and KCNE3 are highly homologous in regions identified by both groups (excluding the modulatory triplet identified by Melman and colleague). Therefore, chimeras containing the modulatory triplet may reside in a KCNE context which is rather native-like (Figure 1-3); containing such a native environment may lead the hypotheses derived from KCNE chimeras astray. This paradox of KCNE modulation is the topic of Chapter II.

KCNE1 is believed to reside near the ion permeation pathway of  $I_{Ks}$  channels. Mutations in the transmembrane domain of KCNE1 are able to coordinate  $Cd^{2+}$  ions. This coordination inhibits potassium efflux and partially occludes the ion conduction pathway (Wang *et al.*, 1996; Tai & Goldstein, 1998; Tapper & George, 2001). Likewise, mutations in the voltage sensor and the pore domain of KCNQ1 are able to mimic some of the effects of KCNE modulation (Melman *et al.*, 2004; Panaghie & Abbott, 2007; Shamgar *et al.*, 2008). However, KCNE1 is still dependent upon the C-terminal domain of KCNQ1 to assemble with and modulate KCNQ1 currents (Schwake *et al.*, 2003).

Single channel recordings of  $I_{Ks}$  have been attempted by several labs. However, interpretation of these recordings is complicated, since the smallest patches of  $I_{Ks}$  contain at least 3-4 functioning channels. Further,  $I_{Ks}$  possesses a form of flickery gating that

allows a subconducting state, obscuring the results from these recordings. Single channel conductance for  $I_{Ks}$  is reported at 4.5, 6 and 16 pS; KCNE1 increases KCNQ1 single channel conductance four-fold or more. For both of the aforementioned reasons, this data should be considered with some skepticism (Pusch, 1998; Sesti & Goldstein, 1998; Yang & Sigworth, 1998).

$I_{Ks}$  currents are enhanced by cAMP-dependent phosphorylation by PKA at KCNQ1 S27 (Kurokawa et al., 2003). Two other putative phosphorylation sites within the C-terminal domain of KCNQ1, S468 and T470, may also be important; mutation of these residues reduces  $I_{Ks}$  sensitivity to the small molecule inhibitor quinidine (Yang et al., 2003). PKA is able to bind the channel complex through an association with the AKAPs, which occurs with a coiled-coil motif found in the C-terminus of KCNQ1. Though AKAP79 and AKAP15/18 both enhance  $I_{Ks}$  in a cAMP-dependent manner, the AKAP Yotiao has been given special attention (Figure 1-2) (Potet et al., 2001). Yotiao does not just coordinate the actions of PKA and PP1 with KCNQ1 (Marx et al., 2002; Kurokawa et al., 2004), but the PKA-dependent phosphorylation of yotiao itself at S43 is able to modulate  $I_{Ks}$  currents (Kurokawa et al., 2004; Chen et al., 2005). cAMP-dependent phosphorylation is required for  $\beta$ -adrenergic stimulation of  $I_{Ks}$ , as KCNQ1 phosphorylation is increased by overexpression of  $\beta$ 2-adrenergic receptors (Dilly et al., 2004). Tubulin may also be required for proper localization of these intracellular signaling molecules, as disruption of microtubules with colchicine reduces cAMP-dependent increases in  $I_{Ks}$  current (Nicolas et al., 2008).

$I_{Ks}$  is also down-regulated through aqueous accessory proteins and signaling cascades. Application of  $17\beta$ -estradiol is able to reduce currents, known through work on the KCNE1 homologue KCNE3 to be mediated by up-regulation in PKC phosphorylation (Moller & Netzer, 2006; O'Mahony & Harvey, 2008). KCNQ1-KCNE1 channels are inhibited by over-expression with Nedd4-2 ubiquitin ligase (also found in the heart). A consensus PxY or "PY" ubiquitin ligase binding-motif is found at the very C-terminal end of KCNQ1, however this motif is not required for Nedd4-2 association with KCNQ1-KCNE1 channel complexes (Jespersen et al., 2007).  $I_{Ks}$  is also down-regulated by association with the muscarinic receptor M1 (Selyanko et al., 2000).

Association of KCNQ1 with KCNE1 also leads to changes in pharmacology, especially with the small molecule inhibitor chromanol 293B. The  $IC_{50}$  for  $I_{Ks}$  is ten-fold lower than in the absence of KCNE1 (3  $\mu$ M versus 30  $\mu$ M). Further, chromanol 293B inhibits the slower, non-instantaneous component of  $I_{Ks}$  (Bett et al., 2006).

Though  $I_{Ks}$  is required for healthy termination of each cardiac action potential, the KCNQ1-KCNE1 complex is also required for potassium recycling into the endolymph of the inner ear (Figure 1-5). Mutations that can give rise to Long QT can also give rise to the recessive Jervell and Lange-Nielsen syndrome, which involves deaf-mutism and QT-prolongation (Jervell & Lange-Nielsen, 1957). Deafness in persons afflicted with JLNS arises from gross morphological changes in cochlear structures within the inner ear. These changes arise from deficiencies in potassium efflux from the stria vascularis into the endolymph of the stria media.

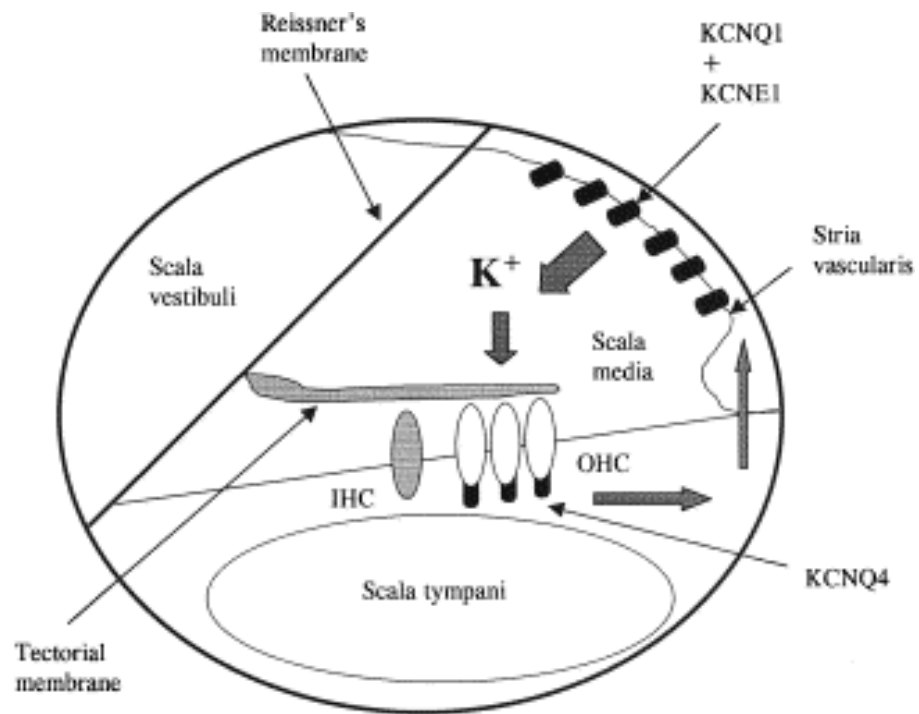


**Figure 1-5.** Cochlear Structure.  $I_{Ks}$  channels reside in the stria vascularis, located on the periphery of the scala media. The direction of the cyclic potassium current is indicated in dark arrows. The high concentration of potassium in the scala media or endolymph results in depolarized membrane potentials in the stria vascularis, allowing  $I_{Ks}$  channels to remain open and participate in potassium efflux required to maintain high endolymph potassium concentrations. Note also that KCNQ4 channels are found on the basolateral membranes of outer (and inner?) hair cells, where they are involved in establishing and adjusting membrane potential in response to auditory stimuli, resulting in potassium efflux that is dissipated through the stria vascularis.

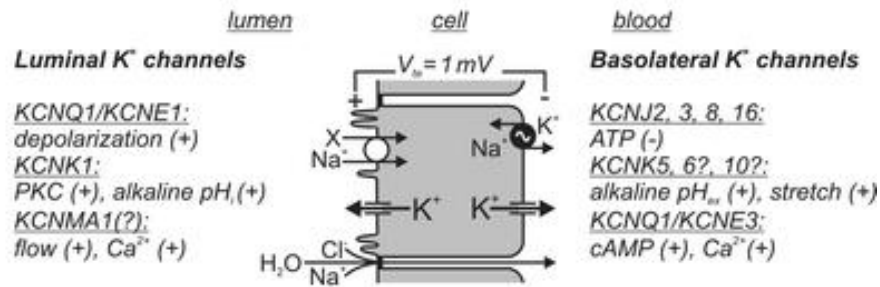
Figure taken from Robbins, J., *KCNQ potassium channels: physiology, pathophysiology, and pharmacology*. Pharmacol Ther, 2001. **90**(1): p. 1-19

Why is KCNQ1-KCNE1 complex able to perform any role in potassium recycling in a non-enervated tissue? High extracellular potassium concentrations in the endolymph result in an altered potassium gradient for cells lining the stria media. This altered electrochemical gradient shifts the Nernst-predicted reversal potential of potassium sufficiently towards positive potentials. Because resting membrane potentials within the inner ear are determined by potassium channels, and membrane potentials are sufficiently positive to allow  $I_{Ks}$  channels to activate, a portion of the  $I_{Ks}$  population remains activated ( $I_{Ks}$  can not inactivate) allowing a continual potassium efflux required to maintain a potassium-rich endolymph (Sakagami et al., 1991; Vetter et al., 1996; Lee et al., 2000; Robbins, 2001).

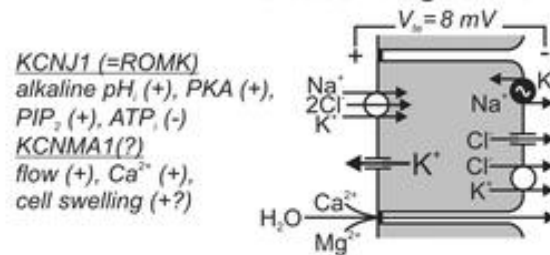
*Epithelial KCNQ1-KCNE complexes* - Potassium currents within epithelial tissues, especially those arising from KCNQ1 channel complexes (Figure 1-6), play many crucial roles in ion permeation. Because the electrochemical gradient of potassium favors efflux at physiologically relevant membrane potentials, leak channels give rise to small potassium currents which in turn establish the membrane potential and allow for a small external pool of potassium ions (Warth, 2003).

Though epithelial tissues are not enervated, those that possess electrogenic transport, for instance the proximal tubule of the kidney, may reach membrane potentials at which voltage-gated potassium channels can activate; this is due to the depolarizing effects of sodium transport into the cytoplasm. Though the identity of the KCNE peptide within KCNQ1-KCNE channel complex is controversial, it appears that luminal secretion

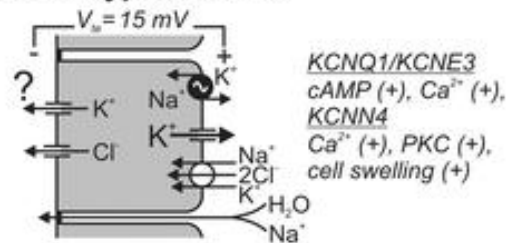
**A Renal proximal tubule / intestinal villus cell**



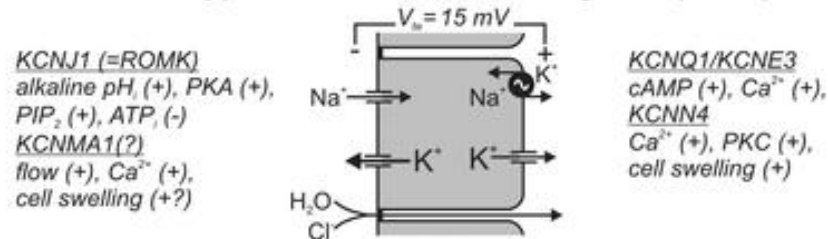
**B Thick ascending limb of Henle's loop**



**C Colon crypt base cell**



**D Colon crypt surface cell / collecting duct principle cell**



**E Gastric parietal cell**

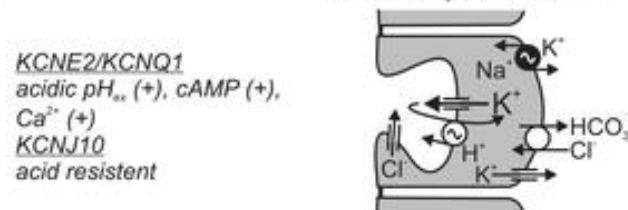


**Figure 1-6.** KCNE-modulated KCNQ1 channels play physiological roles in several types of epithelial cells. **A**,  $I_{Ks}$  is involved in luminal potassium excretion and maintenance of negative membrane potentials in response to electrogenic transport and the resulting depolarization. Further, KCNQ1 channels, modulated by KCNE3, are found on the basolateral membranes of these epithelial cells and are involved in potassium recycling required for sodium efflux into the bloodstream from the kidneys. **C and D**, Colon epithelia (and analogous tracheal epithelium) possess KCNQ1-KCNE3 on their basolateral membranes. KCNQ1-KCNE3 channels provide the potassium efflux required to fuel non-electrogenic transport of chloride into the cells, and produce the electromotive force necessary for chloride secretion from the apical membrane. **E**, Apical KCNQ1-KCNE2 channels in gastric parietal cells. KCNQ1-KCNE2 channels provide potassium efflux into the gastric lumen, where this potassium pool fuels proton efflux and provides the electromotive force required for chloride secretion.

Figure taken from Warth, R., *Potassium channels in epithelial transport*. Pflugers Arch, 2003. **446**(5): p. 505-13.



of potassium ions in the kidneys is mediated in part by  $I_{Ks}$  (Sugimoto et al., 1990; Chouabe et al., 1997; Yang et al., 1997; Schroeder et al., 2000b; Vallon et al., 2005). This luminal potassium current helps to reestablish membrane potential sufficiently close to the reversal potential of potassium and thereby provides the driving force for electrogenic transport. In addition, BK channel protein has also been detected in these cells (Warth, 2003; Levy et al., 2008). As a further level of regulation, the presence of these channels allows both concomitant changes in cell volume due to transport from the kidney lumen as well as changes in intracellular  $Ca^{2+}$  concentration to modulate potassium efflux (Warth, 2003).

Non-electrogenic transport is unable to depolarize epithelial membranes. Potassium channels that are active at hyperpolarizing potentials near the reversal potential for potassium (such as inwardly-rectifying currents, hyperpolarization activated currents or leak currents) would seem to play a more important role in epithelial tissues with non-electrogenic transport. An early example of such a potassium leak current is the basolateral potassium conductance of tracheal epithelia. Ion conductance through the basolateral and apical membranes of the epithelia were distinguishable; the conductance of the apical membrane was dominated by efflux of chloride through CFTR (Engelhardt et al., 1992; Haws et al., 1994; Wine et al., 1994), (observed by a secretagogue-induced increase in current by increasing extracellular chloride concentration). Despite the presence of the chloride conductance, the basolateral potassium conductance establishes the membrane potential. Perturbing potassium channels, either by adjusting extracellular potassium concentrations (changing the reversal potential for potassium) or by

application of  $Ba^{2+}$  externally (blocking potassium currents) led to large changes in membrane potential, resulting in changes in chloride secretion (Smith & Frizzell, 1984).

In epithelia of the gastrointestinal tract and lungs, potassium efflux is coupled to subsequent potassium influx through transporters. The pool of effluxed potassium ions helps fuel co-transport with: 1) sodium and chloride by NKCC1 in colon epithelia, or 2) proton excretion through anti-transport by  $K^+,H^+$ -adenosine triphosphase transporter in gastric parietal cells. As with electrogenic transport, potassium efflux is also responsible for maintaining low membrane potential in these cells. Though potassium efflux occurs mainly basolaterally, the effect on of this voltage shift is seen paracellularly. The establishment of such a hyperpolarized potential on the membranes of these cells leads to the strong electromotive force required for chloride secretion. In the case of colon epithelia, regulation of chloride secretion modulates osmotic balance and plays a role in water retention; in the case of secretory cells of the stomach, chloride secretion is coupled to pH reduction (Warth, 2003).

The aforementioned epithelial currents have been identified. It turns out that voltage-gated KCNQ1 channels are the pore-forming subunits giving rise to these leak currents. How can KCNQ1, an outwardly-rectifying potassium channel, have any function in cells that are not enervated and do not possess electrogenic transport? KCNQ1 is able to activate even at hyperpolarizing membrane potentials when associated with either KCNE2 or KCNE3, an association which (at least partially) removes voltage-dependence (Schroeder *et al.*, 2000b; Tinel *et al.*, 2000a; Dedek & Waldegger, 2001; Gage & Kobertz, 2004).

The interaction between KCNQ1 and KCNE2 (MiRP1) gives rise to a potassium current that shows little voltage dependence (Tinel *et al.*, 2000a; Dedek & Waldegger, 2001; Bendahhou *et al.*, 2005; Lundquist *et al.*, 2005). KCNE2 colocalizes with KCNQ1 mainly in the gastric parietal and oxyntic cells, where with Kir4.1, KCNQ1-KCNE2 provides the hyperpolarized membrane potentials and the potassium efflux required for proton secretion and the driving force for chloride secretion (Dedek & Waldegger, 2001; Heitzmann *et al.*, 2004; Kaufhold *et al.*, 2008). The importance of both KCNE2 and KCNQ1 is underscored by the fact that disruption of either gene in mice leads to abnormal gastric morphology combined with reduced response to histamine stimulation, and an increase in gastric pH. The effects on pH were also observed with chromanol 293B inhibition (Lee *et al.*, 2000; Grahammer *et al.*, 2001a; Lambrecht *et al.*, 2005; Vallon *et al.*, 2005; Roepke *et al.*, 2006). Current arising from KCNQ1-KCNE2 channels is pH sensitive and participates in a positive feedback loop; potassium efflux allows for a decrease in pH, which in turn increases potassium efflux. The feedback loop breaks down when external pH decreases past pH 4.5, as further decreases in pH begin to inhibit KCNQ1-KCNE2 currents. KCNE2/KCNE3 chimeras demonstrate that the extracellular N-terminal segment of KCNE2 provides the pH sensor (Grahammer *et al.*, 2001a; Heitzmann *et al.*, 2007), while the transmembrane domain of KCNE2 is believed to be alpha-helical like that of KCNE1 (Liu *et al.*, 2007).

Co-expression of KCNQ1 with KCNE3 (MiRP2) gives rise to an instantaneous current that is at least partially active at even very hyperpolarized membrane potentials and greater in current density as compared with KCNQ1-KCNE2 complexes (Schroeder

et al., 2000b; Bendahhou et al., 2005; Lundquist et al., 2005). The channel complex is cAMP-sensitive and is localized to the basolateral membranes of various epithelial cells, including the entire gastrointestinal tract, where it provides potassium efflux (Smith & Frizzell, 1984; Lohrmann *et al.*, 1995; Schroeder *et al.*, 2000b; Dedek & Waldegger, 2001; Grahammer *et al.*, 2001a). Just like  $I_{Ks}$ , KCNQ1-KCNE3 currents display heightened sensitivity to chromanol 293B inhibition as compared with those arising from homotetrameric KCNQ1 (with an  $IC_{50}$  reported as low as 1  $\mu$ M (Schroeder *et al.*, 2000b; Gage & Kobertz, 2004; Bett *et al.*, 2006)), and are suppressed by 17 $\beta$ -estradiol (an effect mediated by PKC $\delta$  in a gender-specific manner (O'Mahony et al., 2007)). Unlike  $I_{Ks}$  and KCNQ1-KCNE2 currents, KCNE3 modulated KCNQ1 currents are not sensitive to pH (Grahammer et al., 2001a; Heitzmann et al., 2007).

KCNE3 is able to modulate KCNQ1 channels through the transmembrane modulatory triplet identified by Melman and colleagues discussed above (Melman et al., 2001; Melman et al., 2002a). Transmembrane modulation explains why the C-terminus of KCNE3, which bears great similarity and identity to that of KCNE1, does not lead to KCNE1-like kinetics. The transmembrane domain of KCNE3 may interact directly with the KCNQ1 voltage sensing domain, resulting in increased accessibility to chemical modification (Nakajo & Kubo, 2007; Rocheleau & Kobertz, 2008). However, there is still a paradox regarding KCNE modulation of KCNE1. In order to resolve this controversy, partial truncations of KCNE3 will be examined in Chapter II.

*Other KCNQ1-KCNE complexes* - The remaining two members of the KCNE family are not as well studied nor understood. Depending upon the study, KCNQ1-KCNE4 (MiRP3) channel complexes in over-expression systems are either present on the plasma membrane and do not give rise to a potassium current (Grunnet et al., 2002; Grunnet et al., 2005; Lundquist et al., 2005) or activate at highly positive potentials that are physiologically unreasonable (Teng et al., 2003; Bendahhou et al., 2005). Given that voltage clamp experiments measures conductance as a function of time and voltage, the complete lack of any conductance arising from KCNQ1-KCNE4 channel complexes makes it extremely difficult to ascertain function or electrophysiologically demonstrate any physiologically relevant role.

KCNQ1-KCNE5 (KCNE1-like or Kcne1-l) channels are similarly difficult to study. KCNE5 was first identified as one of several genes disrupted in Alport Syndrome, mental retardation, midface hypoplasia, and elliptocytosis, or AMME; however, loss of KCNE5 does not appear cause this syndrome (Piccini et al., 1999). Although KCNQ1-KCNE5 channels do give rise to delayed outwardly-rectifying currents, the voltage sensitivity has been shifted such that the channel activates only upon reaching very positive membrane potentials. Upon activation the channel expresses currents that are kinetically reminiscent of  $I_{Ks}$ . These two factors make KCNQ1-KCNE5 difficult to identify in any physiological context that includes  $I_{Ks}$ . Since  $I_{Ks}$  activates at far less positive potentials, the small current levels arising from KCNQ1-KCNE5 at a particular membrane potential may indeed be present but overlooked in the presence of  $I_{Ks}$  (Angelo et al., 2002; Bendahhou et al., 2005; Lundquist et al., 2005).

Yet these two channel complexes may play physiologically important roles. Viewed as negative regulators of KCNQ1 channel activity, it is possible that physiologically important currents such as  $I_{Ks}$  are “fine tuned” by KCNE4 and KCNE5. If this is indeed the case, then KCNE4 may act as a negative regulator, reducing current levels, while KCNE5 may shift the collective voltage sensitivity of  $I_{Ks}$ . Given 1) transcripts for every KCNE peptide are present in the heart with KCNQ1, and 2) these expression levels for these transcripts vary spatially and in the context of health within the heart (Bendahhou et al., 2005; Lundquist et al., 2005), it is not unreasonable that there may be multiple populations of KCNQ1-KCNE<sub>x</sub> channel complexes within the same tissue. The role of KCNE4 and KCNE5 could therefore be viewed in much the same way as the role of KCNQ2-5 in generating diversity among M-currents (*vide infra*).

Perhaps even more compelling is the possibility that KCNE4 and KCNE5 may assemble with a KCNQ1 and another KCNE within the same channel complex, a hint of which can be seen with KCNQ1-KCNE1-KCNE2 co-expression (Bendahhou *et al.*, 2005; Lundquist *et al.*, 2005; Toyoda *et al.*, 2006; Morin & Kobertz, 2007; Manderfield & George, 2008). A very powerful technique has just been developed in which only channels expressing a marked subunit can be selectively and conditionally blocked. This technique has demonstrated that complexes including KCNQ1, KCNE1 and KCNE4 can give rise to a current similar to  $I_{Ks}$ . This techniques has also demonstrated that hybrid potassium currents do arise from both KCNQ1-KCNE1-KCNE3 and KCNQ1-KCNE3-KCNE4 potassium conducting complexes in *Xenopus* oocytes (Morin & Kobertz, 2007).

**Promiscuity** - Complicating the story of KCNE peptides even further, most KCNE subunits have been demonstrated to modify the properties of at least one channel in addition to KCNQ1 in over-expression systems. Though there was a great rush to publish any sort of association with a KCNE subunit, there are ultimately two questions that should be asked:

*How is the potassium current being modified?*

Remember our modification of Ohm's Law in an electrochemical gradient,

$$(4) (N_{ion}P_o\gamma_{ion})(V_m - E_{ion}) = I_{ion} ,$$

where  $N$ , number of functioning channels on the cell surface;  $P_o$ , open probability;  $\gamma$ , single-channel conductance; changes in any of these factors can lead to "current modification", an issue which is not unprecedented. For example, artifacts of endogenous gene expression (Jiang et al., 2002a; Anantharam et al., 2003) in over-expression systems have been shown to lead to aberrant changes in the biosynthetic (Krumerman et al., 2004; Chandrasekhar et al., 2006) and biophysical properties (Takumi et al., 1988; Anantharam et al., 2003) of a channel or channel subunits, thus altering their apparent function and identity. Keeping this caveat in mind, one would expect changes in channel function that are either: 1) biophysical in nature (for instance changes in single-cell conductance, voltage sensitivity, and kinetics among others), or 2) not dependent upon expression system, should indicate true  $\beta$ -subunit modulation.

*Is the pairing of channel subunits physiologically relevant?*

The presence of protein or mRNA can be directly assessed in native tissues; however, this does not conclusively demonstrate the presence of a native ionic current. Demonstration that the current arising from a particular channel complex is biophysically reminiscent or identical to a physiologically observed current is more convincing; identification is complicated by the fact that native ionic currents are frequently accompanied by other ionic currents, and may be fine tuned by co-expression with further accessory subunits or by the presence of biophysically heterogeneous populations of ion conducting complexes. Ultimately pharmacological and biophysical tricks are required for isolation and identification of these native currents.

An exhaustive list of channel complexes modified by KCNE association can be found in McCrossan and Abbott (McCrossan & Abbott, 2004). These associations are evidenced by slight changes in voltage sensitivity or kinetics and include evidence of direct KCNE interactions, but otherwise will not be elaborated further (Schroeder et al., 2000a; Tinel et al., 2000b; McCrossan et al., 2003; Lewis et al., 2004). Channel complexes that are particularly noteworthy and require inspection are discussed here.

KCNE1 coexpression with hERG led to an increase in current density and a slight change in voltage sensitivity. This was accompanied by changes in hERG currents in response to Long QT mutations in KCNE1. Though hERG was able to co-immunoprecipitate KCNE1, evidence regarding subcellular localization and any conclusions derived from this evidence were inconclusive. Therefore, it is unclear if



KCNE1 modulates hERG currents in a biophysical or biosynthetic manner (McDonald et al., 1997; Bianchi et al., 1999).

Co-expression of KCNE2 appears to play important roles in three different heart currents, where overexpression cannot recapitulate all of the biophysical properties of the native heart currents.  $I_{Kr}$ , the rapid potassium current in part responsible for terminating each action potential, arises from hERG channels in the heart. KCNE2 alters macroscopic  $I_{Kr}$  by modifying the single channel conductance as well as the voltage sensitivity, pharmacology, kinetics and inactivation of hERG channels. hERG and KCNE2 are also able to co-immunoprecipitate (Abbott et al., 1999). Still, there is some controversy as to whether this interaction is real. Perhaps both camps are correct – KCNE2 transcript levels in the heart have been found to vary spatially and in response to stress induced by heart failure (Yu et al., 2001; Lundquist et al., 2005). Alternatively, KCNE2 may be able to assemble with hERG preferentially in over-expression systems, protecting hERG from down regulation by endogenous KCNE or other accessory subunits (Anantharam et al., 2003).

The second of these three native currents is  $I_f$ , the “funny” pacemaker current that activates in response to increasingly negative membrane potentials. This current prevents the myocardium from becoming too refractory to stimulation. HCN channels, which are weakly potassium-selective but still conduct sodium (Santoro et al., 1998; Ludwig et al., 1999; Snyders, 1999), underlie this current. Co-expression of HCN channels with KCNE2 1) allows  $I_f$  to remain open at higher membrane potentials, 2) increases whole-

cell conductance, and 3) alters  $I_f$  kinetics, speeding gating for HCN1-2 and slowing gating for HCN4 (Yu et al., 2001; Decher et al., 2003).

$I_{to}$ , the transient outward potassium current at the beginning of each action potential, arises mainly from Kv4.3-KChIP2, with some contribution from Kv4.2 channels. While Kv4.2 and Kv4.3 have activation and inactivation delayed by KCNE2 co-expression, Kv4.3-KChIP2 activation kinetics were increased by KCNE2. KCNE2 is also solely responsible for producing “overshoot,” a transient increase in current observed in  $I_{to}$  when action potentials occur in quick succession (Zhang *et al.*, 2001; Deschenes & Tomaselli, 2002; Radicke *et al.*, 2006).

The Kv3.4-KCNE3 channel complex appears to be of great physiological relevance. Mutation of R83H in KCNE3 disrupts a putative PKC phosphorylation site and has been linked to periodic paralysis and hypokalemia in a manner apparently related to blood pH. Mutation S82A, the putative PKC phosphorylation site of KCNE3 in Kv3.4-KCNE3 channel complexes, prevents phosphorylation of KCNE3, though it is unclear if the kinase substrate is removed or if this mutation is allosteric. The observations that pH is also a factor and that protonated R83H inhibits KCNE3 modulation, give credence to the identity of this channel complex. Wild type KCNE3 alters single channel conductance and allows Kv3.4 channels to activate in response to lower membrane potentials (Abbott et al., 2001; Abbott et al., 2006). Transcript and protein levels for both KCNE3 and Kv3.4 are not only present in skeletal muscle but also in hippocampal neurons and PC12 cells, and increase in response to  $A\beta_{1-42}$ , a peptide implicated in Alzheimers disease. Increases observed in protein and transcript levels

mirror increased  $I_A$  potassium current in these tissues. This correlation provides strong evidence that this current arises from the Kv3.4-KCNE3 complex, and implicates increased neuronal potassium efflux in the onset of Alzheimers. It appears that Kv3.4-KCNE3 plays crucial roles in multiple diseases (Pannaccione et al., 2007).

hERG is not only enhanced by KCNE co-expression, but it can be repressed. The association of KCNE3 with hERG, or the closely related *Xenopus laevis* MiRP2, is able to suppress hERG currents, but it is unknown if this association is of any physiological relevance. Transcripts for both hERG and KCNE3 are present in the heart (Schroeder et al., 2000b; Anantharam et al., 2003; Bendahhou et al., 2005; Lundquist et al., 2005).

Recently, KCNE4 and BK were shown to interact in kidney epithelia. Colocalization by immunofluorescence indicates that these channel subunits were localized to the same membranes, and KCNE4 did co-immunoprecipitate with BK, showing a more direct interaction. Co-expression of KCNE4 with BK reduced dwell time at the plasma membrane and protein stability. There was also a shift in BK voltage sensitivity towards more positive membrane potentials with internal  $Ca^{2+}$  concentrations  $\geq 0.1 \mu M$ . The change in BK voltage sensitivity may result from altered  $Ca^{2+}$  sensitivity of the BK-KCNE4 channel complex, modulation which is reminiscent of that seen with KCNMB1 and KCNMB4 subunits (Levy et al., 2008). A similar role had already been described for KCNE4 modulation of Kv1.1 and Kv1.3. Currents arising from homotetramers and heterotetramers of both pore-forming subunits were suppressed by co-expression of KCNE4 (Grunnet et al., 2003). Only one report has surfaced in which KCNE4 has not played an inhibitory role in channel function (*vide infra*) (Strutz-

Seeböhm et al., 2006). Whether or not these KCNE4 interactions actually play physiologically important roles requires further investigation.

KCNE1-4 peptides have also been reported to alter currents arising from KCNQ4 homotetramers, though the nature of this modulation, at least for KCNE1, is biosynthetic (Schroeder et al., 2000b; Chandrasekhar et al., 2006; Strutz-Seeböhm et al., 2006). These interactions will be addressed (*vide infra*).

## **M-CURRENTS**

In 1980, Brown and Adams discovered a potassium current in bullfrog sympathetic neurons that began activating subthreshold and did not inactivate. This current could be studied using a protocol that held membranes at relatively high membrane potentials, followed by stepping to command voltages and measuring tail currents. Currents arising from this channel were relatively slow compared with  $I_A$  currents, and were suppressed by exposure to muscarine. Because of this muscarinic suppression, they named this current  $I_M$  (Brown & Adams, 1980).

In a parallel line of work, homologues of KCNQ1, KCNQ2 and KCNQ3, were identified as localizing to gene loci involved in a benign form of epilepsy, benign familial neonatal convulsion (BFNC), occurring within the first months or year of a child's life, rarely continuing into adulthood (Biervert et al., 1998; Charlier et al., 1998; Singh et al., 1998). Mutations in KCNQ2 have also been identified in myokymia (Dedek et al., 2001). Gene mapping also identified another KCNQ1 homologue, KCNQ4, which mapped to a gene locus involved in autosomal dominant deafness (DFNA2) (Kubisch et al., 1999). A

fifth member of the KCNQ family, KCNQ5, was subsequently identified (Lerche et al., 2000; Schroeder et al., 2000a). KCNQ2-5 all gave rise to potassium selective currents with kinetics slower than those observed for  $I_A$ , and possessing pharmacology reminiscent of  $I_M$ . However, slight biophysical and pharmacological differences still existed. These differences were settled when co-expression of KCNQ2 and KCNQ3 revealed that  $I_M$  arises mainly from homotetrameric KCNQ2/3 channel complexes (Wang et al., 1998) (though there was heated debate whether hERG channels may further diversify M-currents (Marrion, 1997; Stansfeld et al., 1997; Noda et al., 1998; Meves et al., 1999; Selyanko et al., 1999; Selyanko et al., 2002)). KCNQ3 is able to form heterotetramers with KCNQ2, KCNQ4 and KCNQ5 (Schroeder et al., 1998; Wang et al., 1998; Kubisch et al., 1999; Lerche et al., 2000; Schroeder et al., 2000a).

$I_M$  is present throughout much of the nervous system where active  $I_M$  makes neurons more refractory to action potentials, thus decreasing the likelihood of subsequent action potentials (Figure 1-7). Though M-currents are not present in the same tissues as  $I_{Ks}$ ,  $I_M$  like  $I_{Ks}$  plays a crucial role in adjusting membrane potential and preventing tonic firing in excitable cells (Cooper & Jan, 2003).

M-currents and  $I_{Ks}$  do have several analogous properties. Sections of the large, C-terminal domain of KCNQ pore-forming subunits have been crystallized, and structures obtained from these crystals are highly homologous (Figure 1-2) (Howard et al., 2007; Wiener et al., 2008). M-currents and  $I_{Ks}$  are also modulated by the same intracellular and extracellular signals.  $\beta$ -adrenergic stimulation enhances both M-currents and  $I_{Ks}$  (Sims et al., 1988; Dilly et al., 2004), while muscarinic receptors suppresses currents arising from

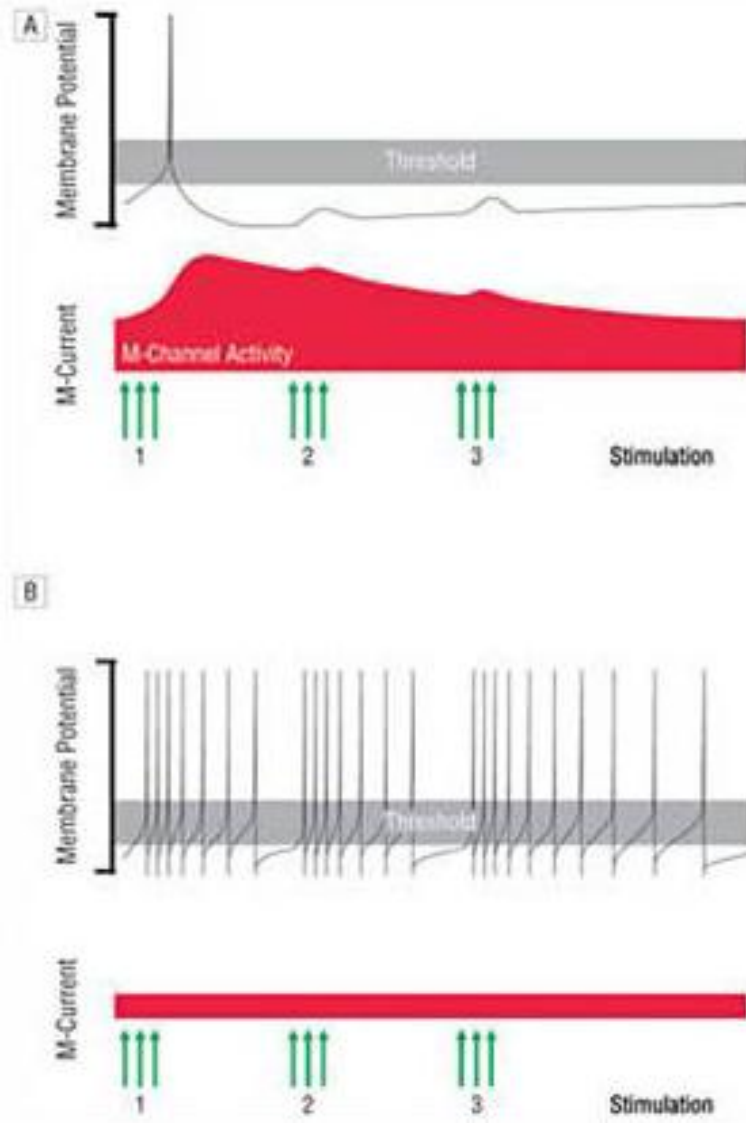


**Figure 1-7.** Related KCNQ channel complexes give rise to M-currents, responsible for regulating neuronal excitability. **A**, neuron in which M-channel function is unperturbed. **B**, neuron in which M-channel function has been lost. *Above*, cartoons depicting membrane potential as a function of time. The top of the shaded range denotes the potential at which voltage-gated sodium channels will activate. If membrane potential reaches threshold, an action potential will result and self-propagate down the length of the neuron. The height of the gray region is the difference in average membrane potential and the threshold for sodium channel activation. This difference in membrane potential and threshold prevents stray neurotransmitters and weak synaptic stimulation from resulting in an action potential. *Below*, M-channel efflux (denoted in solid, vertical height) as a function of time. M-current is slowly activating and deactivating, resulting in an increase in resting potassium conductance and an increase in refractory behavior in these neurons. Green arrows depict excitatory signals stimulating the neuron. If M-currents are absent from the neuron, excitatory signals can result in tonic stimulation.

Figure adapted from Cooper, E.C. and L.Y. Jan, *M-channels: neurological diseases, neuromodulation, and drug development*. Arch Neurol, 2003. **60**(4): p. 496-500.

both (Brown & Adams, 1980; Schroeder *et al.*, 2000a; Selyanko *et al.*, 2000). Down-regulation of M-current is mediated by phosphorylation by PKC. PKC associates with M-channel complexes through AKAPs, again analogous to  $I_{Ks}$  (except that this association can be disrupted by  $Ca^{2+}$  binding to calmodulin) (Hoshi *et al.*, 2003; Higashida *et al.*, 2005). M-currents and  $I_{Ks}$  are also down-regulated by over-expression with ubiquitin transferase enzymes like Nedd4-2 (Ekberg *et al.*, 2007; Jespersen *et al.*, 2007). Both  $I_{Ks}$  and M-currents are also sensitive to intracellular  $Ca^{2+}$  concentrations. For  $I_{Ks}$ , increases in intracellular  $Ca^{2+}$  lead to an increase in current density, decreases in homomeric KCNQ1 inactivation and increased activation at lower membrane potentials through its C-terminal interaction with calmodulin (Ghosh *et al.*, 2006; Shamgar *et al.*, 2006). M-channels also sense intracellular  $Ca^{2+}$  levels through a homologous C-terminal interaction with calmodulin. However, increasing intracellular calcium causes calmodulin to dissociate from KCNQ2, thereby reducing M-current density. The interaction between calmodulin and KCNQ3 or KCNQ4 shows less dependence upon intracellular calcium concentrations, with the strongest association between KCNQ4 and calmodulin (Yus-Najera *et al.*, 2002; Bal *et al.*, 2008).

M-currents and KCNQ1 differ in several ways, though these differences have become less clear as new evidence comes to light. All KCNQ channels possess large intracellular C-termini which are involved in accessory subunit interactions as well as specificity during assembly (Haitin & Attali, 2008). KCNQ1 pore-forming subunits cannot co-assemble with KCNQ2-5, whereas the C-terminus of KCNQ3 is able to mediate heterotetrameric assemblies with KCNQ2, KCNQ4 and KCNQ5. Possession of



a KCNQ1 C-terminal domain is also required for KCNE1 modulation of currents (Maljevic et al., 2003; Schwake et al., 2003).

KCNQ subunits are also found in different tissues. KCNQ1 is found in cardiac and epithelial tissues and in the cochlea but not in the nervous system, adjusting to the tissue-specific potassium conductance requirements by co-assembly with KCNE peptides (Robbins, 2001). KCNQ2-5 subunits are found primarily in the nervous system and auditory pathways (Biervert *et al.*, 1998; Wang *et al.*, 1998; Kubisch *et al.*, 1999; Marcotti & Kros, 1999; Lerche *et al.*, 2000; Schroeder *et al.*, 2000a; Cooper *et al.*, 2001; Devaux *et al.*, 2004; Schwarz *et al.*, 2006), but growing evidence has demonstrated the distinction of tissue specificity is not quite so clear. KCNQ3 and KCNQ5 proteins have been detected in tracheal epithelia (Moser et al., 2008), and KCNQ5 transcripts have been found in skeletal muscle where there is a current that recapitulates some of  $I_M$  pharmacology (Lerche et al., 2000; Schroeder et al., 2000a).  $I_M$  currents have also been observed in bullfrog smooth muscle (Sims et al., 1988).

Much like KCNQ1, M-current subunits form heteromeric potassium conducting complexes, adding to the physiological diversity of potassium conductance. However, KCNQ2-5 achieve this diversity through formation of heterotetrameric channel complexes composed of different pore-forming subunits and not with modulation by KCNE peptides (Schroeder et al., 1998; Wang et al., 1998; Kubisch et al., 1999; Lerche et al., 2000; Schroeder et al., 2000a).

M-channels can also be physiologically expressed as homotetramers, another distinction between KCNQ1 and M-channels. KCNQ4, which gives rise to  $I_{K,n}$ , a

current involved in endolymph potassium recycling, is well established as mediating potassium efflux in outer hair cells (and possibly inner hair cells (Oliver et al., 2003)) of the cochlea (Figure 1-5). Like  $I_{Ks}$ ,  $I_{Kn}$  is required for potassium recycling and normal cochlear physiology (Kubisch *et al.*, 1999; Marcotti & Kros, 1999; Kharkovets *et al.*, 2000; Kharkovets *et al.*, 2006). Homotetrameric M-channels are also found in myelinated peripheral neurons. The slow activating and deactivating potassium current at Nodes of Ranvier,  $K_s$  or  $I_{Ks}$  (this is confusing, but this current is distinct from cardiac  $I_{Ks}$ ), has been demonstrated by immunofluorescence to arise from KCNQ2 homotetramers but can also arise from KCNQ3/2 heterotetramers. It appears the cross-sectional diameter of Nodes of Ranvier correlate with the presence of KCNQ3 – the smaller the diameter, the more likely M-channels will contain KCNQ3 (Devaux et al., 2004; Schwarz et al., 2006), indicative of current diversity arising from gene expression.

Also in contrast to KCNQ1, M-channels are generally not considered to be modulated by association with KCNE peptides. Currents arising from very few KCNQ2-5 or KCNQ3/2,4-5 heteromeric channel complexes have been modified by association with KCNE peptides, but this modification appears to be due to changes in the biosynthetic pathways of the studied over-expression system (Schroeder et al., 2000a; Tinel et al., 2000b; Chandrasekhar et al., 2006; Strutz-Seebohm et al., 2006). The one exception to this rule may be KCNQ4 homotetramers. Co-expression of KCNE3 and KCNE4 with KCNQ4 homotetramers either suppresses or enhances current, respectively, in *Xenopus laevis* oocytes. KCNQ4-KCNE4 is less cation-selective than KCNQ4; this association gives rise to currents that are instantaneous and active at all measured

membrane potentials, with very little observable activation and deactivation kinetics. As there is no data regarding the presence KCNQ4-KCNE3 channel subunits on the plasma membrane, current suppression may result from lack of channel proteins on the cell surface, either through sequestration of channel subunits or through increased internalization. Changes in KCNQ4 due to KCNE4 may also result from perturbation of the biosynthetic pathway; KCNQ4-KCNE4 complexes may be aberrant complexes that would not normally reach the plasma membrane (Schroeder et al., 2000b; Strutz-Seebohm et al., 2006).

Examination of inactivation in KCNQ channels is complicated. While KCNQ1 clearly possesses inactivation, M-currents were identified originally because they lacked any inactivation (Brown & Adams, 1980; Robbins, 2001). Although lack of M-current inactivation would seem to be a fundamental difference, this conclusion is premature. Homotetrameric KCNQ1 currents have not been physiologically observed; co-expression of KCNQ1 with KCNE1 appears to remove all inactivation (or alter the kinetics of inactivation, making them impossible to observe during deactivation), thus one could question whether inactivation of KCNQ1 really plays any physiological role (Pusch et al., 1998). Further, KCNQ4 and KCNQ5 appear to possess inactivation. Homotetramers of KCNQ4 and KCNQ5, as well as KCNQ4 heterotetramers (KCNQ5 was not examined), all possess an inactivation that is dependent upon the depolarizing membrane potential, just like the inactivation observed in KCNQ1 (Pusch et al., 1998; Jensen et al., 2007). Therefore, the ability to possess inactivation may be yet another mechanism for KCNQ subunits to diversity  $I_M$ .

**CHAPTER II**

**KCNE3 TRUNCATION MUTANTS REVEAL A BIPARTITE MODULATION OF  
KCNQ1 K<sup>+</sup> CHANNELS**

**ABSTRACT**

The five KCNE genes encode a family of type I transmembrane peptides that assemble with KCNQ1 and other voltage-gated K<sup>+</sup> channels resulting in potassium conducting complexes with varied channel-gating properties. It has been recently proposed that a triplet of amino acids within the transmembrane domain of KCNE1 and KCNE3 confers modulation specificity to the peptide since swapping of these three residues essentially converts the recipient KCNE into the donor (Melman, Y.F., Domenech, A., de la Luna, S., and T.V. McDonald. 2001 *J. Biol. Chem.* 276: 6439-6444.). However, these results are in stark contrast with earlier KCNE1 deletion studies, which demonstrated that a C-terminal region — highly conserved between KCNE1 and KCNE3 — was responsible for KCNE1 modulation of KCNQ1 (Tapper, A.R., and A.L. George. 2000 *J. Gen. Physiol.* 116: 379-389.). To ascertain whether KCNE3 peptides behave similarly to KCNE1, we examined a panel of N- and C-terminal KCNE3 truncation mutants to directly determine the regions required for assembly with and modulation of KCNQ1 channels. Truncations lacking the majority of their N-terminus, C-terminus, or mutants harboring both truncations gave rise to KCNQ1 channel complexes with basal activation — a hallmark of KCNE3

modulation. These results demonstrate that the KCNE3 transmembrane domain is sufficient for assembly with and modulation of KCNQ1 channels and suggests a bipartite model for KCNQ1 modulation by KCNE1 and KCNE3 subunits. In this model, the KCNE3 transmembrane domain is active in modulation and overrides the C-terminus' contribution, whereas the KCNE1 transmembrane domain is passive and reveals C-terminal modulation of KCNQ1 channels. We furthermore test the validity of this model by utilizing the active KCNE3 transmembrane domain to functionally rescue a non-conducting, yet assembly and trafficking competent long QT mutation located in the conserved C-terminal region of KCNE1.

## **INTRODUCTION**

The KCNE type I transmembrane peptides (~ 125 residues) are a family of tissue specific  $\beta$ -subunits that associate with and fine-tune the electrical properties of several voltage-gated  $K^+$  channels (Abbott et al., 1999; Abbott et al., 2001; Yu et al., 2001; Zhang et al., 2001; Grunnet et al., 2003; McCrossan et al., 2003; Lewis et al., 2004). In expression systems, KCNQ1 (Q1)  $K^+$  channels have affinity for all five KCNE peptides forming  $K^+$  conducting complexes with different voltage-activation, gating kinetics, unitary conductance and pharmacology (Barhanin *et al.*, 1996; Sanguinetti *et al.*, 1996; Sesti & Goldstein, 1998; Schroeder *et al.*, 2000b; Tinel *et al.*, 2000a; Angelo *et al.*, 2002; Grunnet *et al.*, 2002). Of these complexes, the physiological roles of the Q1-KCNE1 (E1) and Q1-KCNE3 (E3) complexes have been well-established. In the heart, Q1-E1 complexes constitute the slowly activating and deactivating cardiac  $I_{Ks}$  current (Barhanin

et al., 1996; Sanguinetti et al., 1996). Mutations in either Q1 or E1 that disrupt channel function and prolong the cardiac action potential have been implicated in several inherited forms of long-QT syndrome (Splawski et al., 2000). Q1-E3 complexes have been detected in the basolateral membranes of several epithelial tissues where these apparently constitutively open channels are critical for cyclic AMP-stimulated chloride secretion in colon and lung (Schroeder et al., 2000b; Grahammer et al., 2001b). Given their connectivity to chloride secretion, Q1-E3 complexes may be potential targets for cystic fibrosis therapies (Cowley & Linsdell, 2002; Cuthbert & MacVinish, 2003).

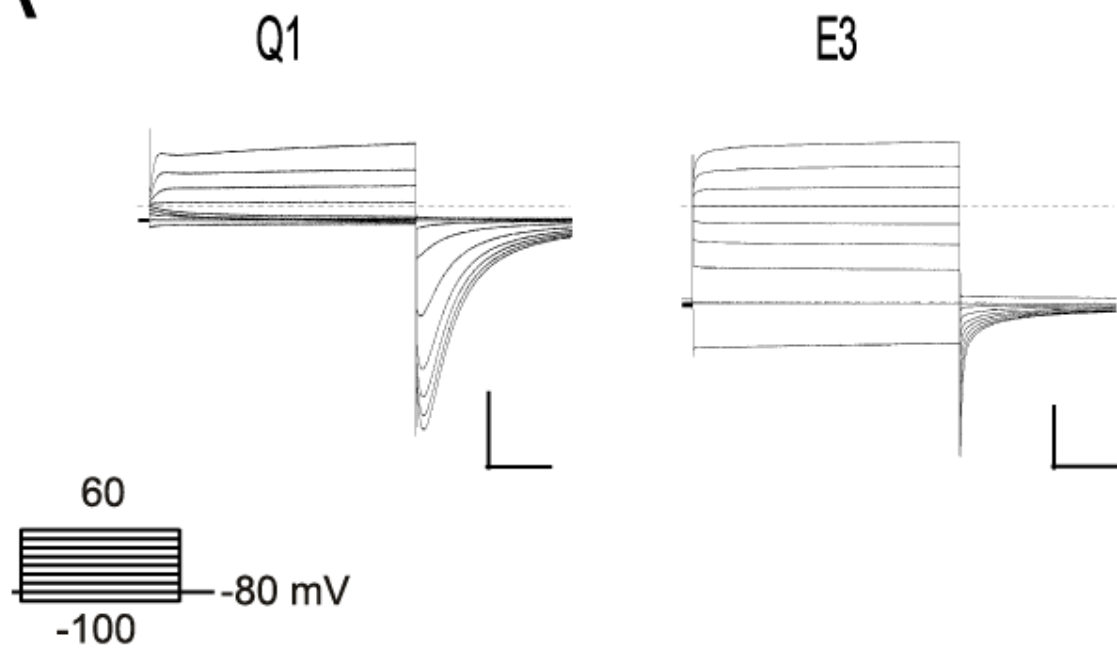
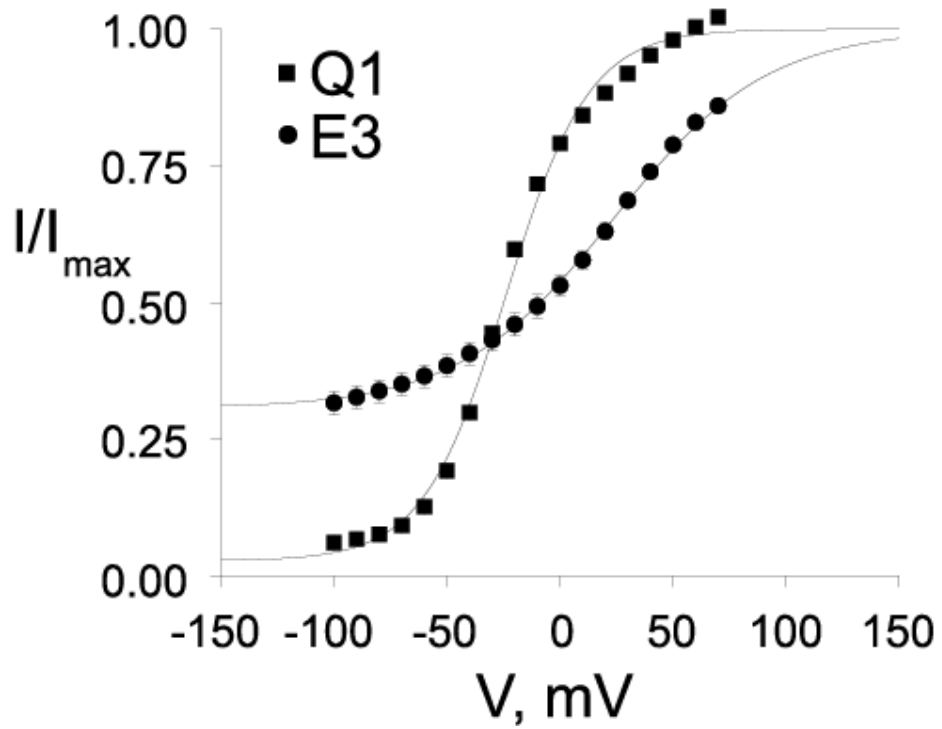
Numerous studies have examined the molecular interactions between E1 and Q1. Two independent cysteine mutagenesis studies have demonstrated that the E1 peptides are intimate with the ion conducting pore unit, yet these studies disagree on the peptides' exact location (Wang *et al.*, 1996; Tai & Goldstein, 1998; Tapper & George, 2001). Deletion studies of E1 have shown that the transmembrane segment is sufficient for assembly with Q1, whereas a C-terminal region of ~ 25 amino acids proximal to the cytoplasmic membrane is necessary for Q1 modulation (Takumi *et al.*, 1991; Tapper & George, 2000). These results are in sync with the long-QT mutations found in E1 that reside within this same region (Splawski et al., 1997; Bianchi et al., 1999). However, recent studies with KCNE1/3 chimeras suggest that a triplet of amino acids within the transmembrane segment of either KCNE is sufficient for modulation of Q1 and it was proposed that the C-terminus – which is so well-conserved between E1 and E3 – is merely required for proper anchoring or positioning of the transmembrane domain (Melman et al., 2001). In a subsequent report, this modulation specificity was further

rendered down to a single amino acid within the triplet: T58/V72 in E1/E3 (Melman et al., 2002a). To date, however, the interaction between E3 and Q1 has not been directly examined.

We sought to determine the regions of E3 responsible for assembly with and modulation of Q1 channels by constructing a panel of E3 truncation mutants and co-expressing them with Q1 channels. We find a double truncation mutant composed essentially of the E3 transmembrane domain assembles with Q1 channels producing  $K^+$  channel complexes that are open at hyperpolarizing potentials. This mutant directly demonstrates that the E3 transmembrane domain is sufficient for assembly with Q1; by analogy we predict this will be the case for all KCNE peptides. These results suggest a bipartite model for modulation of Q1 channels by E3 and E1 where the transmembrane domain is either active in modulation (E3) and masks the contribution of the C-terminus, or is passive (E1) and reveals C-terminal modulation of Q1. We further corroborate the bipartite model by utilizing an “active” E3 transmembrane domain to override a non-functional long QT mutation located in the C-terminus of E1.

## **RESULTS**

Expression of homomeric Q1 channels (Fig. 2-1A, left) gives rise to outwardly rectifying  $K^+$  currents that undergo inactivation, which can be readily detected upon repolarization as a hook in the tail currents since the rate of recovery from inactivation is faster than deactivation (Pusch et al., 1998). In contrast, co-expression of Q1 with E3 produces a  $K^+$  conducting complex that displays no inactivation and has large standing

**A****B**



**Figure 2-1.** KCNQ1/KCNE3 channels have a large standing current at negative membrane potentials. **A**, Two-electrode voltage clamp recordings from *Xenopus* oocytes injected with Q1 (left) or Q1/E3 (right). Traces were recorded in KD98 with a 13 s interpulse interval. Dashed line indicates zero current. **Inset**, “Activation Curve Protocol” of 2 s depolarizations used to elicit currents shown. **B**, Voltage-activation curves from Q1 and Q1/E3 channels. Tail currents were measured 3 ms after repolarization, fit to a Boltzmann, and the data normalized such that the upper asymptote was equal to 1. Squares, Q1; Circles, Q1/E3. Data was averaged from 6 oocytes each  $\pm$  S.E.M. Scale bars represent 1  $\mu$ A and 0.5 s.

currents at hyperpolarizing potentials (Fig. 2-1A, right). The standing currents are caused by the large basal activation of the complex, which is compared to homomeric Q1 channels using the voltage-activation relationship in Fig 2-1B. Using this comparative analysis, the basal activation of the Q1-E3 complex is ~ 30% whereas Q1 channels are relatively closed (3%). To directly determine the regions of E3 required for assembly with and modulation of Q1 channels, we constructed a panel of E3 truncation mutants (Fig. 2-2), co-expressed them with Q1 channels in *Xenopus* oocytes and analyzed them using two-electrode voltage clamp (TEVC).

We first examined whether removal of the N-terminus altered E3's ability to assemble with and modulate Q1 channels. A series of overlapping N-terminal partial truncation mutants were constructed such that every N-terminal amino acid, except for the first 4 residues, was absent in at least one construct. All N-terminal mutants shown in Fig 2-3A rapidly activate and deactivate, lack inactivation, and have large standing currents at negative potentials in response to families of command voltages.

Glycosylation of E3 appears to be required for complex assembly and/or function since severe N-terminal mutants that removed every putative N-linked glycosylation site did not express current when co-injected with Q1 (data not shown). Like WT E3, expression of N-terminal truncation mutants alone did not yield any appreciable current over uninjected controls (data not shown). In fact, all E3 mutants studied did not afford currents above background when injected without Q1 RNA. Functional Q1-E3 N-terminal truncation complexes were compared using voltage activation curves (Fig. 2-3B). This comparison is valid provided that the conducting complexes can be nearly

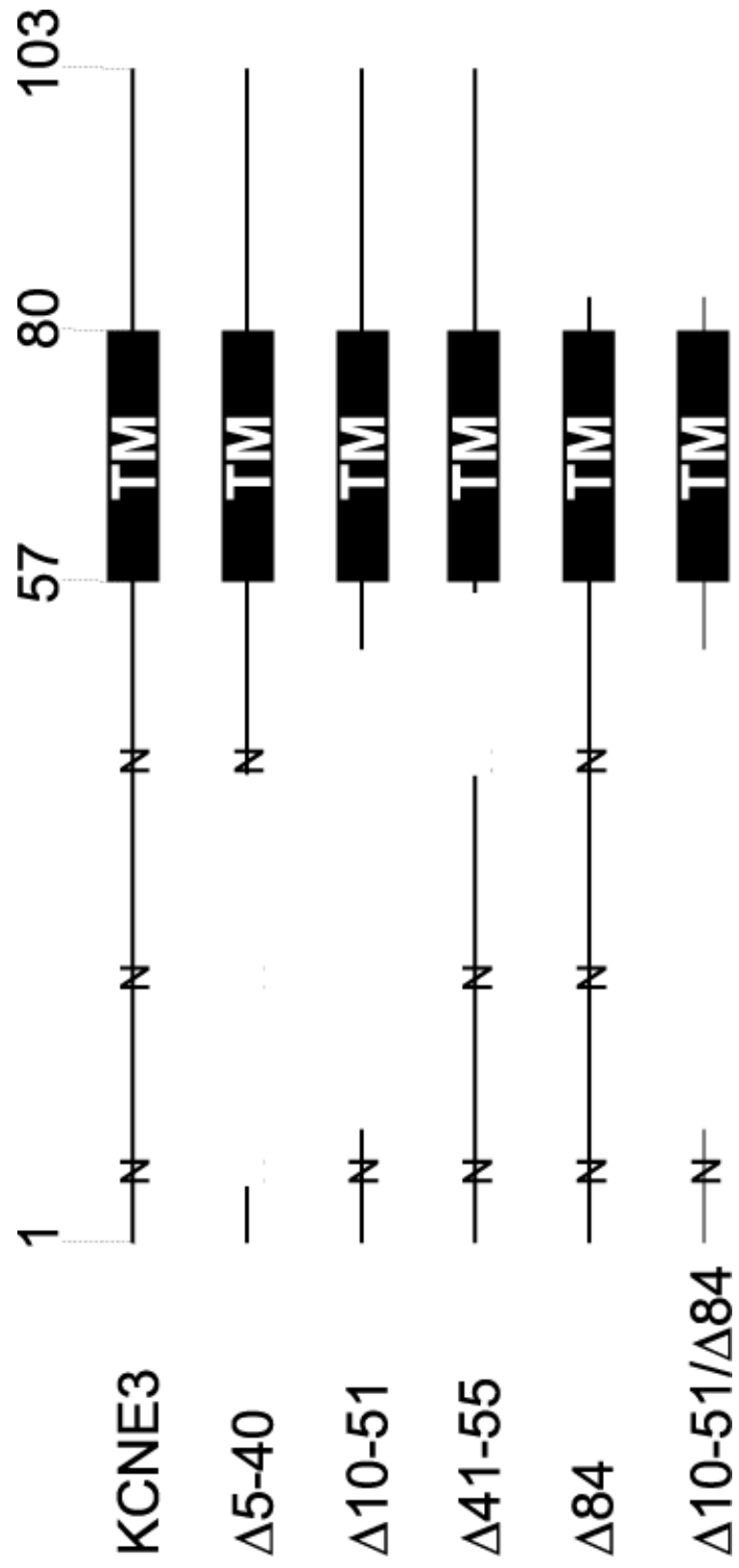


**Figure 2-2.** KCNE3 truncation mutants. Solid lines depict which amino acid residues remain in E3 truncation mutants. Numbers across the top denote amino acid residue number. TM, transmembrane domain; N, putative N-linked glycosylation site.

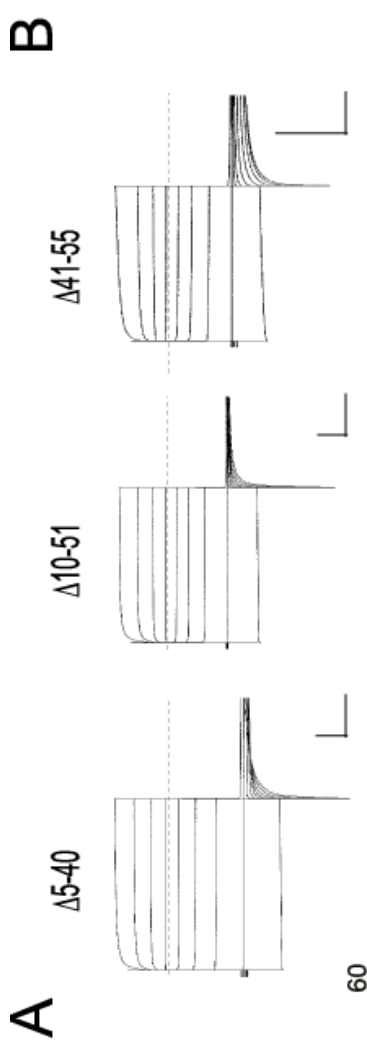
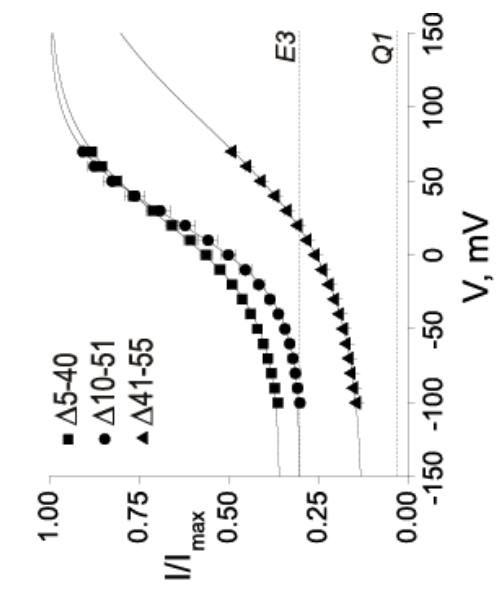


**Figure 2-3.** KCNE3 N-terminal truncation mutants produce standing currents at negative potentials when co-expressed with Q1. **A**, TEVC recordings from *Xenopus* oocytes injected with Q1 and either  $\Delta 5-40$  (left),  $\Delta 10-51$  (center), or  $\Delta 41-55$  (right). Traces were recorded in KD98 with a 13 s interpulse interval. Dashed line indicates zero current. **Inset**, “Activation Curve Protocol” of 2 s depolarizations used to elicit currents shown. **B**, Voltage-activation curves from E3 N-terminal truncation mutants. Activation curve data were fit to a Boltzmann, and the data renormalized as described in Materials and Methods. Squares,  $\Delta 5-40$ ; circles,  $\Delta 10-51$ ; triangles,  $\Delta 41-55$ . Dotted lines indicate the voltage-independent activation of Q1 and Q1-E3 from the lower asymptotes of Q1 the corresponding Boltzmann fits. Data was averaged from 4 – 6 oocytes  $\pm$  S.E.M. Scale bars represent 1  $\mu$ A and 0.5 s.

maximally activated to accurately fit the upper asymptote of the Boltzmann equation, as is the case for  $\Delta 5-40$  and  $\Delta 10-51$ . In the case of the  $\Delta 41-55$  mutant, the curve is markedly right-shifted and not amenable to this comparative analysis. Nonetheless, it is clear from the families of current traces that the N-terminal sequence (barring glycosylation) is not required for Q1/E3 complex assembly and function.

Given the high degree of sequence homology between the C-termini of E1 and E3, we next determined whether the C-terminus of E3 is active in modulation of and assembly with Q1 channels. Figure 2-4 shows representative data from a C-terminal truncation mutant ( $\Delta 84$ ) and a double truncation ( $\Delta 10-51/\Delta 84$ ) mutant co-expressed with Q1. From these data, it is clear that E3 peptides lacking their C-termini can assemble with Q1 channels and form conducting complexes that have standing currents at hyperpolarizing potentials with unaltered  $K^+$  selectivity (Fig. 2-4C). However, removal of the C-terminus does come with a cost; these mutants display some inactivation, slower activation/deactivation kinetics, and a reduction in basal activation. Moreover, roughly equal nanogram amounts of Q1 and C-terminal mutant RNA were required to afford E3-like currents shown in Figure 2-4A; typical injection ratios (1/0.1 Q1/KCNE) afforded currents with more Q1 character (*vide infra*). The electrophysiological properties of C-terminal truncation mutants in Table 1 are compared with WT E3 and the N-terminal truncations, which were also injected at this near equal RNA ratio for comparison.

Since the E3 transmembrane domain is able to modulate Q1 channels without the presence of a C-terminal domain, we next asked whether a dysfunctional mutation within the conserved C-terminus would affect Q1-E3 function. E1 peptides containing the long

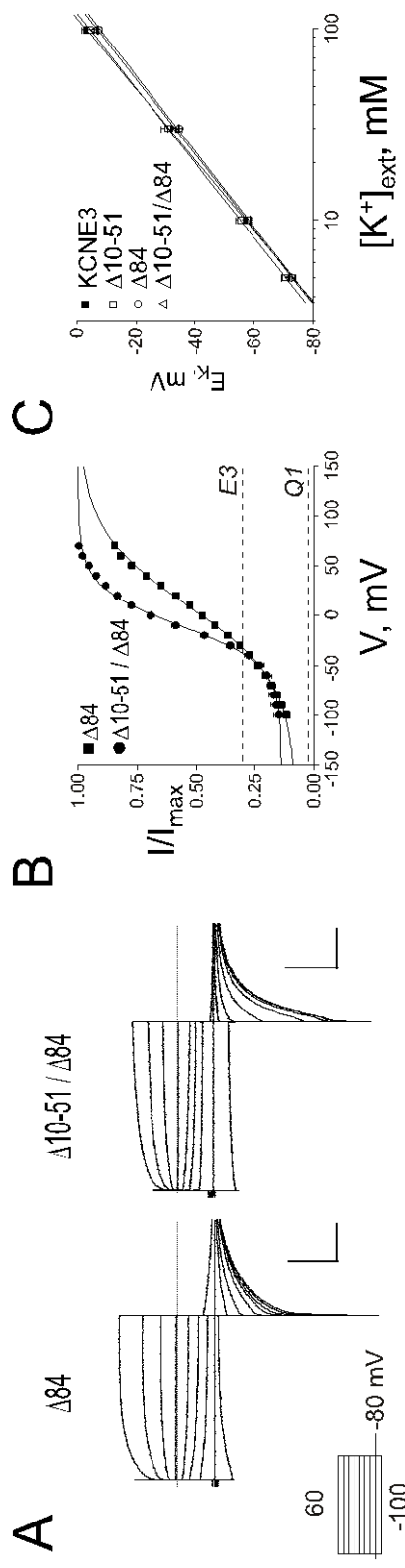




**Figure 2-4.** KCNE3 C-terminal and combined N- and C-terminal truncation mutants also exhibit standing currents at negative potentials when co-expressed with Q1. **A**, TEVC recordings from *Xenopus* oocytes injected with Q1 and either  $\Delta 84$  (left) or  $\Delta 10-51/\Delta 84$  (right). Traces were recorded in KD98 with a 13 s interpulse interval. Dashed line indicates zero current. Scale bars represent 1  $\mu$ A and 0.5 s. **Inset**, “Activation Curve Protocol” of 2 s depolarizations used to elicit currents shown. **B**, Voltage-activation curves from KCNE3 C-terminal and double truncation mutants. Data were fit to a Boltzmann, and normalized as described in Materials and Methods. Squares,  $\Delta 84$ ; circles,  $\Delta 10-51/\Delta 84$ . Dotted lines indicate the voltage-independent activation of Q1 or Q1-E3 (E3). Data was averaged from 4 oocytes each  $\pm$  s.e.m. **C**, External  $K^+$  concentration was varied and the reversal potential was measured.  $\log [K^+]_{\text{ext}}$  is plotted against observed reversal potential. WT and E3 truncation mutants co-expressed with Q1 produced linear fits within error of 53 mV per decade. Data was averaged from 4 – 6 oocytes  $\pm$  S.E.M.

Table 2-1. Electrophysiological Properties of KCNE3 Truncation Mutants<sup>a</sup>

Construct	$V_{1/2}$ (mV)	z	Basal Activation, A2	$\tau_{\text{deactivation}}$ (ms)	
				fast	slow
Q1	-23.8 ± 0.6	1.39 ± 0.03	0.03 ± 0.01	221 ± 10	
E3	23.5 ± 2.5	0.75 ± 0.03	0.31 ± 0.02	14.9 ± 0.3	124 ± 5
$\Delta$ 5-40	25.3 ± 5.1	0.81 ± 0.07	0.35 ± 0.03	19.1 ± 1.2	130 ± 5
$\Delta$ 10-51	24.6 ± 5.5	1.00 ± 0.05	0.30 ± 0.02	14.4 ± 0.6	102 ± 4
$\Delta$ 41-55	86.4 ± 7.4	0.51 ± 0.01	0.12 ± 0.01	10.9 ± 0.2	115 ± 3
$\Delta$ 84	10.1 ± 1.3	0.67 ± 0.02	0.07 ± 0.01	nd	nd
$\Delta$ 10-51/ $\Delta$ 84	-10.0 ± 0.7	1.31 ± 0.05	0.14 ± 0.02	nd	nd
D90N	27.8 ± 4.1	0.59 ± 0.02	0.28 ± 0.02	13.7 ± 0.4	156 ± 28
E1/E3 TM D76N	4.5 ± 4.3	0.82 ± 0.03	0.08 ± 0.01	nd	nd

<sup>a</sup>Data from individual activation curves and deactivation time constants in KD98, obtained from 4 – 6 oocytes. Activation curves were fit to a Boltzmann function as described in Materials and Methods. Values are mean ± S.E.M. Basal activation (A2) for all activation curves was determined by normalizing the data after the Boltzmann fit such that the maximal current fitting parameter (A1) was equal to 1.  $V_{1/2}$  is the voltage of half-maximal activation and z is the slope factor. Time constants of deactivation were fit to a single or double exponential as described in the Material and Methods. nd, not determined.

QT causing mutation D76N have been previously shown to assemble with Q1 channels and traffic to the plasma membrane, but are essentially non-conducting complexes (Fig. 2-5A, left) (Wang & Goldstein, 1995). Incorporation of the corresponding mutation into E3 (D90N) and co-expression with Q1 results in currents nearly indistinguishable from wild type (Fig. 2-5A, right). This functional rescue can be solely attributed to the E3 transmembrane domain since an E1/E3 chimera possessing the E3 transmembrane sequence can also functionally rescue the D76N mutation, albeit with slower activation and deactivation kinetics (Fig. 2-5B). Although these mutants produce functional Q1-E3 complexes, they required injecting more mutant E3 RNA than Q1 to produce currents with primarily E3-character; injection of lower amounts of E3 resulted in currents with more Q1-character, as was previously observed with the E3 D90N mutation (Fig. 2-6A) (Abbott & Goldstein, 2002). These results demonstrate that the E3 transmembrane domain is capable of functionally overriding the modulatory effects of the KCNE C-terminus.

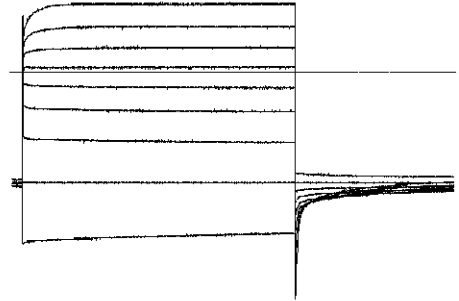
To afford the characteristic Q1-E3 currents with the D90N and C-terminal truncation mutants, an unusually high injection ratio of Q1:E3 RNA was required, suggesting that the C-terminus might be important for cellular assembly and trafficking of the Q1-E3 complex. Supporting this notion was the presence of inactivation in the tail currents with the  $\Delta 84$  and D90N mutants at the lower injection ratios (Fig. 2-6A). This inactivation was not present in either WT Q1-E3 complexes or in complexes where the majority of the E3 N-terminus is removed ( $\Delta 10-51$ ). Therefore, its presence with the  $\Delta 84$  and D90N mutants indicated that a mixed population of Q1 channels (unpartnered and

A

E1 D76N



E3 D90N



B

E1 D76N w/E3 TM

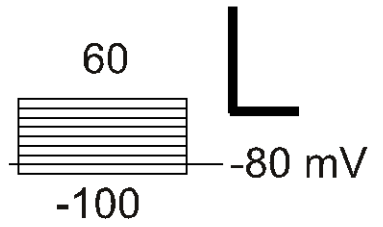
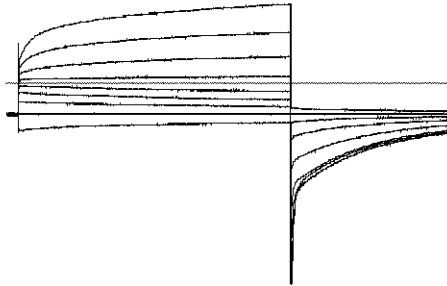


**Figure 2-5.** A Long QT mutation in the C-terminus of KCNE1 is masked by the KCNE3 transmembrane domain. *Inset*, “Activation Curve Protocol” of 2 s depolarizations used to elicit currents shown. Scale bar represents 1  $\mu$ A and 0.5 s for all recordings. **A**, TEVC recording from *Xenopus* oocytes injected with Q1 and either E1 D76N (left) or E3 D90N (right). **B**, Representative TEVC recordings from oocytes co-injected with Q1 and a chimeric partner protein, E1 D76N with the E3 transmembrane (TM) sequence. All oocytes were injected with equal amounts and ratios of Q1 and E1 or E3 RNA, and were recorded in KD98 using a 13 s interpulse interval. Dashed lines indicate zero current.

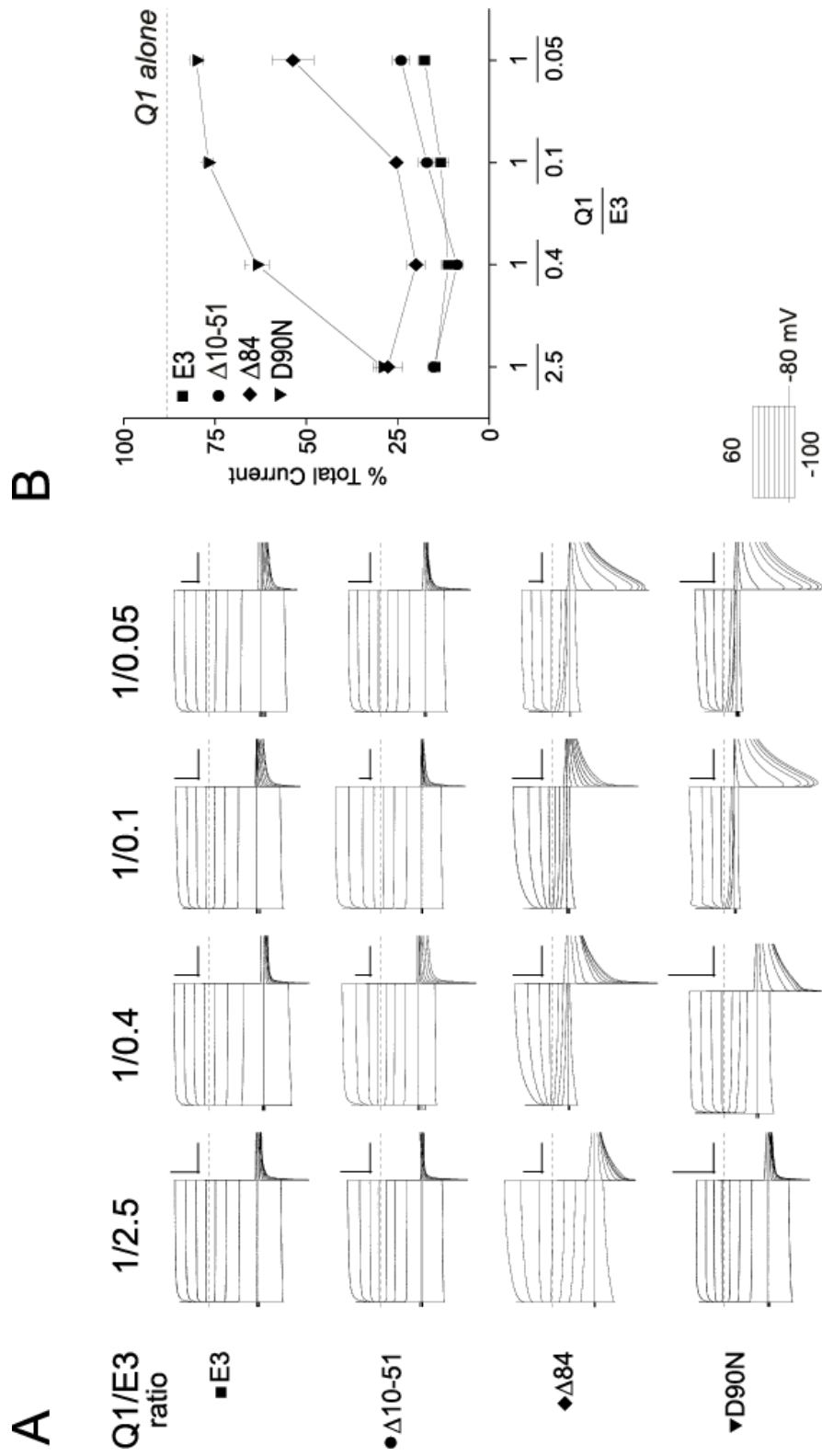


**Figure 2-6.** KCNE3 C-terminal mutants demonstrate a functional dependence on cRNA injection ratios. **A**, Representative two-electrode voltage clamp recordings taken from oocytes injected with varying amounts of E3, between 2.5x and 0.05x of Q1. Currents were recorded in KD98, using a 13 s interpulse interval. The Q1:E3 ratio is labeled across the top. Top row, E3 (square), second row,  $\Delta$ 10-51 (circle), third row,  $\Delta$ 84 (diamond), bottom row, D90N (triangle). Dashed lines indicate zero current. Scale bars represent 1  $\mu$ A and 0.5 s. *Inset*, “Activation Curve Protocol” of 2 s depolarizations used to elicit currents shown. **B**, Percent current remaining after inhibition with 10  $\mu$ M chromanol 293B. Oocytes were held at  $-80$  mV and depolarized for 2 s to  $+40$  mV with a 28 s interpulse interval. Current levels were allowed to stabilize for  $\leq 5$  min before 10  $\mu$ M chromanol 293B was perfused in. Chromanol block typically reached equilibrium within 5 min of wash in. Dashed line indicates the percentage of current remaining in oocytes expressing Q1 alone. Data was averaged from 3 – 11 oocytes  $\pm$  S.E.M.

E3-partnered) was functioning at the cell surface. To confirm that unpartnered Q1 channels were present and functioning at the plasma membrane, we used chromanol 293B, which inhibits Q1-E3 complexes at a 10-fold lower concentration than homomeric Q1 channels (Schroeder et al., 2000b). In the presence of 10  $\mu$ M chromanol 293B, WT and  $\Delta$ 10-51 mutant Q1-E3 complexes were consistently inhibited at  $\sim$  85%, independent of the ratio of RNA injected (Fig. 2-6B). Conversely, as less D90N or  $\Delta$ 84 RNA was injected, chromanol 293B inhibition decreased, approaching the amount of inhibition observed with unpartnered Q1 channels at 10  $\mu$ M chromanol 293B (Fig 2-6B, dotted line). Vehicle (0.1 % DMSO) alone had no effect on WT or mutant Q1-E3 complexes (data not shown). At the highest RNA injection ratio, there was consistently less total current remaining for the  $\Delta$ 84 and D90N mutant than with either WT or the N-terminal truncation mutant ( $\Delta$ 10-51). Attempts to inject even more E3 mutant DNA to determine whether unpartnered Q1 channels remained at the cell surface with the 1/2.5 Q1/E3 ratio were thwarted by extensive oocyte death. Nonetheless, lowering the Q1:E3 RNA injection ratio with the C-terminal and D90N mutants decreased chromanol 293B inhibition and mirrored the increase in inactivation, suggesting that unpartnered Q1 channels were functioning at the plasma membrane. These results implicate the C-terminus in Q1-E3 complex assembly.

We next determined whether the C-terminal and D90N mutant protein was failing to form properly assembled complexes with Q1 and traffic to the plasma membrane, or whether the mutant proteins were merely being degraded. To distinguish injected E3 protein from endogenous KCNE peptides recently identified in *Xenopus* oocytes



(Anantharam et al., 2003), we utilized a HA-tagged version of E3 that has been previously used for biochemical experiments (Abbott et al., 2001; McCrossan et al., 2003; Lewis et al., 2004). Incorporation of the N-terminal HA-tag caused a unique form of  $K^+$ -enhanced, cumulative inactivation in all Q1-E3 complexes, including wild type (Figs. 2-7A & B). Initial recordings in low external  $K^+$  (ND96) required holding at  $-80$  mV for several minutes using test depolarizations to monitor recovery from inactivation. Perfusion of 98 mM  $K^+$  slowly inactivated the HA-tagged Q1-E3 complex, which could not be reversed with hyperpolarizing pulses (Fig. 2-7B). Since the E3-HA-tagged Q1-complex does not recover from inactivation with voltage in high external  $K^+$ , no recovery “hooks” in the tails were observed upon repolarization. Subsequent perfusion with ND96 could partially relieve cumulative inactivation, but the currents never returned to their original values. To ameliorate  $K^+$ -enhanced cumulative inactivation of the HA-tagged Q1-E3 complexes, we replaced the external  $K^+$  with 10 mM  $Rb^+$  (Fig. 2-7C). At this concentration of  $Rb^+$ , we could readily detect the “hook tails” associated with homotetrameric Q1 inactivation since inward currents are about threefold larger with external  $Rb^+$  in comparison to  $K^+$  (Seebahn et al., 2003). Using these conditions, Q1-complex assembly with the C-terminal truncation mutant ( $\Delta 84$ ) remained dependent on the ratio of RNA injected and homotetrameric Q1 channels could be detected at both injection ratios. Remarkably, addition of the epitope tag to the D90N mutant essentially rescued the assembly defect of this mutant (Fig. 2-7C).

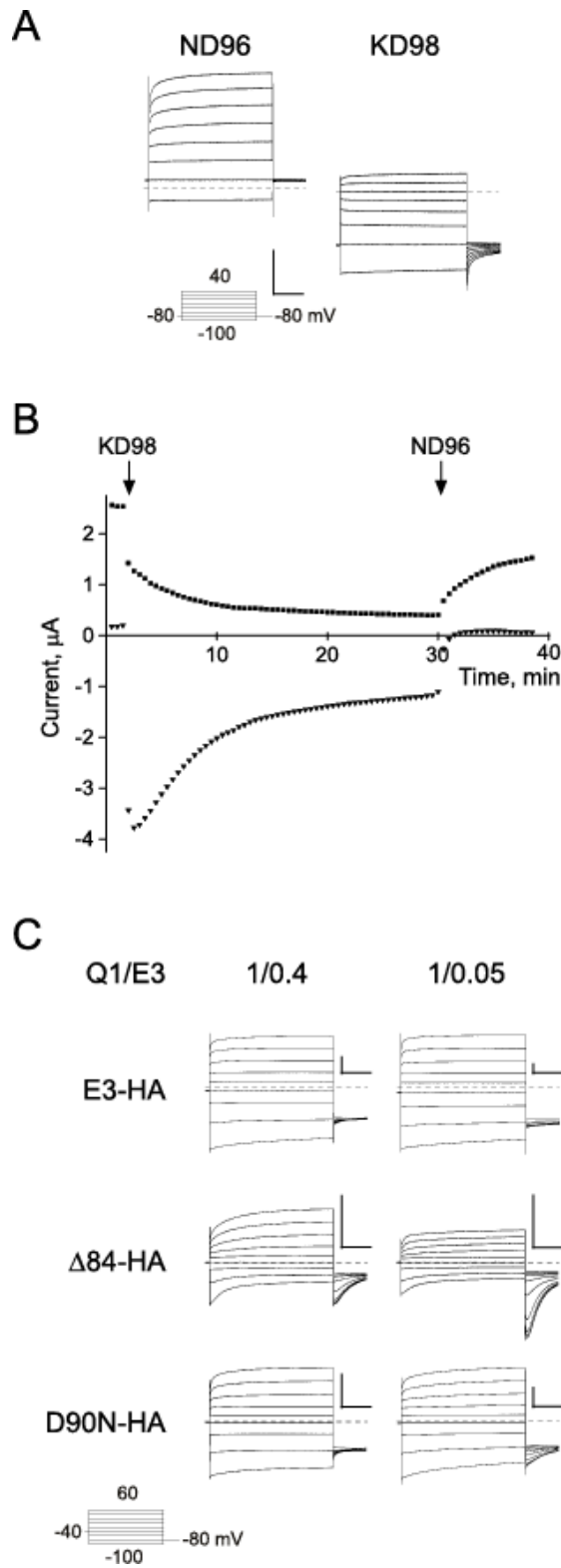


**Figure 2-7.** Functional characterization of KCNQ1/KCNE3-HA complexes. **A**, Q1 complexes formed with HA-tagged E3 exhibit potassium dependent inactivation. TEVC recordings of oocytes expressing Q1 and E3-HA were bathed in ND96 (left) and KD98 (right). Both recordings are shown at the same scale, and use a 13 s interpulse interval. *Insets*, “Activation Curve Protocol” of 2 s depolarizations used to elicit currents shown. **B**, Current versus time plotted for potassium concentration changes for the Q1-E3-HA complex shown in **A**. Oocytes were held at  $-80$  mV, and depolarized for 2 s to  $+40$  mV, with a 28 s interpulse interval. Squares denote the current measured at  $+40$  mV, triangles at  $-80$  mV 100 ms before the respective capacitive transients. **C**, HA-tagged E3 shows altered dose-dependence for the C-terminal truncation mutant. TEVC measurements of oocytes injected with 0.4x (left) or 0.05x (right) E3-HA relative to Q1. Currents were recorded with 10 mM  $Rb^+$  (RD10), and oocytes were held at  $-40$  mV, with an 11.5 s interpulse interval. Top, E3-HA, middle,  $\Delta 84$ -HA, bottom, D90N-HA. Scale bars represent 1  $\mu A$  and 0.5 s.

Since Q1-complex assembly with the HA-tagged  $\Delta 84$  mutant remained dependent on the amount of RNA injected in functional experiments, we next determined whether the E3 C-terminal mutants were proteolytically stable. HA-tagged E3 proteins were isolated from crude oocyte membranes after 3 – 5 days of co-expression with Q1. Three oocytes worth of membranes from each sample at the 1/0.4 Q1/E3 ratio were analyzed by SDS-PAGE and transferred to nitrocellulose for E3 detection. Immunoblots in Figure 2-8A showed a similar complex pattern of bands for both WT E3 and D90N, which is consistent with several N-linked glycoforms. The  $\Delta 84$  C-terminal truncation mutant protein also afforded an abundant signal on the immunoblot; however, only a single, intense band was observed at 20 kD. The  $\Delta 84$  protein was also detected at the lower 1/0.05 Q1/E3 ratio (Fig. 2-8B).

The markedly different pattern of protein bands for WT and  $\Delta 84$  suggested that the C-terminal truncation mutant was largely residing in the endoplasmic reticulum (ER), which could be directly tested utilizing E3's N-linked glycosylation. N-glycosylated membrane proteins in the ER possess immature glycans (~ 3 kD/glycan), whereas the N-linked glycans on membrane proteins that have trafficked through the Golgi mature and often increase in size due to the various trimming and additions of glycosides. To identify the maturity of the N-linked glycans on WT and  $\Delta 84$ , two glycosidases were used: endoglycosidase H (Endo H), which cleaves only the immature glycoform, and PNGase F, which removes all forms of N-linked glycosylation. SDS-solubilized membranes containing WT and  $\Delta 84$  protein were enzymatically deglycosylated and separated on Tris-Tricine gels to resolve the ~ 10 – 20 kD unglycosylated proteins (Fig.

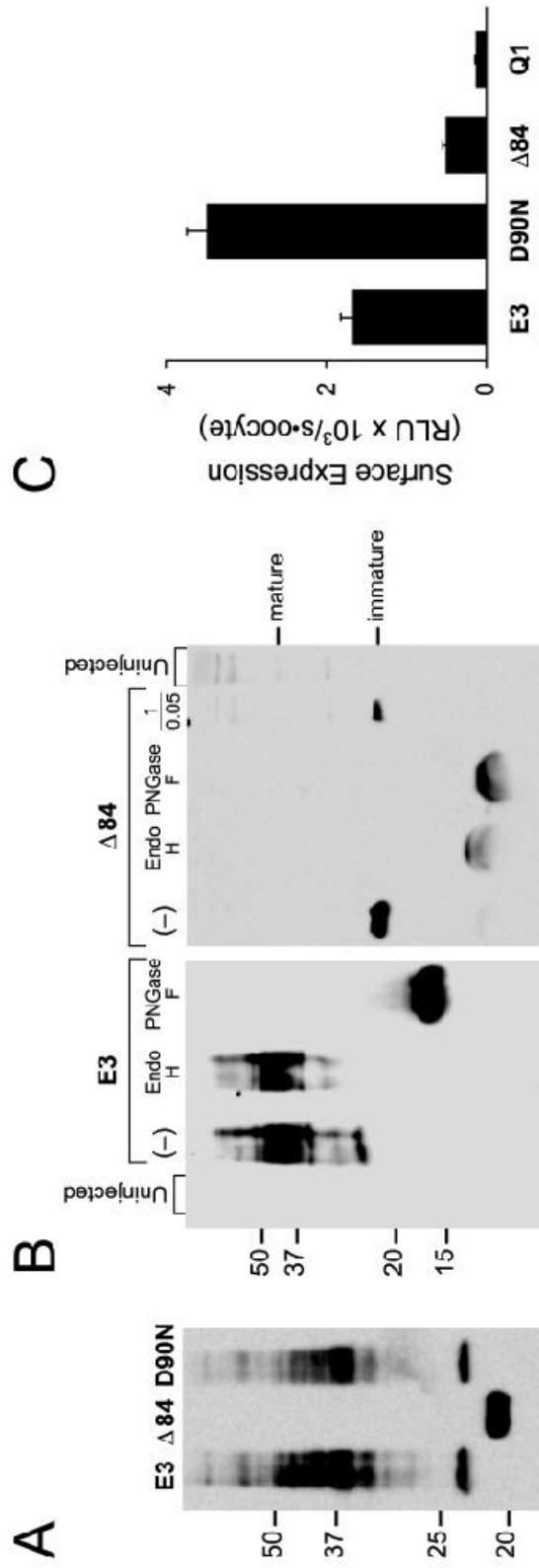


**Figure 2-8.** WT and C-terminal mutant HA-tagged KCNE3 peptides are glycosylated and not proteolytically degraded in oocytes. Crude membranes for the immunoblots were prepared 3 – 5 days after co-injection with Q1 and the indicated E3 construct. **A**, Immunoblot of HA-tagged E3 peptides from SDS-solubilized membranes isolated from oocytes injected at a Q1/E3 ratio of 1/0.4. Membranes from 3 oocytes were loaded in each lane and resolved with a 15% Tris-glycine SDS gel. Molecular weight standards are labeled on the left for both blots. **B**, Immunoblots of enzymatically deglycosylated E3 and  $\Delta 84$  HA-tagged proteins were separated on 16.5% Tris-tricine SDS gels. E3 (4 oocytes/lane) and  $\Delta 84$  (6 oocytes/lane) were digested with endoglycosylase H<sub>f</sub> (Endo H) or PNGase F. Lane marked (–) represents untreated samples. Loaded in the lane marked 1/0.05 are solubilized membranes from 17 oocytes expressing Q1/ $\Delta 84$  injected at the lowest Q1/E3 ratio examined. Membranes from uninjected oocytes are denoted and were loaded at the left (4 oocytes) and right (17 oocytes). Mature and immature glycosylation is denoted, as determined by enzymatic deglycosylation. **C**, Cell surface expression of HA-tagged E3 proteins was quantitated by single oocyte chemiluminescence. Oocytes were injected with a 1/0.4 Q1/E3 ratio, allowed to incubate for 5 days, and the cell surface tagged proteins were labeled with an anti-HA antibody followed by a secondary HRP-conjugated antibody. Single oocyte luminescence was quantitated in a luminometer and is reported in relative light units (RLU). Q1 sample is from control oocytes injected with only Q1 RNA. Error bars are standard error measurement from 15 – 19 oocytes.

2-8B). Endo H treatment of WT E3 removes only a single band at 23 kD. Although the deglycosylated product cannot be observed at this exposure, extended exposures revealed a faint band at 17 kD, suggesting that the majority of the protein has mature N-linked glycosylation (data not shown). PNGase F treatment of WT E3 demonstrated that the remaining, slower mobility bands were due to N-linked glycosylation, as all bands collapsed to a single species at ~ 17 kD. In contrast, both glycosidases equally acted on the single band in the  $\Delta 84$  sample identifying the N-linked glycan as the immature form found in the ER. Given the small size of the  $\Delta 84$  mutant, the slight difference in protein mobility for the differently deglycosylated samples is presumably due to the remaining monosaccharides left behind after Endo H treatment. PNGase F, in contrast, removes all of the carbohydrate from each N-glycosylation site resulting in a protein with a smaller molecular weight. These results demonstrate that the C-terminus is important for assembling Q1-E3 complexes that efficiently exit the ER.

As shown in Figure 2-8B, the PNGase F treated  $\Delta 84$  samples were routinely stronger in intensity than when treated with Endo H. This difference suggested that some mature glycoforms of  $\Delta 84$  may have been present, but were not detectable in the immunoblot due to the heterogeneity of mature glycosylation that often causes an under representation of the protein signal. To ensure that a small portion of the HA-tagged  $\Delta 84$  was reaching the plasma membrane, we used whole oocyte cell surface labeling in combination with chemiluminescence to detect the extracellularly HA-tagged E3 proteins on the cell surface (Zerangue et al., 1999). Oocytes co-expressing Q1 with HA-tagged E3 proteins were labeled with anti-HA antibody followed by labeling with a secondary-

HRP conjugated antibody. The amount of secondary antibody on the cell surface of each oocyte was quantitated using a luminometer. Strong cell surface signals were observed for WT and D90N (Fig. 2-8C). Cell surface expression of  $\Delta 84$  was easily detected over Q1 injected background controls, but was noticeably less than WT and D90N. These cell surface expression data are in agreement with the biochemistry and electrophysiological experiments, which in total, demonstrate that the E3 C-terminus aids in cellular assembly and trafficking of the Q1-E3 complex.

## **DISCUSSION**

In this study, we have used the dramatic changes in Q1 channel function to assess Q1-E3 complex assembly, and by definition, the region of E3 responsible for basal activation of the complex. Through a series of truncation mutants, exemplified by a 41-residue double truncation mutant that is active, yet lacks the majority of its N- and C-termini, we have shown that the transmembrane domain of E3 is sufficient for assembly with and modulation of Q1 channels. A comparative analysis of gating revealed that truncation of the majority of the N-terminus does not appreciably alter Q1-E3 basal activation as long as one putative N-linked glycosylation site is retained. The importance of N-linked glycosylation in Q1-KCNE complex formation and function has been previously observed with E1 (Takumi et al., 1991; Freeman et al., 2000). A requirement of using tail current analysis to compare the basal activation of these mutants is that the channel complexes must be sufficiently activated past their midpoint of activation to fit the data accurately to a Boltzmann. Any uncertainty in the upper asymptote of the fit will



greatly affect the value determined for the basal activation. The  $\Delta 41-55$  highlights this caveat since its basal activation is apparently reduced; however, this mutant clearly forms complexes with Q1 channels that are open at hyperpolarizing potentials, which cause a substantial lowering of the oocyte resting potential similarly to WT E3.

Mutants that allow unpartnered Q1 channels to escape the ER and function at the plasma membrane would also affect the measurement of basal activation. The lower basal activation of the C-terminal truncation mutants may be due in part to unpartnered Q1 channels affecting the activation curve analysis, which was supported by the following three observations in electrophysiological experiments where the Q1/E3 RNA injection ratio was systematically varied. 1) The C-terminal truncation and D90N point mutants required injecting more E3 RNA than Q1 to afford the characteristic Q1-E3 currents. Moreover, as relatively less E3 RNA was injected, the resulting currents resembled unpartnered Q1 channels. In contrast, Q1-complexes with WT and the N-terminal E3 truncation mutant ( $\Delta 10-51$ ) always afforded Q1-E3-like currents over a similar 50-fold range of E3 RNA. 2) The presence of homotetrameric Q1 inactivation, as observed by the hook in the tails currents upon repolarization, was detected only with the C-terminal mutants and increased as less E3 RNA was injected. 3) The chromanol 293B sensitivity, an indirect measurement of Q1-E3 complex assembly, was reduced for the C-terminal mutants and was also dependent on the Q1/E3 RNA injection ratio. These observations strongly imply that a heterogeneous population of Q1 channels is at the cell surface when co-expressed with E3 C-terminal mutants; however, these observations do not rule out the possibility that there are more than two populations of Q1 channels

functioning at the plasma membrane. The diminished assembly capacity of the C-terminal mutants, which allows unpartnered Q1 channels to traffic to the plasma membrane, also explains an apparent inconsistency with a previous investigation of the D90N mutant. Injection at more typical Q1/KCNE RNA ratios (1/0.1) results in currents with primarily Q1-character, as was previously observed with this mutant (Abbott & Goldstein, 2002). It is not until a large excess of D90N RNA is injected that Q1-E3 currents are consistently observed.

Biochemical examination of the E3 C-terminal mutant proteins necessitated the use of an epitope-tagged E3 construct since oocytes contain endogenous KCNE peptides (Anantharam et al., 2003). Although this particular HA-tagged E3 construct has been previously used in biochemical experiments (Abbott et al., 2001; McCrossan et al., 2003; Lewis et al., 2004), in our hands, we observed a unique form of inactivation when it assembled with Q1 that was enhanced by high external  $K^+$  and not reversible with hyperpolarizing pulses under these high  $K^+$  conditions. Surprisingly, incorporation of the HA-tag into the D90N mutant enabled this assembly defective mutant to readily assemble with Q1 channels. We observed efficient Q1-D90N-HA complex assembly in all three assays tested: RNA titration, maturation of glycosylation and cell surface expression. The HA-tag had little effect on the  $\Delta 84$  mutant, as it remained assembly impaired and dependent on RNA injection ratios. While the addition of the HA tag does add 2 extra negative charges per KCNE subunit, and it has been shown that these charges are in the vicinity of the outer vestibule of the Q1 channel (Chen et al., 2003), any proposed mechanisms for either of these two observed phenomena would be conjecture.

The finding that the majority of the  $\Delta 84$  mutant protein possesses the immature form of N-linked glycosylation indicates that the C-terminus assists in the proper assembly of Q1-E3 complexes that can efficiently exit the endoplasmic reticulum. In addition, the fact that only the immature core oligosaccharide is observed for the  $\Delta 84$  mutant, and not the unglycosylated peptide, demonstrates that C-terminal truncation mutant is recognized by oligosaccharyltransferase and is treated as a bona fide substrate. The presence of the immature glycan on  $\Delta 84$  is also consistent with Q1-KCNE complex formation occurring in the ER, which is in agreement with several recent studies that suggest Q1-KCNE complex formation occurs in the ER (Bianchi et al., 2003; Krumer et al., 2004). Although no mature form of  $\Delta 84$  was directly observed in the Western Blots, cell surface labeling of individual oocytes confirmed that at least a small portion of the  $\Delta 84$  mutant protein was indeed at the cell surface. The presence of immature  $\Delta 84$  protein in both the low and high RNA injection ratios indicates that the protein resides in the ER, but is unable to prevent unpartnered Q1 channels from escaping the ER. These results, however, do not directly address whether the majority of the  $\Delta 84$  protein is retained in the ER, and not assembled with Q1, or whether the assembled Q1-E3 complexes lacking an E3 C-terminus are not passing the protein quality control (QC) mechanisms in the ER. The most likely QC proteins involved in ER retention are calnexin/calreticulin since the  $\Delta 84$  mutant lacks a C-terminus eliminating the possibility of a cytoplasmic ER retention signal (Ellgaard & Helenius, 2003). The lack of an ER retention signal also argues that  $\Delta 84$  mutant is retained in the ER and not refluxing back

from the cis-Golgi since COPI proteins require these motifs for retrograde trafficking (Ellgaard & Helenius, 2003).

Our findings directly bear on the controversy regarding the locations of the assembly and modulation domains of E1 and E3. The current debate revolves around assigning assembly and modulatory properties to two distinct locations: the transmembrane domain and a highly conserved region within the C-terminus. Deletion analysis of E1 initially demonstrated that the transmembrane domain was sufficient for assembly with Q1 channels, but the C-terminus was required for modulation (Tapper & George, 2000). More recent E1/E3 chimeras suggest exactly the opposite: the transmembrane sequence houses the modulatory domain while the C-terminus anchors and properly positions the KCNE peptide within the Q1 channel complex (Melman et al., 2001). In the context of these previous reports, the results from our E3 truncation and point mutants suggest a bipartite model for assembly and modulation. In this model (Fig. 2-9), the transmembrane domain and the conserved C-terminal region both play a role in assembly. The transmembrane domain is the primary player in Q1-KCNE complex assembly, but the C-terminus also aids in assembling competent complexes, as evidenced by the “assembly-challenged” E3 C-terminal truncation mutants, E3 D90N mutant and D76N E1/E3 chimera. For modulation, the KCNE transmembrane sequence is either active or passive in basal activation. In the case of E3, the transmembrane domain is active and overrides the C-terminus, affording a Q1 channel complex with large basal activation. Conversely, the E1 transmembrane domain is passive and reveals C-terminal modulation of Q1, producing slowly activating and deactivating  $I_{Ks}$  currents. The

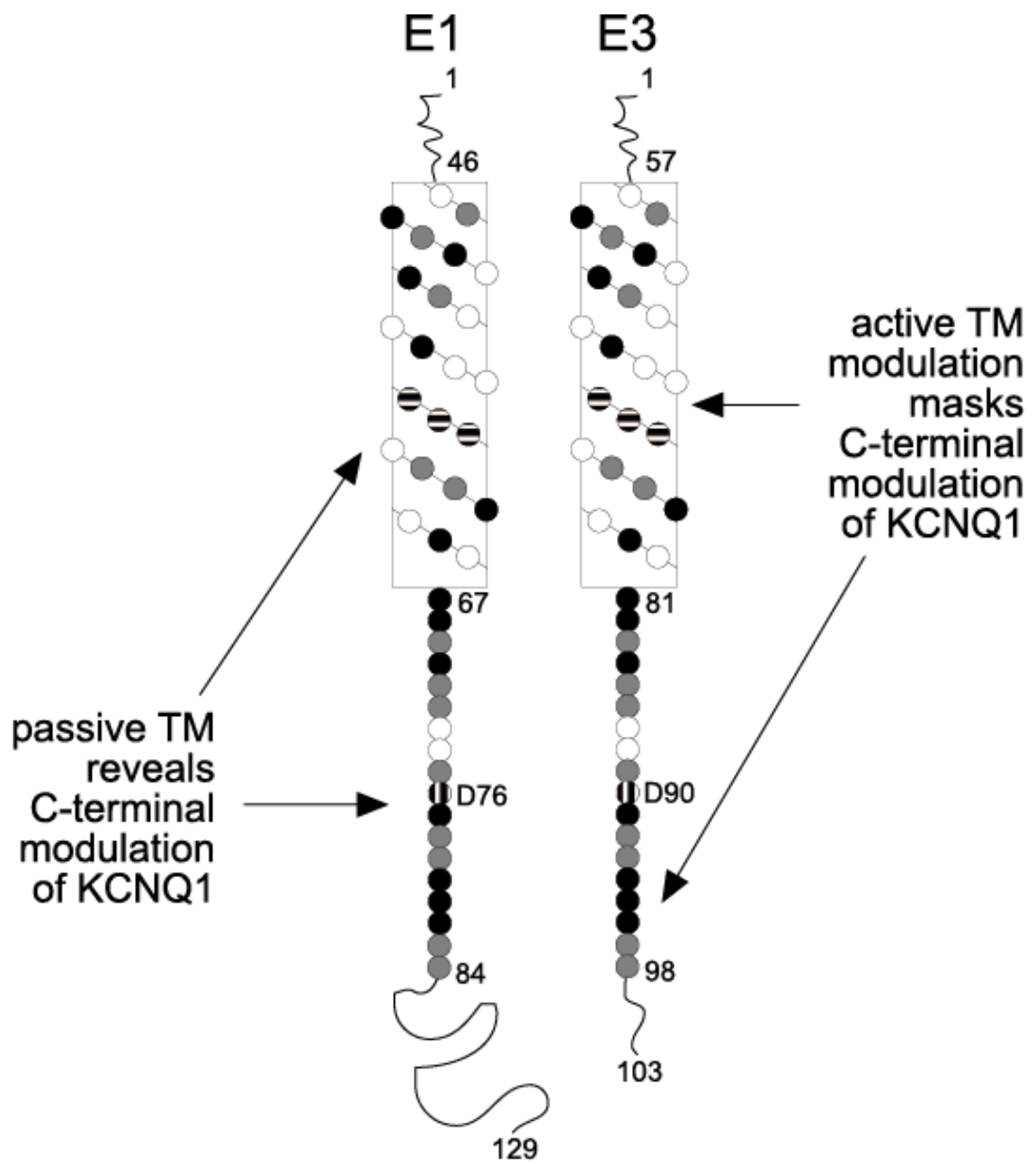


**Figure 2-9.** A bipartite model for modulation of KCNQ1 by KCNE1 and KCNE3. Net diagrams of the transmembrane domains of E1 and E3 are aligned; amino acid residues, denoted as circles, are shaded based on conservation. Black circles, identical amino acids; gray circles, similar amino acids; horizontally striped circles, high-impact amino acids identified by chimeric studies; vertically striped circles, D76 and D90; no fill, non-similar amino acids; TM, transmembrane domain.

bipartite model also predicts that a dysfunctional C-terminus would have no effect on E3 modulation of Q1, but would be detrimental to Q1-E1 complex function. Incorporation of such mutation into E3 (D90N) had no effect on Q1-E3 complex function, whereas this same Long QT mutation in E1 renders the complex non-functional. And with some ghoulish tinkering (placing the E3 transmembrane sequence into the E1 D76N mutant), we demonstrated that the E3 transmembrane domain alone was sufficient to mitigate the disruptive effects of this C-terminal mutation.

Is bipartite assembly and modulation exclusive to E1 and E3? Based on sequence homology, previous deletion studies with E1 (Tapper & George, 2000) and our E3 truncation mutants show that the KCNE transmembrane segment is a general, minimal Q1 assembly domain. Although the KCNE C-terminus is not as conserved as the transmembrane domain throughout the entire family, there is some evidence that the E1 C-terminus may also be important for Q1-E1 complex assembly. Previous E1 deletion studies initially suggested that the C-terminus was solely involved in modulation since removing it did not prevent complex formation with Q1 channels (Tapper & George, 2000). However, complex formation was not readily apparent from the current traces (the raw data was nearly indistinguishable from unpartnered Q1 currents) and a cysteine residue had to be incorporated into the E1 transmembrane domain so that Q1-E1 complex formation could be detected by cadmium inhibition. Although cadmium inhibition was clearly detected in these mutants, it was noticeably less than WT Q1-E1 complexes (Tapper & George, 2000), suggesting that a population of unpartnered Q1 channels may have also been present and functioning at the cell surface. Further examination of the C-

terminus of E1, as well as the remaining KCNE peptides, will reveal whether this region facilitates Q1-KCNE complex formation in the entire KCNE family.

Transmembrane modulation, and thus the bipartite model, may be limited to KCNE modulation that involves altering the basal activation of Q1 channels. Given the reported proximity of the KCNE transmembrane segment to the S6 helix (Wang *et al.*, 1996; Tai & Goldstein, 1998; Tapper & George, 2001), we view E3 transmembrane modulation of Q1 similarly to the constitutively activated S6 mutants in the Shaker K<sup>+</sup> channel described by Swartz and co-workers (Hackos *et al.*, 2002). Whether the basal activation of the Q1-E3 complex is due to a sub-conducting leaky closed state, a perturbed closed to open equilibrium, or a supplantation of an obliterated cytoplasmic gate by an alternative voltage-activated gating mechanism is yet to be determined. This perspective of channel gating provides a rationalization of the E1/E3 chimera data where a single point mutation (Melman *et al.*, 2002a; Melman *et al.*, 2002b) can essentially convert E1 into E3 by inducing basal activation by one of the aforementioned gating mechanisms.

Our discovery of C-terminal E3 mutants that are assembly compromised brings up an important issue that has not been directly addressed in the KCNE literature. Several elegant studies have shown significant electrophysiological changes when KCNE peptides are co-expressed with many types of voltage-gated K<sup>+</sup> channels; however, the percent of functioning K<sup>+</sup> channels assembled with KCNE peptides at the cell surface was never directly determined. While we could show that the C-terminal E3 mutants were “assembly-challenged” using RNA ratio titration experiments in combination with



chromanol 293B pharmacology, we could not accurately determine the fraction of unpartnered Q1 channels at the cell surface. The development of new methods that directly determine the ratio of partnered and unpartnered K<sup>+</sup> channels functioning at the plasma membrane would be of great value in structure/function studies of K<sup>+</sup> channel-KCNE complexes and may help corroborate the physiological relevance of many of these newly identified complexes.

## **MATERIALS AND METHODS**

***Mutagenesis and cRNA preparation*** - KCNQ1 and KCNE3 were subcloned into vectors containing the 5' and 3' UTRs from the *Xenopus*  $\beta$ -globin gene for optimal protein expression. KCNE3 mutations were introduced using Quikchange (Stratagene) and confirmed by DNA sequencing. The HA-tag, PYDVPDYA, was incorporated into the N-terminus of E3 between residues 11 and 12 (Abbott et al., 2001). Plasmids were linearized with MluI, and RNA synthesized by run-off transcription using SP6 (Promega).

***Oocyte preparation and cRNA injection*** - Mature oocytes were surgically extracted from anesthetized *Xenopus laevis*. Isolated oocytes were mechanically separated and bathed in OR2 (mM): 82.5 NaCl, 2.5 KCl, 1 MgCl<sub>2</sub>, 5 HEPES, pH 7.4 + 2 mg/ml collagenase (Worthington Biochemical Corp.) for 85-95 minutes to remove ovarian material and follicles. After rinsing, oocytes were incubated overnight at 18 °C in ND96-bathing (ND96B) solution + gentamicin (mM): 96 NaCl, 2 KCl, 1.8 CaCl<sub>2</sub>, 1

MgCl<sub>2</sub>, 5 HEPES, 50 µg/ml gentamicin (Sigma), pH 7.4. Oocytes were microinjected with RNA 12-50 hours after extraction with 27.6 nl total volume of cRNA solution. Oocytes were injected with (ng/oocyte): Q1, 15; Q1/E3, 7.5/3.5; Q1/E3 truncation, 5/3.5; Q1/KCNE D→N mutant, 7.5/18.5. For experiments in which E3 cRNA injection ratios were compared, Q1 was kept constant at 7.5 ng/oocyte, while the quantity of E3 was varied, 18.5, 3.0, 0.7, and 0.4 ng/oocyte. Likewise, in experiments utilizing HA-tagged E3 constructs, Q1 was kept constant at 7.5 ng/oocyte, and was co-injected with E3 (3.0 or 0.4 ng/oocyte). In controls where only Q1 or E3 was injected, an equivalent volume of DEPC water was also injected. Injected oocytes were incubated at 18 °C in ND96B for 2 – 7 days before conducting experiments.

***Electrophysiology*** - Currents were measured using two-electrode voltage clamp (OC-725-C, Warner Instrument Corp.) and data acquired with Digidata 1322A (Axon Instruments) running Clampex 8.2 (Axon Instruments) at RT. Electrodes were filled with 3M KCl, 5 mM EGTA, 10 mM HEPES, pH 7.6, and had resistance between 0.2 – 1.5 MΩ. A home-made gravity-fed perfusion chamber was used, in which complete solution exchange occurred within ~ 10 s.

Q1-E3 channels are open at negative membrane potentials, and thus several steps were taken to ensure that the currents measured are from K<sup>+</sup> selective currents and not from non-specific leak. Oocytes injected with wild type (WT) and mutant E3 cRNA were only recorded from if the resting membrane potential was more negative than – 75 mV in ND96 since oocytes with more positive resting potentials routinely had non-

specific leak and/or were dead. ND96 (mM): 96 NaCl, 2 KCl, 0.3 CaCl<sub>2</sub>, 1 MgCl<sub>2</sub>, 5 HEPES, pH 7.0. For experiments utilizing solutions with K<sup>+</sup> concentrations greater than ND96, the current at – 80 mV was measured in ND96 before and after each experiment. Data was only included if current at – 80 mV returned to the original level in ND96 after treatment with high K<sup>+</sup> solution. The majority of the E3 mutants had positive current at – 80 mV due to outward “leak” of potassium, presumably through the Q1-E3 channels. For Q1, the leak current at – 80 mV was between – 0.01 and – 0.04 μA in ND96. All traces shown were not leak subtracted.

Tail currents for activation curves were measured in KD98 (mM): 98 KCl, 0.3 CaCl<sub>2</sub>, 1 MgCl<sub>2</sub>, 5 HEPES, pH 7.0. Upon switching the external solution to KD98, oocytes were held at – 80 mV until the inward current plateaued. The tail current protocol was a series of command pulses to potentials between – 100 and + 60 mV in 10 mV increments for 2 s, after which oocytes were returned to – 80 mV. The interpulse interval was 13 s.

Reversal potentials were measured at several external potassium concentrations, each isotonicly balanced with sodium. The reversal potential protocol was a holding potential of – 80 mV, depolarizing to + 40 mV for 2 s, followed by repolarization to potentials around the Nernst-predicted value of E<sub>K</sub> in 2 mV steps to determine the reversal potential.

Chromanol 293B inhibition was measured in ND96C (mM): 96 NaCl, 2 KCl, 1.8 CaCl<sub>2</sub>, 1 MgCl<sub>2</sub>, 5 HEPES, pH 7.4. Chromanol 293B (Tocris) was added to ND96C from a 10 mM stock in DMSO. The final concentration of DMSO in ND96C was 0.1%.

Oocytes were held at  $-80$  mV and subjected to  $+40$  mV depolarizations for 2 s every 30 s until the current level stabilized ( $\leq 5$  min). After the current stabilized,  $10 \mu\text{M}$  Chromanol 293B was perfused until inhibition was complete ( $\sim 5$  min), and the remaining current was measured.

Oocytes expressing complexes with HA-tagged E3 proteins became appreciably inactivated during incubation at  $18^\circ\text{C}$  in ND96B. Cumulative inactivation was removed by holding at  $-80$  mV in ND96 with periodic test depolarization to  $+40$  mV to monitor relief of inactivation. After relieving inactivation, oocytes were subjected to a family of depolarizations from  $-100$  to  $+40$  mV in 20 mV steps with a 13 s interpulse interval. Cumulative inactivation was monitored utilizing a 2 s test depolarization from  $-80$  to  $+40$  mV at 30 s intervals. At first, isochronal current measurements were taken 100 ms before the respective capacitive transients at  $-80$  and  $+40$  mV in ND96 solution. Then, the bath solution was changed to KD98, and the current was then measured until there was no change in current between test depolarizations. A family of currents was then measured in KD98 using the same depolarization protocol used with ND96. Recovery from cumulative inactivation was monitored by returning the bath solution to ND96 and measuring the current at  $-80$  mV and  $+40$  mV as described above.

To detect the voltage-dependent inactivation of homotetrameric Q1 channels with the HA-tagged E3 constructs, the oocytes were held at  $-40$  mV and in bathed RD10 solution, which minimized cumulative inactivation, yet enabled the visualization of inward currents (mM): 88 NaCl, 10 RbCl, 0.3 CaCl<sub>2</sub>, 1 MgCl<sub>2</sub>, 5 HEPES, pH 7.4). The pulse protocol used a holding potential of  $-40$  mV, a 2 s test pulse between  $-100$  and  $+$

60 in 20 mV increments, followed by a tail pulse to – 80 mV for 1.5 s. The interpulse interval was 11.5 s.

**Data Analysis** - The amplitude of the tail currents were measured 3 ms after return to – 80 mV and plotted versus the depolarized potential. The resultant activation curves were initially fit to a Boltzmann function,  $y = A2 + (A1-A2)/(1+e^{(V-V_{1/2})*(-zF/RT)})$ , where  $V_{1/2}$  is the midpoint of activation and  $z$  is the maximum slope. The upper and lower asymptotes,  $A1$  and  $A2$ , respectively, were left to vary, allowing data to be fit in cases where channels did not fully close or were not fully activated in the voltage ranges that can be used with oocytes (-100 to +60 mV). After the initial fit, the tail current amplitudes were normalized such that the upper asymptote ( $A1$ ) was equal to 1. These data were refit to the Boltzmann function, and the lower asymptote ( $A2$ ) of the second fit was used to compare basal activation of the wild type and mutant Q1-E3 complexes. Deactivation time constants were measured by fitting the current at – 80 mV following a (40 – 60 mV) depolarization to a single or double exponential. Time constants of deactivation were not determined in samples where recovery from inactivation obscured the fast component of deactivation.

**Oocyte membrane preparation** - 3 – 5 days after injection with 7.5 ng Q1 and E3 (3.0 or 0.4 ng cRNA/oocyte), several oocytes were checked for functional  $K^+$  conducting complexes and each batch of oocytes was homogenized at 4 °C in 0.9 ml homogenization buffer, 100 mM HEPES, pH 7.6, 1 mM EDTA, 50 mM DTT, and 100 µg/ml PMSF.

Subsequent steps were performed 4 °C. The cell debris from the homogenate was pelleted (3000g, 10 min), and the supernatant was collected. The pellet was vigorously resuspended in homogenization buffer (0.9 ml) and cell debris was pelleted again (3000g, 10 min). The supernatants were combined and overlaid on a 15% sucrose cushion, prepared with 100 mM HEPES, pH 7.6, and 10 mM N-ethyl maleimide. Samples were subjected to ultracentrifugation (175,000g, 75 min) and pelleted membranes were detergent solubilized at RT in: 1% SDS, 150 mM NaCl, 100 mM DTT, 10 mM TRIS-HCl pH 7.5. Since a proportionally smaller volume of solubilization buffer was used for oocytes injected with 0.4 ng of mutant E3 cRNA, these membranes were solubilized with 5% SDS to aid in solubilization.

***SDS-PAGE and Western*** - SDS solubilized membranes were diluted with 1/5 volume of 6x SDS-PAGE loading buffer and the proteins were separated on either a 15% SDS-PAGE (TRIS/glycine) or 16.5% (TRIS/tricine) (Schagger & von Jagow, 1987). Proteins were transferred to nitrocellulose (0.2 µm pore size) at constant amperage (0.2 – 0.3 A) for 1 hr. Blots were blocked for 45 min at RT in blocking buffer (5% non-fat milk in western wash (150 mM NaCl, 10 mM TRIS-HCl, pH 7.4, and 0.2% Tween-20)). The blots were incubated overnight at 4 °C with 100 ng/ml rat monoclonal α-HA (Roche) in blocking buffer. Blots were washed in western wash (3 x 5 min) and incubated for 45 min at RT with 200 ng/ml goat α-rat HRP (Santa Cruz) in blocking buffer. After washing (3 x 5 min) in western wash, the blot was developed in SuperSignal West Dura

Extended Duration Substrate (Pierce) for 5 min and the immunoreactive bands were captured using a Fujifilm LAS-3000 CCD Camera.

***PNGase F and Endo H analysis*** - SDS solubilized membranes as described above were diluted to 0.5% SDS with an equal volume of water, then raised to 1% NP40 and 50 mM sodium citrate, pH 5.5, or 50 mM sodium phosphate, pH 7.5, and digested with Endo H<sub>f</sub> or PNGase F (New England Biolabs), respectively, at 37 °C for 1 hr. After digestion, samples were raised to a total of 75 mM DTT and 3.5% SDS, then mixed with 6x gel loading buffer and the proteins were resolved on SDS-PAGE and analyzed by western blot as described before.

***Cell Surface Labeling and Luminometry*** - The level of cell surface HA-tagged E3 proteins were measured by luminometry as reported (Zerangue et al., 1999). Oocytes were injected with 7.5 ng Q1 and WT or mutant E3-HA (3.0 or 0.4 ng). Control oocytes were injected with only 7.5 ng Q1 cRNA. On day 5 post injection, a few oocytes were checked for functioning channel complexes, and then the oocytes were cooled to 4 °C in ND96B to prevent further trafficking. Oocytes were blocked for 30 min with 1% BSA in ND96B. Oocytes were then incubated for 1 hr with 1 µg/ml Rat monoclonal α-HA (Roche) in 1% BSA in ND96B . Oocytes were washed (8 x 5 min) with 1% BSA in ND96B and incubated for 40 min with secondary α-rat F(ab)<sub>2</sub> antibody (Jackson ImmunoResearch) added at 2 µg/ml in 1% BSA in ND96. Secondary antibody was removed and washed once with 1% BSA ND96 for 1 hr followed by a second wash in

ND96B for 1 hr. Oocytes were individually placed in wells with 50  $\mu$ l of ND96B solution, mixed with 50  $\mu$ l of SuperSignal ELISA Femto Maximum Sensitivity Substrate (Pierce) and the signal at 405 nm was integrated for 15 s using a Mediators PhL Luminometer (Aureon Biosystems). Data is given in relative light units, RLU, and comes from the same batch of oocytes.



## **CHAPTER III**

### **SECONDARY STRUCTURE OF A KCNE CYTOPLASMIC DOMAIN**

#### **ABSTRACT**

Type I transmembrane KCNE peptides contain a conserved C-terminal cytoplasmic domain that abuts the transmembrane segment. In KCNE1, this region is required for modulation of KCNQ1 K<sup>+</sup> channels to afford the slowly activating cardiac I<sub>Ks</sub> current. We utilized alanine/leucine-scanning to determine whether this region possesses any secondary structure and to identify the KCNE1 residues that face the KCNQ1 channel complex. Helical periodicity analysis of the mutation-induced perturbations in voltage-activation and deactivation kinetics of KCNQ1-KCNE1 complexes defined the KCNE1 C-terminus is  $\alpha$ -helical when split in half at a conserved proline residue. This helical rendering assigns all known Long QT mutations in the KCNE1 C-terminal domain as protein-facing. The identification of a secondary structure within the KCNE1 C-terminal domain provides a structural scaffold to map protein-protein interactions with the pore-forming KCNQ1 subunit as well as the cytoplasmic regulatory proteins anchored to KCNQ1-KCNE complexes.

## **INTRODUCTION**

KCNE type I transmembrane peptides are a class of membrane-embedded  $\beta$ -subunits that assemble with and modulate the function of voltage-gated  $K^+$  channels (McCrossan & Abbott, 2004). The physiological importance of these small (~ 100 – 150 aa)  $\beta$ -subunits on  $K^+$  channel function is underscored by the genetic mutations in KCNE1 (E1) and KCNE2 (E2) that cause abnormalities in the cardiac rhythm (Splawski et al., 2000). Outside of the heart, mutations in E1 also cause endolymphatic collapse in the developing ear and a C-terminal mutation in KCNE3 (E3) has been implicated in periodic paralysis since it alters Kv3.4 channel function (Letts et al., 2000; Abbott et al., 2001). All five KCNE peptides have been shown to assemble with and differentially modulate KCNQ1 (Q1)  $K^+$  channels (McCrossan & Abbott, 2004). Q1-E1 complexes produce the slowly activating and deactivating cardiac  $I_{Ks}$  current whereas Q1 assembly with either E2 or E3 gives rise to constitutively conducting complexes that rapidly activate and deactivate. Complexes with E4 and E5 slow the activation kinetics of Q1 channels similarly to E1; however, co-assembly with these recently discovered KCNEs results in  $K^+$  channel complexes that conduct only at extremely depolarizing potentials. Q1-KCNE complex gating is also modulated by several intracellular proteins. Calmodulin, PKA, protein phosphatase I (PP1), and A-kinase anchoring proteins (AKAPs) are all cytoplasmic proteins that interact with membrane-embedded Q1-KCNE complexes (Marx et al., 2002; Kurokawa et al., 2003; Shamgar et al., 2006).

Although KCNE peptides modulate Q1 function differently, 4 KCNE peptides share a conserved cytoplasmic sequence (~ 20 aa) that is adjacent to the transmembrane

domain. Function-structure studies with E1 have shown that this domain is required for Q1 channel modulation (Takumi *et al.*, 1991; Tapper & George, 2000). Moreover, one-third of the known genetic missense point mutations in E1 that cause Long QT syndrome reside in this cytoplasmic region (Splawski *et al.*, 2000; Schulze-Bahr *et al.*, 2001; Ma *et al.*, 2003; Lai *et al.*, 2005; Napolitano *et al.*, 2005). Therefore, we utilized perturbation mutagenesis to determine whether this cytoplasmic domain possesses any secondary structure and to identify residues that face the Q1 channel complex. Alanine and tryptophan scanning have been previously used to examine the secondary structure and protein-facing residues of both water-exposed and membrane-embedded domains of voltage-gated K<sup>+</sup> channels (Monks *et al.*, 1999; Hong & Miller, 2000; Li-Smerin *et al.*, 2000a, 2000b). Using alanine and leucine mutagenesis, we observed two distinct classes of E1 mutants: those that strongly shift the voltage-dependence of activation favoring the closed state, and those that resemble the wild type complex. Periodicity analysis of our results revealed that the cytoplasmic C-terminal domain of E1 is helical when broken into two segments separated by a proline residue. This suggests that either the E1 C-terminus is a kinked  $\alpha$ -helix, or the helix experiences two different protein environments above and below this junction point. Moreover, this helical projection defines 4 out of 4 dysfunctional mutations that cause Long QT syndrome as facing the Q1 channel complex. Given that this C-terminal domain is conserved in all but one of the known KCNE peptides, our E1 results predict that E2, E3 and E5 will possess a domain with similar structure when associated with Q1 channel subunits. In total, these results

provide a structural motif from which to interpret the link between Q1-KCNE gating and intracellular regulation.

## **RESULTS**

The C-terminal sequence that abuts the predicted transmembrane domain of E1 has been shown to be vital for Q1 modulation (Tapper & George, 2000), which suggests that a protein-protein interaction exists between Q1 and E1 in this region. To identify the C-terminal residues of KCNE peptides that face the Q1 channel complex and to determine whether this region possesses any secondary structure, we individually mutated each residue in E1 to alanine, expressed these mutants with Q1 channels in *Xenopus* oocytes, and measured the changes in Q1-E1 complex gating using TEVC. For native alanine residues, leucine was used to induce a perturbation; for native serine residues, both alanine and leucine mutants were examined.

Of the 19 E1 C-terminal residues examined, only one mutant, D76A, did not express current. This was expected given that the Long QT mutation (D76N) and the equivalent mutation in rat affords a non-functional Q1 channel complex (Wang & Goldstein, 1995; Splawski *et al.*, 1997; Bianchi *et al.*, 1999). Currents elicited from voltage depolarizations of wild type (WT) and representative mutant Q1-E1 complexes in high external  $K^+$  are shown in Figure 3-1A. To compare the voltage-gating of the WT and mutant Q1-E1 complexes, we generated activation curves by measuring the tail current after repolarization and plotted it versus the depolarization potential. Standard tail-current analysis requires that the channel reaches equilibrium between the open and

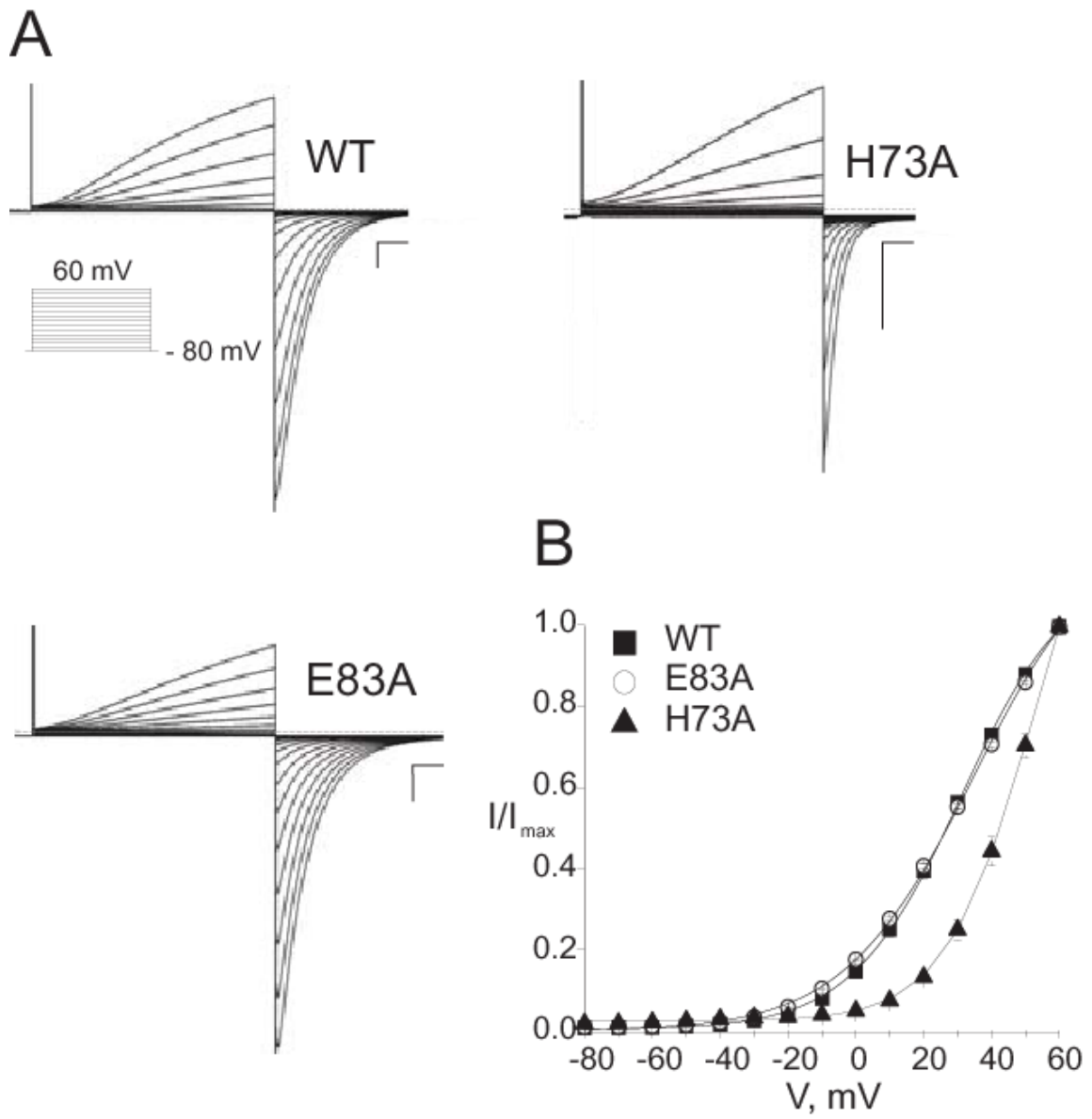


**Figure 3-1.** KCNE1 alanine mutants show diverse gating properties. **A**, two-electrode voltage clamp recordings of wild type, H73A, and E83A mutant channels expressed in *Xenopus* oocytes. Currents were recorded in KD98 solution. Dotted line indicates zero current. Scale bars represent 1  $\mu$ A and 0.5 s. **Inset**, protocol of 4 s depolarizations from  $-80$  mV to  $60$  mV at  $10$  mV increments used to elicit currents shown. **B**, voltage activation curves for wild type and representative mutant channel complexes calculated from tail current analysis. Solid curves represent Boltzmann fits to the data. Data was averaged from 5 – 10 oocytes each  $\pm$  S.E.M.

closed states before repolarization; however, Q1-E1 complexes do not reach equilibrium even after 90-second depolarizations (Takumi et al., 1988), which necessitated an isochronal (4 s) tail current measurement. Normalized tail currents were plotted against depolarization potentials and the resultant activation curves (Figure 3-1B) were fit to a Boltzmann equation. From the Boltzmann fit, the voltage of half maximal activation ( $V_{1/2}$ ) and slope factor ( $z$ ) were determined for WT and each mutant Q1-E1 complex (Table 3-1). These parameters were used to calculate the isochronal free energy of Q1-E1 complex opening at zero voltage ( $\Delta G_{\text{iso}}$ ), and for each mutant,  $\Delta\Delta G_{\text{iso}}$  was also determined ( $\Delta G_{\text{iso}}^{\text{mutant}} - \Delta G_{\text{iso}}^{\text{WT}}$ ). As in previous perturbation studies (Monks *et al.*, 1999; Hong & Miller, 2000; Li-Smerin *et al.*, 2000a, 2000b), we defined residues with a  $|\Delta\Delta G_{\text{iso}}| > 1$  kcal/mol as high impact. Using this arbitrarily defined cut-off, 9 mutants scored as high impact, all of which resulted in stabilization of the closed state and acceleration of the deactivation kinetics when compared to WT. For the native serine residues, where alanine and leucine substitutions were individually examined, both S68A and S68L were defined as high impact, only S74L scored as high impact, and both S84 mutants were low impact.

To determine whether there was a periodicity of high and low impact mutants, the C-terminal residues were plotted on a helical wheel (Figure 3-2, center). An  $\alpha$ -helical pattern was not immediately apparent by simple visual inspection, nor by Fourier periodicity analysis (*vide infra*). While plotting our data on a helical wheel diagram, we initially observed a helical pattern for the bottom half of the region that abruptly disappeared conspicuously after a proline residue. Proline disruption of helical segments

Table 3-1. Electrophysiological Properties of KCNE1 Mutants<sup>a</sup>

Construct	$V_{1/2}$ (mV)	$z$	$\Delta G$	$\Delta\Delta G$	$\tau_{\text{deactivation}}$ (ms)
E1	31.3 ± 1.1	1.56 ± 0.03	1.02 ± 0.05	--	665 ± 80
S68A	60.0 ± 1.2	2.20 ± 0.06	3.04 ± 0.09	2.02 ± 0.10	131 ± 5
S68L	51.8 ± 1.6	1.90 ± 0.13	2.26 ± 0.15	1.24 ± 0.16	139 ± 7
S68D	43.6 ± 1.0	1.90 ± 0.07	1.91 ± 0.08	0.89 ± 0.09	156 ± 6
S68E	44.8 ± 1.0	2.05 ± 0.12	2.11 ± 0.09	1.09 ± 0.10	145 ± 14
K69A	28.1 ± 1.6	1.84 ± 0.03	1.19 ± 0.06	0.17 ± 0.08	350 ± 28
K70A	56.1 ± 0.6	2.24 ± 0.06	2.90 ± 0.09	1.88 ± 0.10	105 ± 4
K70Q	54.5 ± 0.8	2.04 ± 0.08	2.27 ± 0.08	1.25 ± 0.09	132 ± 3
L71A	42.6 ± 2.6	2.04 ± 0.08	2.02 ± 0.18	1.00 ± 0.19	256 ± 16
E72A	43.0 ± 0.8	1.90 ± 0.02	1.88 ± 0.03	0.86 ± 0.06	362 ± 18



H73A	$52.3 \pm 3.2$	$2.03 \pm 0.02$	$2.40 \pm 0.10$	$1.38 \pm 0.11$	$176 \pm 3$
S74A	$34.1 \pm 0.9$	$1.61 \pm 0.03$	$1.27 \pm 0.04$	$0.25 \pm 0.06$	$496 \pm 32$
S74L	$53.4 \pm 1.5$	$1.94 \pm 0.09$	$2.37 \pm 0.09$	$1.35 \pm 0.10$	$200 \pm 12$
S74I	$44.4 \pm 1.4$	$2.17 \pm 0.03$	$2.22 \pm 0.08$	$1.20 \pm 0.09$	$189 \pm 10$
S74M	$30.3 \pm 2.1$	$1.90 \pm 0.03$	$1.35 \pm 0.11$	$0.33 \pm 0.12$	$255 \pm 22$
N75A	$27.9 \pm 1.5$	$1.65 \pm 0.02$	$1.06 \pm 0.06$	$0.04 \pm 0.08$	$644 \pm 42$
D76A	NF	NF	NF	NF	NF
P77G	ND	ND	ND	ND	ND
P77A	$38.4 \pm 2.7$	$1.65 \pm 0.05$	$1.41 \pm 0.08$	$0.39 \pm 0.09$	$406 \pm 9$
P77L	$39.5 \pm 1.7$	$1.52 \pm 0.08$	$1.38 \pm 0.04$	$0.36 \pm 0.06$	$381 \pm 19$
F78A	$69.5 \pm 6.4$	$1.50 \pm 0.10$	$2.14 \pm 0.12$	$1.12 \pm 0.13$	$161 \pm 14$
N79A	$45.6 \pm 0.9$	$2.12 \pm 0.04$	$1.98 \pm 0.07$	$0.96 \pm 0.09$	$179 \pm 4$
V80A	$43.7 \pm 1.3$	$1.55 \pm 0.02$	$1.39 \pm 0.04$	$0.37 \pm 0.06$	$258 \pm 13$

Y81A	74.7 ± 1.0	1.85 ± 0.02	2.88 ± 0.15	1.86 ± 0.16	112 ± 3
I82A	59.4 ± 1.2	2.20 ± 0.03	2.67 ± 0.04	1.65 ± 0.06	145 ± 5
E83A	34.6 ± 0.8	1.34 ± 0.02	1.06 ± 0.02	0.04 ± 0.05	630 ± 50
S84A	44.6 ± 1.2	1.90 ± 0.06	1.95 ± 0.05	0.93 ± 0.05	317 ± 16
S84L	37.5 ± 4.2	1.13 ± 0.03	0.97 ± 0.09	-0.05 ± 0.10	449 ± 52
D85A	48.0 ± 2.5	1.98 ± 0.04	2.18 ± 0.13	1.16 ± 0.14	297 ± 20
A86L	24.8 ± 0.8	1.61 ± 0.03	0.92 ± 0.03	-0.10 ± 0.06	874 ± 57

---

<sup>a</sup> Data from individual activation curves and deactivation time constants in KD98, obtained from 4–12 oocytes. Activation curves were fit to a Boltzmann function as described in Materials and Methods.  $V_{1/2}$  is the voltage of half-maximal activation and  $z$  is the slope factor. Time constants of deactivation were fit to a single exponential as described in the Materials and Methods. Values are mean ± S.E.M. NF, non-functional mutant, ND, no current detected.

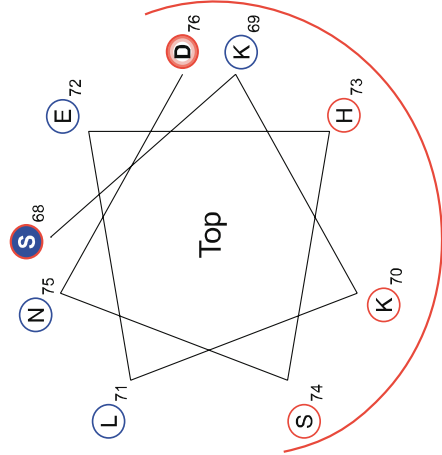
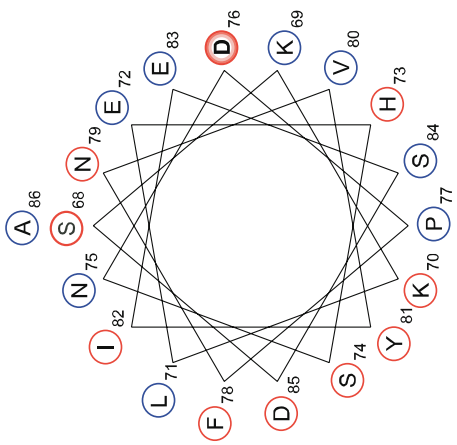
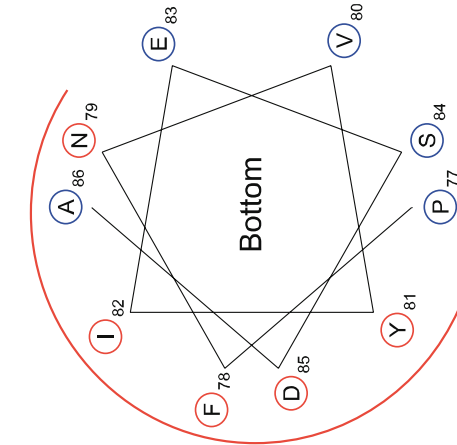


**Figure 3-2.** Periodicity of gating perturbations in the KCNE1 C-terminal domain.

*Center*, helical wheel diagram of the 19 C-terminal E1 residues examined. Red circles indicate residues with  $\Delta\Delta G_{\text{iso}} > 1$  kcal/mol, blue circles indicate  $\Delta\Delta G_{\text{iso}} \leq 1$  kcal/mol.

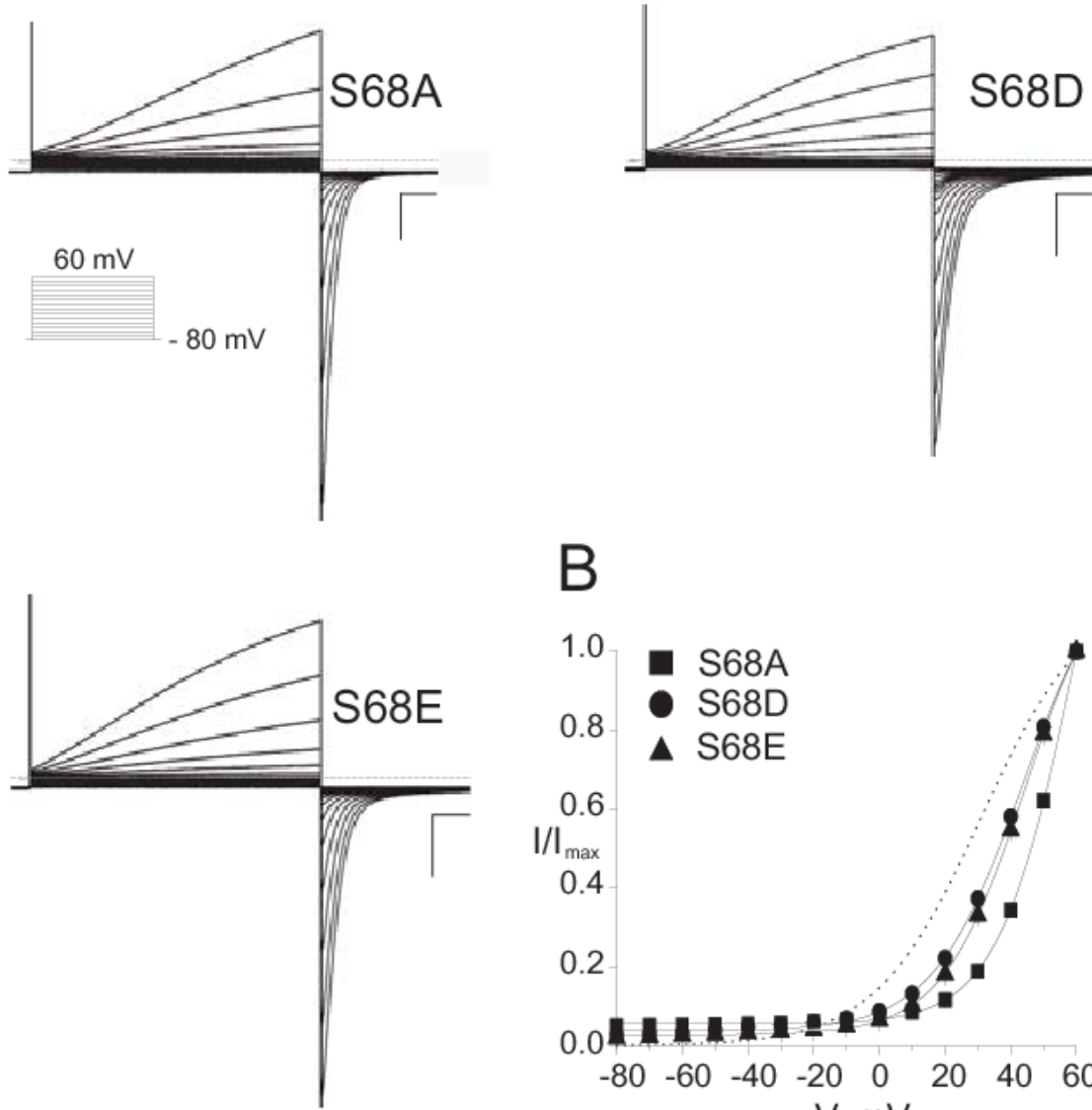
Power spectrum analysis indicates a peak angle of  $125^\circ$  and  $\alpha$ -PI of 1.77 for the entire C-terminal segment.

When residues above and below P77 are plotted on separate helical wheels (Left and Right), high impact residues (red) and low impact residues (blue) segregate to separate faces of each helical diagram. Each high impact face is denoted by a red line. S68A is a high impact residue on the low impact face (filled blue with red outline). D76A is a non-functional mutant at the plasma membrane, as determined by cell surface luminometry (red fill).

has been previously detected in transmembrane segments of two voltage-gated K<sup>+</sup> channels by perturbation mutagenesis (Hong & Miller, 2000; Li-Smerin *et al.*, 2000a). Therefore, we plotted amino acids above and below the proline on two separate helical diagrams. The residues on the bottom helical wheel (Figure 3-2, right) segregated into two distinct faces. Clustering of the high and low impact residues was also observed for the top helical diagram (Figure 3-2, left); however, there were two high impact serines (S68 and S74) and the non-functional mutant (D76A) that warranted further experimental investigation.

S68A is a noticeable outlier in the top helical wheel landing in the low impact face. Sequence analysis indicates that S68 is within a putative protein kinase C (PKC) consensus sequence, suggesting that this serine may be phosphorylated. Since the premise of perturbation mutagenesis is that alterations in side chain volume lead to disruption of protein-protein interactions and thus channel function, we wondered whether S68A scored as high impact due to the inability to posttranslationally place a negative charge at this position, and not due to a change in side chain volume. To test this hypothesis, we mutated S68 to aspartic and glutamic acid: two commonly used imperfect isosteres of phosphorylated serine. Figure 3-3A shows the current-voltage relationships of the S68A, D, and E mutants. Activation curves (Figure 3-3B) show that substitution with either aspartic or glutamic acid had less of an effect ( $\Delta\Delta G_{\text{iso}} \sim 1$  kcal/mol) than the alanine mutant ( $\Delta\Delta G_{\text{iso}} \sim 2$  kcal/mol). If S68 is phosphorylated by PKC, mutation of the surrounding consensus sequence should also have a similar effect on Q1-E1 complex function. Substituting K70 with glutamine is predicted by oriented

**A**



**B**

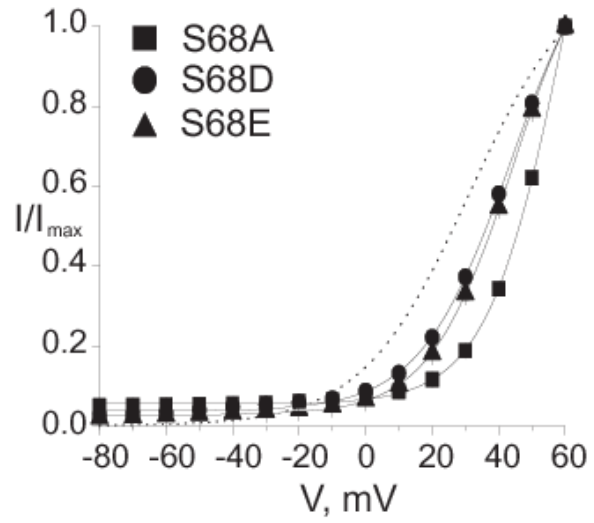


**Figure 3-3.** Negatively charged side chains produce smaller perturbations than alanine at position S68. **A**, TEVC recordings of S68A and S68D channels expressed in *Xenopus* oocytes. Currents were recorded in KD98 solution. Dotted line indicates zero current. Scale bars represent 1  $\mu$ A and 0.5 s. **Inset**, protocol of 4 s depolarizations from  $-80$  mV to  $60$  mV at  $10$  mV increments used to elicit currents shown. **B**, voltage activation curves for S68A, S68D and S68E mutant channels calculated from tail current analysis. Solid curves represent Boltzmann fits to the data. Dashed line indicates Boltzmann fit of WT activation curve. Data was averaged from 8 – 10 oocytes each  $\pm$  S.E.M.

peptide libraries to disrupt the PKC consensus sequence (Nishikawa et al., 1997), yet this polar residue produces a nominal change in side chain volume. Like S68A, the K70Q mutant shifts the voltage-dependence of activation of the Q1-E1 complex in favor of the closed state (Table 3-1).

Of the native serines in the E1 C-terminal region, S74 was unique in that the alanine mutant was defined as low impact whereas the leucine mutant was high impact. Upon breaking the region in two halves, S74 was positioned at the high/low impact interface of the helical wheel (Figure 3-2, left). We hypothesized that if S74 was at the water-protein interface, side chains with a higher degree of rotational freedom could utilize the adjacent aqueous environment to adopt a conformation that would maintain productive protein-protein interactions without steric clashes whereas the more rigid, branched side-chains could not. Conveniently, leucine, isoleucine and methionine have approximately the same Van der Waals volume (Creighton, 1992), yet their flexibility and the 3-dimensional space that they occupy is significantly different. Figure 3-4 shows that mutating E1 S74 to the straight-chain methionine afforded a Q1-complex similar to WT whereas mutation to the  $\beta$ -branched isoleucine resulted in a Q1-E1 complex similar to leucine, which was defined as high impact (Table 3-1).

D76A was the only alanine mutation that did not express measurable current when co-injected with Q1 mRNA. There are two possibilities to explain the negligible current observed with this mutation: (1) the Q1-D76A complex is non-functional. (2) The Q1-D76A complex cannot reach the plasma membrane. To discern between these



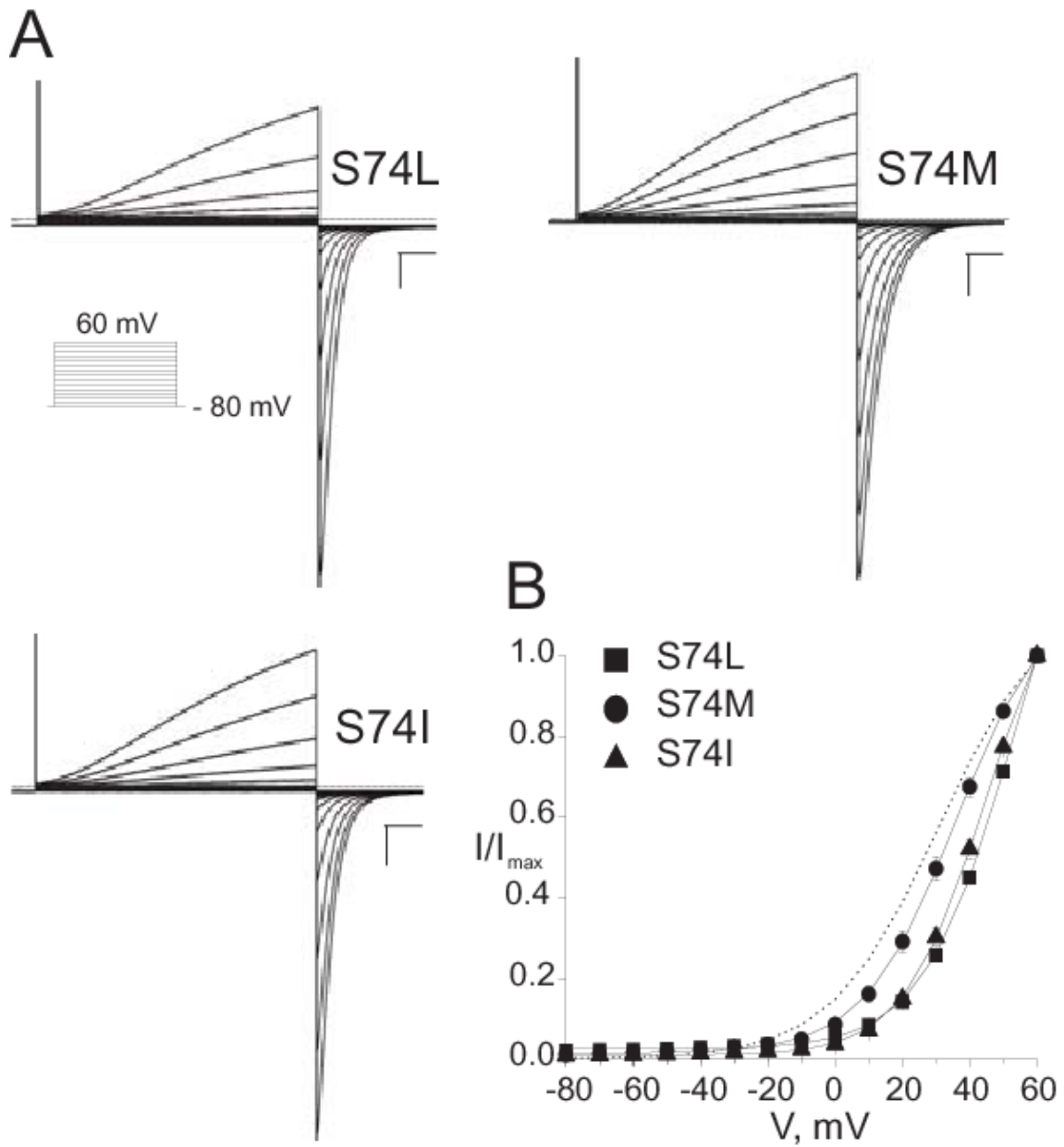


**Figure 3-4.** Branched amino acids cause larger perturbations at position S74. **A**, TEVC recordings of S74L, S74M and S74I channels expressed in *Xenopus* oocytes. Currents were recorded in KD98 solution. Dashed line indicates zero current. Scale bars represent 1  $\mu$ A and 0.5 s. **Inset**, protocol of 4 s depolarizations from  $-80$  mV to  $60$  mV at  $10$  mV increments used to elicit currents shown. **B**, voltage activation curves for S74 mutant channels calculated from tail current analysis. Solid curves represent Boltzmann fits to the data. Dashed line indicates Boltzmann fit of WT activation curve. Data was averaged from 6 – 10 oocytes each  $\pm$  S.E.M.

two, we used whole oocyte cell surface luminometry to determine whether an extracellularly HA-tagged version of D76A could reach the plasma membrane. Figure 3-5A shows that D76A protein is present at the plasma membrane similarly to WT and the Long QT causing mutant D76N, which has also been shown to be non-functional at the cell surface (Wang & Goldstein, 1995; Gage & Kobertz, 2004). Since the Q1-D76A complex is at the plasma membrane but not conducting, this mutant was scored as a high impact residue.

Splitting the E1 C-terminal region into two domains was based on our observation that the periodicity of high and low impact mutants shifted at P77, suggesting a kink or turn at this position. To experimentally test whether the presence of a helix breaking residue at this position was required for proper Q1-E1 complex function, we mutated this proline to amino acids that are known to either induce flexibility or maintain  $\alpha$ -helicity. Both alanine and leucine are often found in helical regions and are considered helix-inducing (Rohl et al., 1996). Substitution of either of these residues at position 77 produced Q1-complexes similar to WT (Table 3-1). Exchanging the proline for the highly flexible glycine residue did not afford currents above uninjected controls.

The lack of an obvious trend with this mutagenic discourse prompted us to use Fourier transform periodicity analysis to determine the amount of helicity in each segment and the location of the helical phase change. This non-biased analysis has been used to define the helical segments within an entire voltage-sensing domain of a mammalian  $K^+$  channel (Li-Smerin et al., 2000a). Determining the periodicity of a region using a power spectrum requires a  $\Delta\Delta G_{\text{iso}}$  value for every residue. To satisfy this

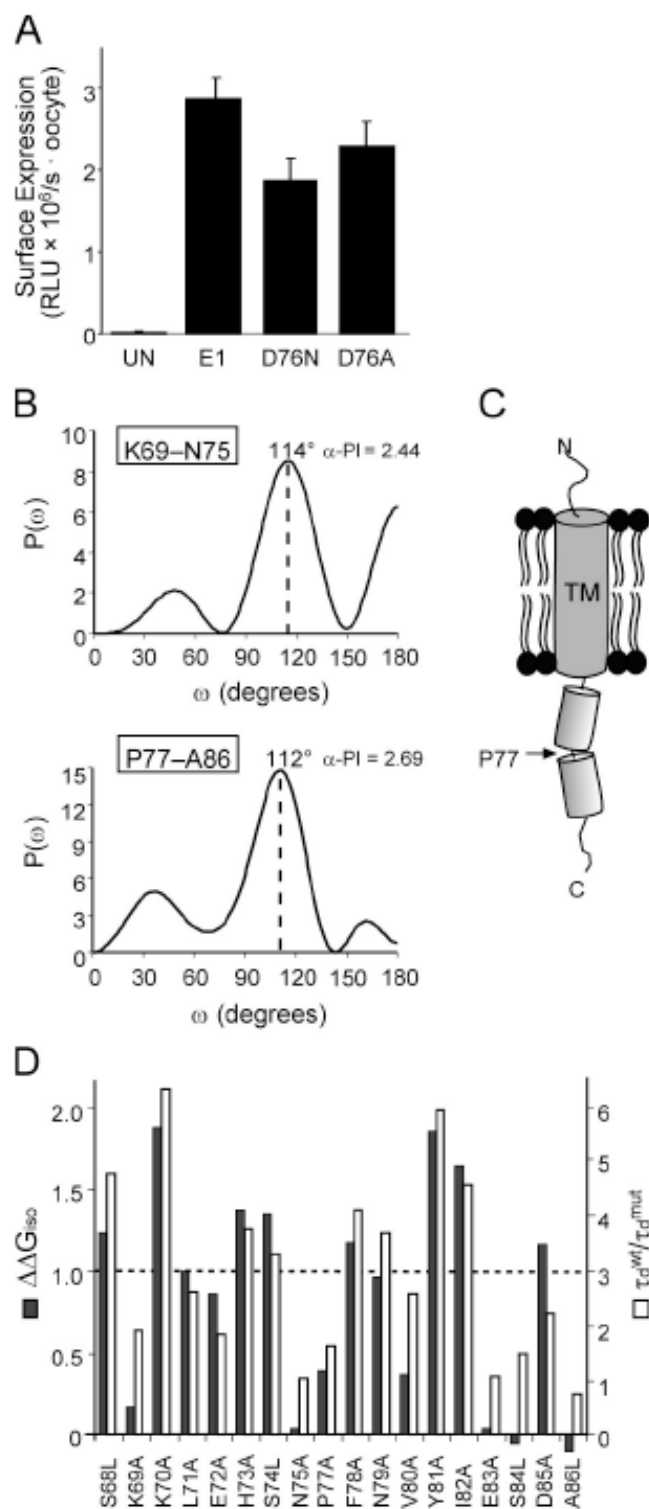


**Figure 3-5.** The transmembrane-abutting C-terminal domain is comprised of two helical regions. **A**, whole oocyte luminometry was used to quantify the surface expression of HA-tagged E1 peptides (E1, D76N, D76A) and uninjected controls (UN). Luminescence is reported in relative light units (RLU). Error bars represent standard error measurement (s.e.m.) from 10 – 20 oocytes. **B**, periodicity analysis of the top (K69–D76) and bottom (P77–A86) segments of the E1 C-terminal domain.  $P(\omega)$  is plotted as a function of angular frequency ( $\omega$ ) to generate a power spectrum of the  $\Delta\Delta G_{\text{iso}}$  values for each segment. A value of 1 kcal/mol was assigned for the non-functional D76A mutant. The primary peak occurs at  $114^\circ$  for the top segment and  $112^\circ$  for the bottom. **C**, a cartoon of the cytoplasmic E1 C-terminal domain split into two helical regions by a kink or turn. **D**, changes in deactivation rates mirror isochronal  $\Delta\Delta G$  measurements for the E1 C-terminal domain mutants. Double bar graph comparing  $\Delta\Delta G_{\text{iso}}$  and deactivation rates ( $\tau_d$ ) for the E1 C-terminal alanine and leucine mutants. Solid bars indicate  $\Delta\Delta G_{\text{iso}}$ , open bars  $\tau_d^{\text{WT}}/\tau_d^{\text{mutant}}$ . The dashed denotes the cut-off values for  $\Delta\Delta G_{\text{iso}}$  and  $\tau_d^{\text{WT}}/\tau_d^{\text{mutant}}$ .

requirement, we excluded D76A since it was non functional and S68A given the uncertainty of the native state of this side chain in the functioning Q1-E1 complex. Figure 3-5B shows the power spectra for K69 – N75 and P77 – A86 when the E1 C-terminal region is broken into two halves at P77. Both spectra show a peak angle within the boundaries of helicity ( $90^\circ - 120^\circ$ ) and with  $\alpha$ -periodicity index ( $\alpha$ -PI) greater than 2. These results are highly indicative of two helical domains (Figure 3-5C), as was observed using simple helical wheel models (Figure 3-2). We then varied the position of the breakpoint to determine whether P77 was the ideal spot to divide the E1 C-terminal domain. Since we cannot assign a  $\Delta\Delta G_{iso}$  value for D76A, we used a placeholder value for D76 to maintain the helical trajectory of the K69 – N75 segment and asked whether this helical domain extended beyond this residue. Propagation of the domain to include P77 and F78 resulted in sharp drop in  $\alpha$ -PI, indicating that residues past D76 should not be included in the top segment (Table 3-2). For the bottom segment, the  $\alpha$ -PI increased as the analysis was extended to include the proline while the peak angle remained consistent for a helix. However, inclusion of D76 using any high impact value greater than 1 kcal/mol decreased the  $\alpha$ -PI, indicating that this high impact residue was out of helical phase with the bottom segment. Taken together, dividing the entire E1 C-terminal domain at any position other than P77 resulted in less helical character for either the top or the bottom segments.

## **DISCUSSION**

We have used perturbation mutagenesis and helicity analysis to identify secondary structural elements in the conserved cytoplasmic region of the E1  $\beta$ -subunit. Previous perturbation studies have primarily relied on comparing the free energy of channel opening of mutant channels versus wild type (Monks *et al.*, 1999; Hong & Miller, 2000; Li-Smerin *et al.*, 2000a, 2000b). To utilize this parameter for Q1-E1 complexes, which do not reach equilibrium under standard-length test depolarizations, we measured isochronal  $\Delta\Delta G$ s. Although these values are not free energies, they allowed for a comparative analysis of the effect of mutations in E1 on Q1 function. Half of the mutations studied in the E1 C-terminus gave  $|\Delta\Delta G_{\text{iso}}| > 1$  kcal/mol—an arbitrarily defined cut-off for a high impact residue, but an empirically supported definition (Monks *et al.*, 1999; Hong & Miller, 2000; Li-Smerin *et al.*, 2000a, 2000b). Changes in deactivation kinetics have also been used to define high impact residues, though a specific cut-off value has not emerged from previous reports (Monks *et al.*, 1999; Hong & Miller, 2000). Graphing the deactivation kinetics of the E1 mutants reveals that a 3-fold acceleration of channel closing rate mirrors the trend observed with isochronally measured  $\Delta\Delta G_{\text{iso}}$  (Figure 3-5D). Only one mutant, D76A, was refractory from this straightforward functional analysis since it did not generate measurable currents. However, cell surface labeling experiments show that this mutant is at the plasma membrane and is non-functional, and thus we can define it as high impact. Although only two mutations (D76A and the Long QT causing D76N) have been examined at this

Table 3-2.  $\alpha$ -helical Characteristics of C-terminal E1 Segments<sup>b</sup>

Segment	$\alpha$ -PI	Peak angle	Segment	$\alpha$ -PI	Peak angle
K69 – N75	2.44	114°	P77 – A86	2.69	112°
K69 – P77	1.61	123°	F78 – A86	2.53	109°
K69 – F78	1.51	126°	N79 – A86	2.20	111°

<sup>b</sup> Data from power spectrum periodicity analysis of  $\Delta\Delta G_{\text{iso}}$  for residues in each segment. Power spectra,  $\alpha$ -PI and peak angle values were calculated as described in Materials and Methods. For the top segments that contain D76, a placeholder value of 1 kcal/mol was used, which maintains the helical trajectory of the K69 – N75 segment.



position, it is interesting that both substitutions render the Q1-E1 complex non-functional, yet the complex traffics to the plasma membrane efficiently.

Plotting the residues on a helical wheel resulted in no obvious clustering of high impact residues (Figure 3-2, center). Periodicity analysis using a power spectrum confirmed that no helical pattern was present: both the peak angle ( $125^\circ$ ) and  $\alpha$ -PI (1.77) were inconsistent with the region being a continuous helix. However, breaking the cytoplasmic region into two domains at a conserved proline (P77) segregated the high and low impact residues to distinct faces on helical wheels. In addition, Fourier periodicity analysis indicate that both domains have significant helical character (Table 3-2), which supports the arbitrarily defined 1 kcal/mol cut-off value used for the helical wheel diagrams (Figure 3-2). Moreover, this depiction places all known Long QT mutants in this region on the high impact face. Given that the mutants in the high impact face markedly shift the gating of Q1-E1 complexes, we predict that these residues directly interact with Q1. This prediction is supported in high resolution detail with the crystal structures of voltage-gated  $K^+$  channels (Jiang et al., 2003a; Jiang et al., 2003b; Long et al., 2005a), which have verified that the high impact faces identified by previous perturbation studies are involved in protein-protein interactions within the voltage-sensing domain.

Although we observed a convincing pattern with helical wheel diagrams for the E1 C-terminal domain, S68A did not segregate to the high impact face, yet it had the highest  $\Delta\Delta G_{iso}$  calculated. S68 is within a putative PKC consensus sequence. Disruption of the PKC site by mutation of the critical +2 basic residue (K70) to either glutamine or

alanine resulted in Q1-E1 complexes with right-shifted activation curves similar to S68A, which cannot be phosphorylated. Although phosphorylation of E1 at this serine has not been observed experimentally, it has been detected in the homologous serine in E3 (Abbott et al., 2006). Substitution of S68 to either aspartic or glutamic acid, to mimic phosphoserine, showed that the more voluminous, but negatively charged side chains had less of an effect on Q1-E1 gating than the removal of hydroxyl group by alanine mutagenesis. These preliminary data suggest that E1 may be phosphorylated at S68, but requires further biochemical support and verification in native tissues.

Unlike S68 and S84, S74 was uniquely sensitive to changes in amino acid side chain volume in that only the bulkier S74L mutant scored as high impact. Helical analysis revealed that this residue was at the edge of the high impact face, which prompted us to experimentally examine whether this was the case. Isovoluminous substitution showed that branched amino acids (isoleucine, leucine) were less tolerated than the straight chain methionine side chain, which scored as a low impact residue using both criteria ( $\Delta\Delta G_{\text{iso}}$  and  $\tau_d$ ). These results are consistent with the notion that S74 lies at the water-protein boundary since the flexible methionine side chain can adopt a productive protein-protein interaction between E1 and the Q1-channel complex while utilizing the adjacent aqueous environment without energetic penalty.

Previous perturbation studies of voltage-gated  $K^+$  channels had identified a proline residue in the S3 helix that disrupted the helical pattern of this transmembrane domain (Hong & Miller, 2000; Li-Smerin *et al.*, 2000a). This functional analysis proposed that the S3 helix would be kinked at this proline residue, which was

subsequently confirmed by three high resolution crystal structures of voltage sensing domains (Jiang et al., 2003a; Jiang et al., 2003b; Long et al., 2005a). Since our perturbation results afforded a strong helical pattern when the E1 C-terminal domain is divided in half at a proline residue, we hypothesized that P77 is inducing a kink or turn at this position. We attempted to mimic this kink by mutation to the helix breaking residue, glycine, but were unable to measure any currents above background when this mutant was expressed with Q1. To determine if the proline geometry was required for proper modulation of Q1 channels, we mutated P77 to alanine and leucine, two residues that have a high helix propensity (Rohl et al., 1996). When these mutants were expressed with Q1 subunits, K<sup>+</sup> currents and gating characteristics similar to wild type Q1-E1 complexes were observed. Identical results (with alanine and tryptophan) were also obtained for the helix kinking proline in the S3 segment of K<sup>+</sup> channel voltage sensors (Hong & Miller, 2000; Li-Smerin *et al.*, 2000a), suggesting that detection of proline kinks using channel function and simple site-directed mutagenesis may not be possible. This conclusion is further supported by a systematic investigation of conserved proline residues in membrane proteins, which has shown that many protein-protein interfaces evolve ancillary interactions to stabilize kinked helices thus obviating the need for proline residues to maintain the bent geometry (Yohannan et al., 2004).

Since mutagenesis could not elucidate whether a turn or kink was present at P77, we relied on power spectrum analysis to identify the location of the phase change in the E1 C-terminal domain. Using this mathematical approach, breaking the domain at P77 resulted in two segments with the greatest  $\alpha$ -PI and peak angles most consistent with

helices that are adjacent to transmembrane domains (Table 3-2). This analysis indicates that the E1 C-terminal domain is helical with either a kink at P77 (Figure 3-5C) or the domain experiences a different protein environment above the proline residue, which may also be influenced by PKC phosphorylation. Sequence similarity of this membrane-abutting domain predicts that E2, E3 and E5 will possess a similar structural motif and protein environment when co-assembled with Q1 subunits.

This conserved structural scaffold adds to the growing body of evidence that the E1 C-terminal domain is critical for Q1 channel modulation. Initial E1 deletion studies showed that removal of the membrane-abutting cytoplasmic domain eliminates the hallmark slow activation/deactivation kinetics of the Q1-E1 complex (Tapper & George, 2000). In addition, a recent E3 deletion study also concluded that the E1 C-terminus was required for Q1 modulation, but not necessary for E3 modulation (Gage & Kobertz, 2004). Our alanine mutants also support this separation of KCNE modulation of Q1. Alanine mutants in E1 had significant effects on the voltage-dependence and deactivation kinetics of Q1-E1 complexes whereas the equivalent mutations in E3 had no measurable effect on the constitutively conducting Q1-E3 complex (unpublished results). Similarly, tryptophan mutants in the E1 transmembrane domain—though structurally informative—were consistently less perturbative on Q1-E1 complex function than C-terminal E1 alanine mutants (SAN Goldstein, personal communication).

The cytoplasmic E1 C-terminal domain also provides a structural platform for potential interactions with tethered water soluble regulatory proteins. Calmodulin was recently shown to bind to the Q1 C-terminus relatively close to the S6 transmembrane

segment and facilitates channel assembly and calcium sensitivity (Shamgar et al., 2006). Adjacent to the Q1 calmodulin binding site is a leucine zipper sequence that is required for yotiao, an A-kinase anchoring protein, to bind (Marx et al., 2002). Anchoring of yotiao to the Q1 C-terminus targets cAMP-dependent protein kinase (PKA) and protein phosphatase 1 (PP1), which control the phosphorylation state of the Q1 N-terminus. Moreover, this PKA-mediated modulation can be disrupted by genetic mutations within the E1 cytoplasmic domain (Kurokawa et al., 2003). Thus, the manifold nature of Q1-E1 complex regulation suggests that high impact regions identified in the C-terminus of E1 may be revealing protein-protein interactions not only with Q1  $\alpha$ -subunits, but also with tethered cytoplasmic regulatory proteins.

## **MATERIALS AND METHODS**

***Mutagenesis and in vitro transcription*** - Human Q1 and E1 were subcloned into vectors containing the 5' and 3' UTRs from the *Xenopus*  $\beta$ -globin gene for optimal protein expression. Single point mutations were introduced into E1 using Quickchange site-directed mutagenesis (Stratagene) and confirmed by DNA sequencing of the entire gene. For all surface luminometry experiments, the hemagglutinin A (HA) tag, YPYDVPDYA, was incorporated into the N-terminus of E1 between residues 22 and 23 (Wang & Goldstein, 1995). The cDNA plasmids were linearized by MluI digestion, and cRNA synthesized by run-off transcription using SP6 or T7 RNA polymerase (Promega).

**Electrophysiology** - Oocytes were surgically removed from *Xenopus laevis* and defolliculated using 2 mg/mL collagenase (Worthington Biochemical Corp.) in OR2 containing (mM): 82.5 NaCl, 2.5 KCl, 1 MgCl<sub>2</sub>, 5 HEPES, pH 7.4 for 75-90 min. Isolated oocytes were rinsed with and stored in ND96 bathing solution (ND96B) containing (mM): 96 NaCl, 2 KCl, 1.8 CaCl<sub>2</sub>, 1 MgCl<sub>2</sub>, 5 HEPES, 50 µg/mL gentamicin (Sigma-Aldrich), pH 7.4 at 18°C. Approximately 24 h after extraction, oocytes were microinjected with 27.6 nL total volume of cRNA containing Q1 (7.5 ng/oocyte) and E1 (3.75 ng/oocyte). After 3–6 days, currents were recorded using Warner Instrument (OC-725) two-electrode voltage clamp (TEVC) and the data were acquired with Digidata 1322A using pClamp 8 or 9 (Axon Instruments). Electrodes were filled with 3 M KCl, 5 mM EGTA, 10 mM HEPES, pH 7.6, and had resistance between 0.2 and 1.0 MΩ. For each experiment, oocytes were held at – 80 mV in ND96 (in mM): 96 NaCl, 2 KCl, 0.3 CaCl<sub>2</sub>, 1 MgCl<sub>2</sub>, 5 HEPES, pH 7.4, and pulsed to a command potential of 40 mV. Oocytes injected with Q1 and wild type or mutant E1 RNA were only recorded from if a 4-s pulse to 40 mV produced current greater than 1 µA to ensure that currents were coming from exogenously injected channel complexes. Tail currents for activation curves were measured in KD98 (in mM): 98 KCl, 0.3 CaCl<sub>2</sub>, 1 MgCl<sub>2</sub>, 5 HEPES, pH 7.4. Oocytes were held at – 80 mV and the tail current protocol was a series of 4 s test pulses to potentials between – 100 and + 60 mV in 10 mV increments. For severely right-shifted mutants (F78A and Y81A), test pulses between – 100 and + 80 mV were used.

**Data Analysis** - The amplitude of tail currents was measured 6 ms after repolarization to  $-80$  mV and normalized such that the maximal current was equal to 1. Normalized tail currents were plotted versus the depolarized potential to produce activation curves for wild type and mutant E1 channel complexes. Activation curves were fit to a Boltzmann function,  $I/I_{\max} = A2 + (A1 - A2) / (1 + e^{(V - V_{1/2}) * (-zF/RT)})$ , where  $I/I_{\max}$  is the normalized tail current amplitude,  $V_{1/2}$  is the midpoint of activation,  $z$  is the maximum slope,  $F$  is Faraday's constant,  $R$  is the gas constant and  $T$  is temperature in Kelvin. The upper and lower asymptotes,  $A1$  and  $A2$ , were left to vary, allowing data to be fit since Q1-E1 complexes did not fully activate in the voltage ranges that can be used with oocytes (Gage & Kobertz, 2004). The isochronal free energy of channel opening,  $\Delta G_{\text{iso}}$ , was calculated for wild type (WT) and each mutant Q1-E1 complex using the equation  $\Delta G_{\text{iso}} = zFV_{1/2}$ . For each mutant,  $\Delta\Delta G_{\text{iso}}$  was calculated as  $\Delta G_{\text{iso}}^{\text{mutant}} - \Delta G_{\text{iso}}^{\text{WT}}$ . The deactivation time constant ( $\tau_d$ ) was measured by fitting the current at  $-80$  mV following a 40 mV depolarization to a single exponential.

**Periodicity Analysis** - The periodicity of  $\Delta\Delta G_{\text{iso}}$  was determined as previously reported by Swartz et al. using the following equation (Li-Smerin et al., 2000a):

$$P(\omega) = \sum_{j=1}^n [(V_j - \langle V \rangle) \sin(j\omega)] + \sum_{j=1}^n [(V_j - \langle V \rangle) \cos(j\omega)] ,$$

where  $P(\omega)$  is the power spectrum as a function of angular frequency,  $\omega$ , and was determined for E1 C-terminal segments of 7 to 10 residues where  $\langle V \rangle$  is the average  $|\Delta\Delta G_{\text{iso}}|$  for each segment,  $V_j$  is the  $\Delta\Delta G_{\text{iso}}$  at position  $j$ , and  $n$  is the number of residues in

a segment. Since  $\alpha$ -helices are defined as having 3.6 residues per turn, a peak angle at  $100^\circ$  indicates an ideal  $\alpha$ -helix. Transmembrane helices have shown peak angles shifted to higher frequencies, and since this membrane abutting C-terminal region is presumably an extension of the membrane spanning helix, we centered our analysis at  $105^\circ$  (Rees et al., 1989; Li-Smerin et al., 2000a). The  $\alpha$ -periodicity index ( $\alpha$ -PI) is the average value of  $P(\omega)$  in this helical range ( $90^\circ - 120^\circ$ ) relative to the average value of  $P(\omega)$  over the entire power spectrum and is a quantitative assessment of helical character:

$$\alpha\text{-PI} = \left[ \frac{1}{30} \int_{90^\circ}^{120^\circ} P(\omega) d\omega \right] / \left[ \frac{1}{180} \int_{0^\circ}^{180^\circ} P(\omega) d\omega \right],$$

values for  $\alpha$ -PI greater than 2 are considered indicative of an  $\alpha$ -helix. For mathematical analyses that necessitated the inclusion of the non-functional D76A mutant, a  $\Delta\Delta G_{\text{iso}}$  value of 1 kcal/mole was used to maintain the  $\alpha$ -PI and peak angle calculated for the K69 – N75 segment.

***Cell Surface Luminometry*** - The surface expression of HA-tagged E1 proteins was measured by luminometry (Zerangue et al., 1999). Oocytes were injected with 7.5 ng Q1 and 3.75 ng wild type (WT) or mutant E1-HA. After 3-5 days, currents were recorded from a few oocytes expressing WT E1-HA complexes to ensure that functioning complexes were present at the cell surface. ND96 containing 1% bovine serum albumin (BSA) was used to block and wash oocytes, as well as dilute antibodies. Oocytes were cooled to  $4^\circ\text{C}$ , blocked for 30 min, and primary antibody (1  $\mu\text{g}/\text{mL}$  rat monoclonal  $\alpha$ -HA, Roche) was applied for 1 h at  $4^\circ\text{C}$ . Oocytes were washed ( $8 \times 5$  min), incubated for



40 min with secondary antibody (2  $\mu\text{g}/\text{mL}$   $\alpha$ -rat F(ab)<sub>2</sub>, Jackson ImmunoResearch Laboratories), and washed again (5  $\times$  10 min). Oocytes were finally washed with ND96 containing no BSA for 1 h at 4°C, individually placed in wells with 50  $\mu\text{L}$  of ND96 solution and mixed with 50  $\mu\text{L}$  of the SuperSignal ELISA Femto Maximum Sensitivity Substrate (Pierce Chemical Co.). The signal at 405 nm was integrated for 10 s after a 20 s delay using a Veritas Microplate luminometer (Turner Biosystems). Data is reported in relative light units, RLU.

**CHAPTER IV**  
**THE INTRACELLULAR, JUXTAMEMBRANOUS DOMAIN OF KCNE1**  
**INTERACTS DIRECTLY WITH THE CYTOPLASMIC FACE OF THE KCNQ1**  
**PORE DOMAIN**

**ABSTRACT**

KCNQ1 forms a homotetrameric, voltage-gated potassium channel found in a variety of tissues including heart muscle and epithelial cells. To generate the diversity of potassium currents required by these different tissues, KCNQ1 subunits assemble with KCNE type I transmembrane peptides to produce membrane-embedded complexes with varied gating kinetics. In cardiomyocytes, KCNQ1/KCNE1 (Q1/E1) complexes produce the  $I_{Ks}$  current, which contributes to the termination of action potentials and provides cardiac repolarization reserve.  $I_{Ks}$  is essential for normal heart rhythmicity. Mutations in both E1 and Q1 give rise to Long QT syndrome, a congenital arrhythmia that can cause *torsade de pointes*, fibrillation and sudden death. The slow gating kinetics of  $I_{Ks}$  stem from potential interactions ostensibly between Q1 and the cytoplasmic C-terminal domain of E1 (Rocheleau et al. 2006 *Journal of General Physiology* **128**, 721-729; Tapper & George 2000 *Journal of General Physiology* **116**, 379-389). We used oxidant-mediated cysteine cross-linking to further resolve these protein-protein interactions to faces and discrete amino acid pairings between Q1 and E1 peptides. We found within the

membrane-abutting C-terminal region of E1 side chains residues which are associated with discrete amino acids in the Q1 S4-S5 linker and the S6 gate; many of these pairings correspond well with Long QT mutations in both Q1 and E1. Co-expression of cysteine pairings give rise to  $I_{Ks}$  oxidation sensitive currents in whole-cell perforated patch clamp experiments. Our results demonstrate that Q1 and E1 interact on their cytoplasmic exposed surfaces and suggest Long QT mutations in this region of the channel complex disrupt native protein-protein interactions required for  $I_{Ks}$  function.

## **INTRODUCTION**

KCNQ1 (Q1) forms homotetrameric, voltage-gated, potassium-conducting complexes found in a variety of tissues. Despite the presence of Q1 in many different tissues, currents arising from over-expressed Q1 channels have not been physiologically observed. When Q1 assembles with and is modulated by small, type I transmembrane peptides of the KCNE family, Q1 acquires its proper physiological and biosynthetic properties; it is through KCNE-interactions that Q1 channels are able to meet the tissue specific requirements for potassium conduction (McCrossan & Abbott, 2004). In complexes shared with KCNE1 (E1), Q1 channels give rise to the  $I_{Ks}$  potassium current (Barhanin et al., 1996; Sanguinetti et al., 1996).  $I_{Ks}$  is essential for normal heart rhythmicity because  $I_{Ks}$  is responsible in part for repolarizing heart muscle after every depolarization and provides cardiac repolarization reserve. Mutation in either  $I_{Ks}$  subunit can cause the cardiac dysfunction Long QT Syndrome, a lengthening of the Q-T time interval which can lead to seizures, *torsades de pointes* and fibrillation. Recessive Long

QT syndrome associated with  $I_{Ks}$  is called Jervell and Lange-Nielsen syndrome and occurs with bilateral deafnesses (Splawski *et al.*, 1997; Wollnik *et al.*, 1997; Splawski *et al.*, 2000; Keating & Sanguinetti, 2001; Silva & Rudy, 2005).

The mechanism of KCNE modulation of Q1 channel complexes is not fully understood. Chimeric and partially truncated KCNE peptides demonstrated KCNEs possess a bipartite modulation of Q1 channel complexes (Chapters II & III). The modulation of KCNE peptides residing in the transmembrane domain is either permissive and allows C-terminal KCNE modulation, or it is active and masks the modulation of the KCNE C-terminus (Tapper & George, 2000; Melman *et al.*, 2001; Melman *et al.*, 2002a; Gage & Kobertz, 2004). The KCNE transmembrane domain is in close proximity to both the pore and the voltage sensor of Q1 (Wang *et al.*, 1996; Tai & Goldstein, 1998; Tapper & George, 2001; Melman *et al.*, 2004; Panaghie & Abbott, 2007; Shamgar *et al.*, 2008); therefore, the simplest model for KCNE modulation would entail KCNEs acting directly on the Q1 voltage sensor. This appears to be the case with the active KCNE3 transmembrane domain (Nakajo & Kubo, 2007; Rocheleau & Kobertz, 2008). Measurements of voltage sensor accessibility to chemical modification within Q1/E1 complexes have demonstrated voltage sensor movement and gating movements are uncoupled, an observation which neither confirms nor denies a transmembrane interaction (Nakajo & Kubo, 2007; Rocheleau & Kobertz, 2008). E1 may also be able to interact with and alter the activity of the calmodulin-Q1 interaction (Ghosh *et al.*, 2006; Shamgar *et al.*, 2006).

Our understanding of KCNE modulation is also complicated by subunit stoichiometry within channel complexes. Not only is E1 able to break the four-fold symmetry of Q1 channel complexes (MacKinnon, 1991; Schulteis *et al.*, 1996; Doyle *et al.*, 1998; Robbins, 2001; Zhou *et al.*, 2001; Jiang *et al.*, 2002b; Jiang *et al.*, 2003a; Long *et al.*, 2005a; Long *et al.*, 2007; Morin & Kobertz, 2008), but E1 may be able to form complexes with other members of the KCNE family (Bendahhou *et al.*, 2005; Lundquist *et al.*, 2005; Toyoda *et al.*, 2006; Morin & Kobertz, 2007; Manderfield & George, 2008). Were the 2:4 stoichiometry of KCNE:Q1 not disturbed in complexes containing other KCNEs, a single E1 peptide may be able to bestow upon four Q1 subunits the properties of  $I_{Ks}$ .

We set out to better understand how E1 is able to modulate Q1. Our goal in this work was to test potential protein-protein contact points between Q1 and E1. Through oxidant-mediated disulfide bond formation between exogenous cysteine point mutations in a cysteine-null background (Schulteis *et al.*, 1996; Kobertz *et al.*, 2000), we demonstrated both proximity and juxtaposition of side chain residues between Q1 and E1 in assembled channel complexes. The particular cysteine pairings we identified occur within natively assembled and functional channel complexes on the plasma membrane, confirmed by a combination of cell-surface biotinylation, co-immunoprecipitation, PNGase F sensitivity, and  $I_{Ks}$ -like channel function determined by whole-cell perforated patch clamp. The disulfide crosslink pairings we have identified occur between the C-terminus of E1 and the cytoplasmic face of the pore region of Q1. All amino acids in E1 identified as interacting with Q1 were either previously identified as Long QT mutations

or proximal to Long QT mutations (Splawski et al., 2000). Interacting E1 residues also corresponded precisely with high-impact amino acids identified by an alanine-substitution scan performed on the C-terminus of E1 (Rocheleau et al., 2006). These findings suggest the importance of a direct interaction between the C-terminal, juxtamembranous domain of E1 and both the gate and S4-5 linker helix of Q1, and confirm the importance of the C-terminus in giving rise to E1-like KCNE modulation.

## **RESULTS**

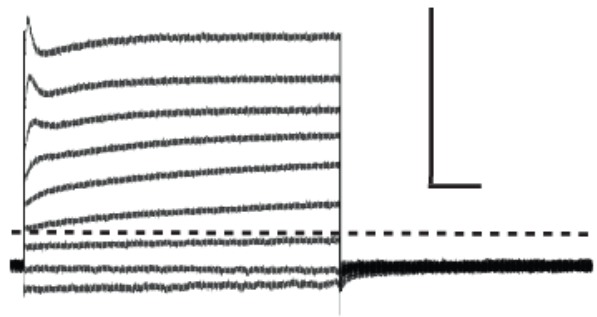
In order to biochemically test whether side chain residues in Q1 and E1 are both close in proximity and juxtaposed to one-another within functional  $I_{Ks}$  channels, we had to be certain only non-native, engineered cysteines in both subunits were able to form disulfide bound heterodimers. Therefore, we replaced all native membrane-embedded cysteines with alanine and all aqueously exposed cysteines with serine. The utilization of cysteine-deficient constructs of Q1 and E1 precluded the possibility of false-positive disulfide bond formation involving native cysteine residues. Our predictions of side chain environment were based on the X-ray crystal structure of highly homologous rKv1.2 (Long et al., 2005a) and hydrophobicity plots.

However, cysteine replacement left an important caveat – did mutation of each of these cysteines result in channel complexes with a non-native structure? We decided to indirectly test the structure of “cysless”  $I_{Ks}$  by assaying the mutant channel complexes for their biophysical properties and comparing these biophysical properties with those of the wild type channels. Perforated patch clamp was used in order to prevent “rundown” of

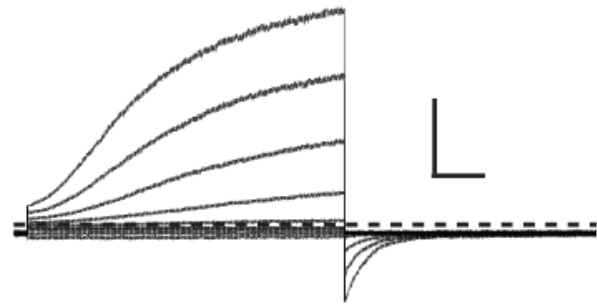
$I_{Ks}$  function observed by us and others (Selyanko et al., 2000; Kurokawa et al., 2004; Dong et al., 2006). Shown in Figure 4-1, whole-cell perforated patch clamp experiments demonstrate  $I_{Ks}$  and “ $I_{Ks}$ -cys” are mutually reminiscent, each possessing extremely slow activation and deactivation kinetics. There were two differences we observed between wild type  $I_{Ks}$  and  $I_{Ks}$ -cys. Activation curves for cysless  $I_{Ks}$  were left-shifted as compared with wild type channels; cysless  $I_{Ks}$  channels activated in response to much more negative membrane potentials. We also observed a large increase in current density – CHO-K1 cells expressing cysless constructs possessed measurable currents a full day earlier after transfection as compared with wild type constructs (data not shown). Expression of Q1 or “Q1-cys” alone gave rise to currents with much faster activation kinetics relative to  $I_{Ks}$ . Q1 currents also possess obvious inactivation; this inactivation can be easily observed as a transient decrease in current upon membrane depolarization (please refer to Figure 2-1 (Gage & Kobertz, 2004), wild type Q1 recordings taken from *Xenopus laevis* oocytes using two-electrode voltage clamp running a similar voltage-pulse protocol). Because cysless Q1 and E1 gave rise to currents reminiscent of those arising from wild type Q1 and E1, we concluded our cysless construct possess native-like function and, therefore, native-like structure.

With our native structure indirectly confirmed, we commenced our scan of cysteine point mutant pairings (Figure 4-2). We conducted this scan in hypotonically lysed membranes. Hypotonic lysis removes all non-specific aqueous proteins endogenous to CHO cells, preventing many native cysteines from forming disulfide bonds with our engineered cysteine point mutations. After hypotonic lysis we maintained

Q1-cys



Q1+E1



Q1-cys+E1-cys

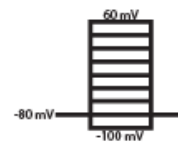
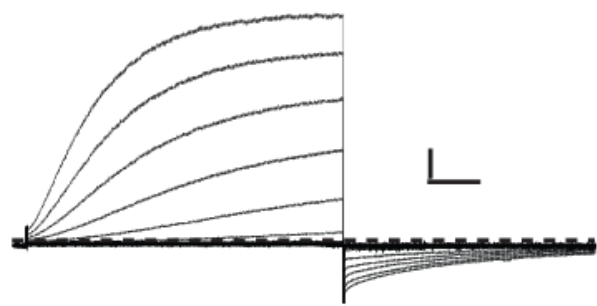




**Figure 4-1.** Native and “cysless”  $I_{Ks}$  subunits give rise to currents which are mutually reminiscent. Whole-cell perforated patch clamp recordings from CHO-K1 cells transiently transfected with  $I_{Ks}$  subunits as indicated. Scale bars denote 25 pA/pF and 0.5 s. Dashed line indicates no net current. Data are representative of  $n = 2 - 6$  recordings per pairing. **Above**, Q1-cys and empty vector. Homotetrameric Q1-cys channels give rise to current which activates much more quickly compared with  $I_{Ks}$  (*center*), and displays inactivation, visualized by a transient decrease in current occurring just after very strong depolarizations. Cysteine mutation in Q1 does not appear to substantially alter gating kinetics of Q1 homomeric channels (compare with Figure 2-1). **Center**, heteromeric Q1/E1 channels give rise to  $I_{Ks}$ .  $I_{Ks}$  lacks observable inactivation, and current increase for  $I_{Ks}$  is much slower compared with Q1-cys. **Below**, Q1-cys/E1-cys channels give rise to  $I_{Ks}$ -cys.  $I_{Ks}$ -cys also lacks inactivation and possesses very slow gating kinetics compared with Q1-cys alone. However, cysteine mutation allows Q1-cys/E1-cys channels to activate at much more negative membrane potentials as compared with native Q1/E1. **Inset**, voltage-pulse protocol used to elicit these recordings. Membranes were held at  $-80$  mV, and depolarized for 3 s to potentials between  $-100$  mV and  $+60$  mV in 20-mV increments. Depolarizations occurred every 15 s.

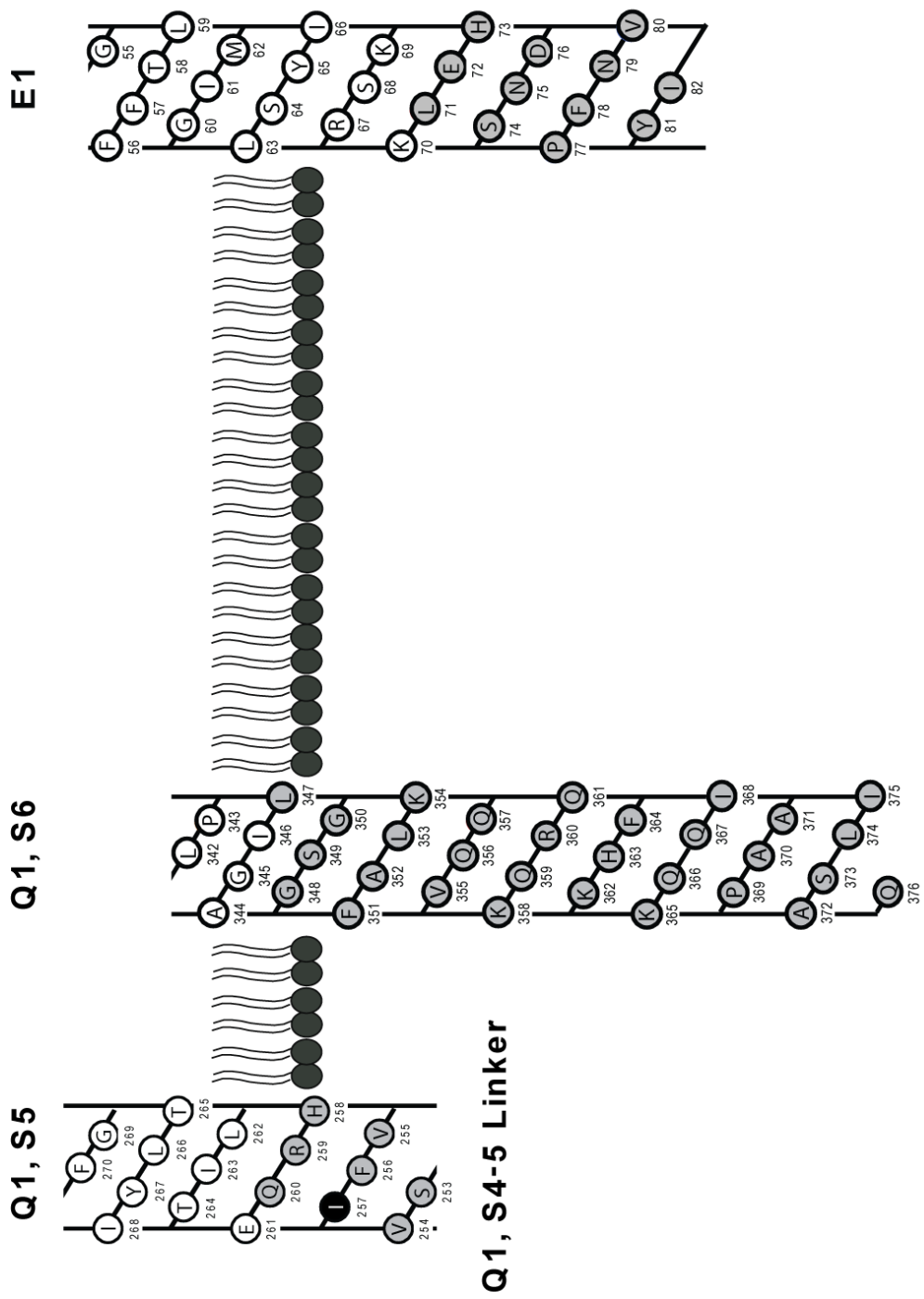


**Figure 4-2.** The positions of exogenous cysteine mutants scanned in this study. Residues are projected onto net diagrams, and though helices in this region are known to contain joints and “kinks” (Long et al., 2005a; Rocheleau et al., 2006), this projection assumes native alpha-helical secondary structure for ease of presentation. Exogenous cysteines at positions highlighted in gray or black were able to form (any) higher molecular mass species upon oxidation with greatly varying efficiency. *Left*, the cytoplasmic side of the S5 and S6 helices of Q1 are labeled, with membrane topology (relative to the intracellular face of the plasma membrane) based on homology to the crystal structure of Kv1.2 (Long et al., 2005a). I257, highlighted in black, is the joint between the S5 helix and the S4-5 linker helix. *Right*, transmembranous and C-terminal amino acid side chains of E1. The membrane topology of E1 was *a priori* estimated by hydrophobicity.

hypotonic conditions for fear of membranes resealing and preventing free aqueous access for H<sub>2</sub>O<sub>2</sub> to all parts of the channel complex. Formation of a disulfide bond must invariably result in an observable mass-shift of proteins resolved on SDS-PAGE (bound cysteine point mutant protein is covalently attached to a second sulfhydryl-containing species).

We began our scan of Q1 and E1 pairings with Q1 residues lining the aqueous reservoir on the cytoplasmic side of the selectivity filter within Q1 channel complexes. Engineered cysteine mutations were located in the fifth and sixth transmembrane helices of Q1. *A priori* we also knew the high-impact transmembrane triplet identified by Melman and colleagues is believed to interact with membrane-embedded regions of Q1 (Melman et al., 2001; Melman et al., 2002a). Only a hydrophilic environment would allow a deprotonated sulfhydryl to exist transiently before losing an electron to H<sub>2</sub>O<sub>2</sub>; therefore, attempting disulfide bond formation within the transmembrane domains of both I<sub>Ks</sub> subunits was a gambit, considering membrane-embedded side chain residues, even those in close proximity to the aqueous vestibule, might not be able to participate in disulfide bond formation.

We were not able to visualize any disulfide bond formation in the transmembrane domain of E1, nor could we visualize any disulfide bond formation with putatively aqueous cysteines replacing R67, S68, R69, or K70 (summarized in Figure 4-2, no fill). Co-expression of all E1 cysteine point mutants (except E1 G60C) resulted in maturely glycosylated E1 peptides resolving between 37 – 50 kDa (Chandrasekhar et al., 2006), indicating our E1 mutant proteins were not rapidly degraded and were able to assemble

with Q1-cys. The nature of the lack of E1 G60C expression was never explored. Our results allow two interpretations: the transmembrane domain of E1 is not close to the pore domain of Q1, or disulfide bond formation cannot occur with side chain residues located within the KCNE transmembrane domain.

Failing to find any *bona fide* disulfide-bonding pairs within the aqueous vestibule, we turned our attention towards the cytoplasmic face of Q1 channels. For these experiments we would not have to worry about the hydrophobicity of the local environment preventing disulfide bond formation, making our results easier to interpret. We identified E1 L71C and cysteine point mutants C-terminal to L71 which were readily able to form disulfide crosslink species (Figure 4-2, gray). However, the number of erstwhile crosslinks, combined with relatively poor efficiency of disulfide bond formation, led to more stringent requirements for consideration. We continued our scan until we observed disulfide bonding patterns demonstrating both periodicity in E1 (another *a priori* expectation, given the results of the alanine scan performed by Rocheleau and colleagues (Rocheleau et al., 2006)) and greater efficiency. We defined our “hits” as all of our crosslinking combinations in which the percentage of signal in the crosslinked band is significantly greater than three separate negative controls. A “bloody good” example of these crosslink pairings is presented in Figure 4-3.

Q1-cys, H363C was co-expressed with a panel of E1-cys cysteine point mutants, resolved on 15% SDS-PAGE, and immunoblotted with antibodies raised against the HA tag of E1 (Fig. 4-3A). Each pairing of Q1 and E1 yields a strong signal (observed as either a single, wide band or a doublet) measuring between 37 – 50 kDa, corresponding

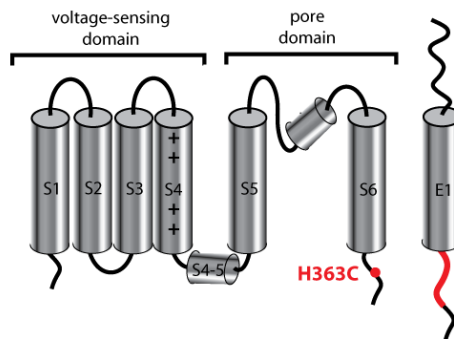
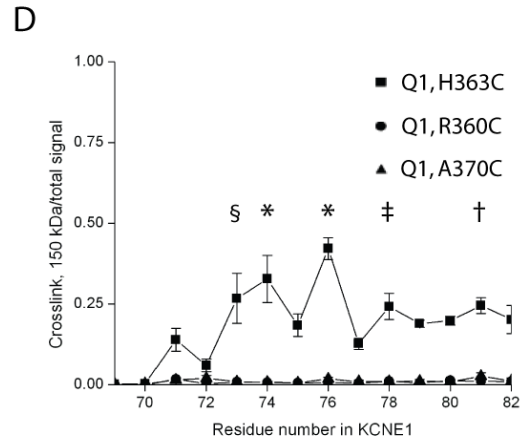
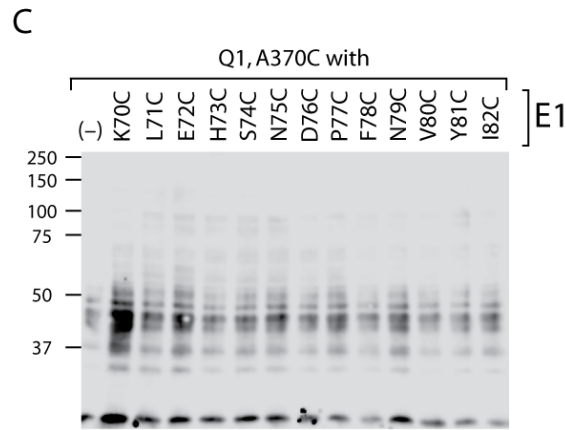
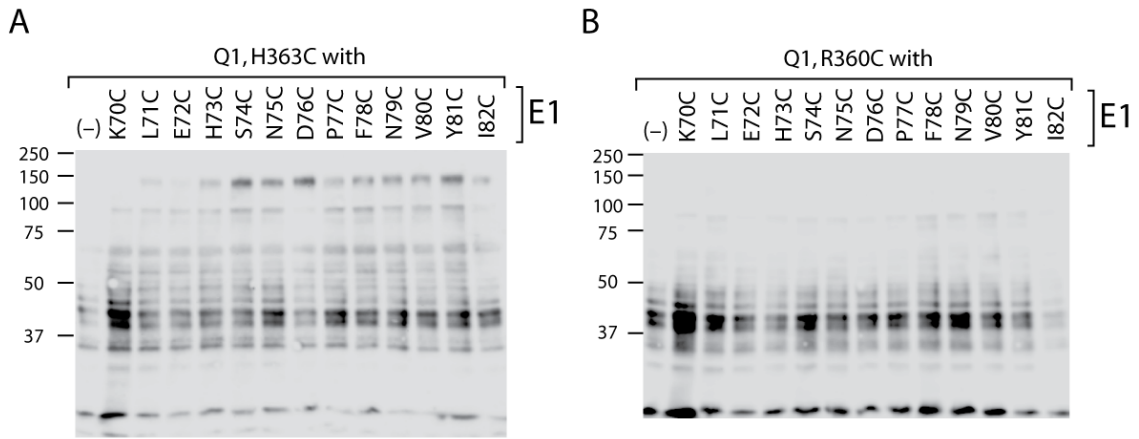


**Figure 4-3.** Q1-cys, H363C is able to form higher molecular mass species with a panel of E1-cys point mutations. **A – C**, Representative western blots of proteins oxidized by 10 min application of 0.01% H<sub>2</sub>O<sub>2</sub> in hypotonically lysed membranes, resolved on non-reducing SDS-PAGE and immunoblotted with  $\alpha$ -E1. E1-cys point mutants are labeled above and molecular weight markers are labeled on the left. “(-)” indicates our internal negative control, E1 C106S. All E1 point mutants produce a strong banding between 37 and 50 kDa, corresponding to maturely glycosylated E1 peptides (Chandrasekhar et al., 2006). **A**, Q1-cys, H363C was co-expressed with E1-cys or E1-cys cysteine point mutants in CHO cells through transient transfection. Oxidation results in the observation of several higher molecular weight bands between 50 and 150 kDa. **B & C**, Q1-cys, R360C (**B**) or Q1-cys, A370C (**C**) were co-expressed with the same panel of cysteine point mutants of E1-cys assayed with Q1-cys, H363C. Mutant E1 also forms many higher molecular weight species running between 50 – 100 kDa, but lacks the high-intensity species weighing just under 150 kDa. **D**, absorbance for our putative crosslinked species normalized to the “total” absorbance for each transfection pairing. The normalized absorbance is plotted against the position of the interacting cysteine in E1. The strength of the ~ 150 kDa band varies depending upon the crosslink pairing and is highly reproducible. Signal denotes the mean for n = 3 – 4 experiments  $\pm$  S.E.M. The statistical significance of each experiment (individually compared against three negative controls) is binned according to least significance: † ( $p < 0.05$ ), ‡ ( $p < 0.01$ ), § ( $p < 0.001$ ), \* ( $p < 0.0001$ ). **Legend**, the identity of the Q1-cys point mutant. **Inset**, cartoon depicting the location of H363C on the S6 gate of Q1 pore-forming subunits as well as

the location of our panel of cysteine point mutation in E1 (red peptide backbone).



to maturely glycosylated E1 (Chandrasekhar et al., 2006). Many other E1-containing species can also be observed with masses between 50 and 150 kDa. Of these species, the band resolving to just below 150 kDa is of particular interest. This 150 kDa band depends upon the presence of a cysteine in E1 and, of all of the higher molecular weight bands larger than 50 kDa, the signal intensity for the 150 kDa band is greatest and changes reproducibly depending upon the position of each E1 cysteine mutant. In a reciprocal scan, in which a single cysteine point mutant of E1 is crosslinked with a panel of Q1 cysteine point mutants, we identified several Q1 cysteine point mutants which showed little propensity for crosslink formation in the vicinity of H363 (data not shown). Two of these Q1 point mutations, R360C and A370C, each within approximately two  $\alpha$ -helical turns of H363, were used as the other two of our aforementioned negative controls (Fig. 4-3B & C). No positive control exists for this experiment. Both control disulfide bond scans almost completely lack our putative disulfide bound ~ 150 kDa species, but otherwise possess all of the features observed upon H363C co-expression. We plotted percentage of crosslink at 150 kDa (normalized to “total” protein signal) against position of cysteine replacement in E1 (Fig. 4-3D). The percentage of protein in the ~ 150 kDa band is also highly reproducible. The statistical significance of pairings of H363C with each cysteine point mutant in E1 mirror the measured “isochronal  $\Delta\Delta G$ ” of alanine replacement (Rocheleau et al., 2006).

During our investigation we identified other Q1 cysteine point mutants which displayed intriguing crosslinking patterns with E1 cysteine point mutants. Crosslink formation ends abruptly C-terminal to the cysteine mutant P369C. P369C is unique in

that it forms a strong intensity ~ 150 kDa species only upon co-expression with a single E1 point mutant, D76C (Fig. 4-4A & E). One other Q1 cysteine mutant displayed statistically significant disulfide bond formation with E1, I257C. We discovered this cysteine point mutant by extending our scan towards the cytoplasmic, N-terminal end of the fifth transmembrane domain. I257C, the amino acid residue homologous to the hinge between the S4-5 linker helix and S5 in Kv1.2, forms crosslinked species with the same residues that were identified by H363C (Fig. 4-4B). However, crosslink formation required five-fold more oxidant relative to oxidation involving S6 cysteine mutants. In order to generate background disulfide bond formation for the S4-5 linker, V254C and F256C were used as negative controls (Fig. 4-4C & D). Neither residue, nor any other residue between V254C and H258C (data not shown), was able to generate the 150 kDa crosslinked species. A comparison of the percentage of mass shift for experiments involving I257C and background controls was plotted (Fig. 4-4F). Lastly, S253, a residue on the cytoplasmic side of the S4-5 linker helix, was able to form disulfide bound species with much less oxidant as compared with I257C. However, the higher molecular weight species identified with S253C did not include our suspect 150 kDa species, nor was there any evidence of a discernable crosslinking pattern (data not shown).

Having found these putative crosslinked species, we sought to demonstrate the 150 kDa species was the Q1-E1 disulfide-bound heterodimer of Q1 and E1. Our expected mass of a Q1-E1 heterodimer would be ~ 120 kDa (Q1 is ~ 70 kDa while maturely glycosylated E1 is ~ 50 kDa); the species we identified could be one of several experimental artifacts. These artifacts include E1 covalently linked with any membrane-

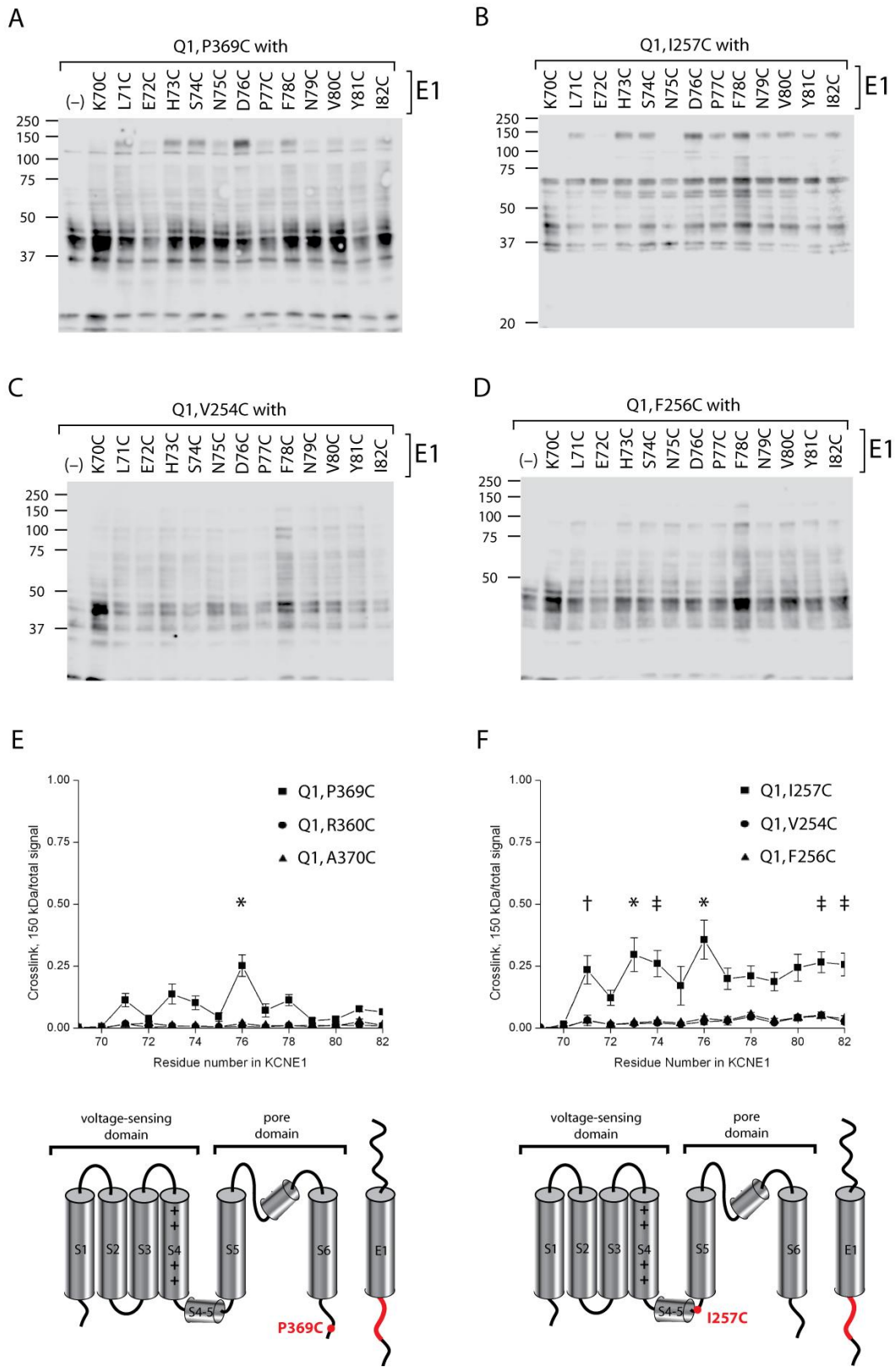


**Figure 4-4.** Cysteine point mutations residing in the S6 gate and the S4-5 linker are able to form higher molecular mass species with E1 cysteine point mutants. **A – D**, representative western blots of proteins oxidized as described (*vide infra*) but otherwise treated and presented as in Figure 4-3A – C. All combinations of cysteine point mutants shown give rise to maturely-glycosylated E1. The identity of the co-transfected Q1 and E1 cysteine point mutants is labeled above and molecular mass markers are labeled on the left. **A**, Q1-cys, P369C is co-expressed with our panel of E1 cysteine point mutants and oxidized with 0.01% H<sub>2</sub>O<sub>2</sub> for 10 min prior to resolution on non-reducing SDS-PAGE. Oxidation of only one pair of Q1 and E1 cysteine point mutants, P369C with D76C, results in a significantly intense ~ 150 kDa band. **B**, Q1-cys, I257C co-expressed with our panel of E1 cysteine point mutants and oxidized with 0.05% H<sub>2</sub>O<sub>2</sub> for 10 mins. Oxidation results in many of the higher molecular weight species observed with H363C or P369C co-expression, including the suspect 150 kDa species identified before. **C & D**, cysteine point mutants Q1-cys, V254C (**C**) or Q1-cys, F256C (**D**), located within one helical turn of I257 on the S4-5 linker helix of Q1, are co-expressed with our panel of E1 cysteine point mutations. Samples were oxidized for 10 min with 0.05% H<sub>2</sub>O<sub>2</sub>. Oxidation results in many of the higher molecular weight species resolving between 50 and 100 kDa, however there is very little signal from the ~ 150 kDa band. **E & F**, normalized signal intensity of the ~ 150 kDa species of Q1-cys, P369C co-plotted with R360C and A370C (**E**) or Q1-cys, I257C co-plotted with V254C and F256C (**F**), as presented in Figure 4-2D. Signal denotes the mean for n = 3 – 6 experiments ± S.E.M. The statistical significance of each experiment (individually determined versus three

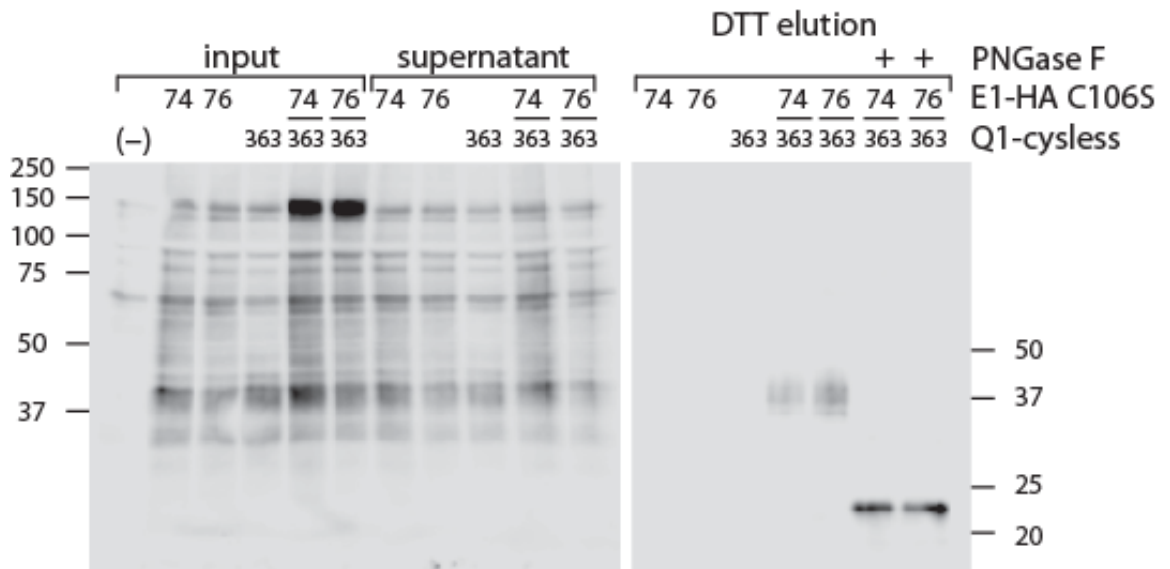
negative controls) is binned according to least significance: † ( $p < 0.05$ ), ‡ ( $p < 0.01$ ), \* ( $p < 0.0001$ ).

associated endogenous CHO-K1 protein, an E1 homodimer, or any non-specific proteins which can be recognized by our  $\alpha$ -HA antibodies. Alternatively, our crosslinked species may resolve at a different apparent molecular mass due to the species being a disulfide bound dimer.

We could not test our crosslink band directly for the presence of Q1 on an immunoblot. Immunoblots with  $\alpha$ -Q1, in the absence or presence of a co-expressed E1 subunit, reveal an aggregation band around 150 kDa, obscuring the crosslink species we sought (data not shown). However, we were able to immunoprecipitate the channel complex using the  $\alpha$ -Q1 antibody. In Figure 4-5A, ghosts were first oxidized, then subsequently immunoprecipitated using  $\alpha$ -Q1 antibodies and probing for E1 in the immunoblot. Only the ~ 150 kDa band was both dependent upon co-expression of Q1 and E1 cysteine mutants, and was depleted in the supernatant of the immunoprecipitation. Please note several of the other higher molecular weight species identified by oxidation must result from endogenous CHO proteins, as these bands were present in the absence of transfection.

Upon DTT elution of our crosslink band from  $\alpha$ -Q1 antibodies, all HA-containing E1 peptides pulled down by Q1 immunoprecipitation collapsed to between 37 and 50 kDa, consistent with our 150 kDa band possessing multiple disulfide bound species. The size of this HA-tagged peptide corresponds well to maturely glycosylated E1, the E1 species expressed on the cell surface. We confirmed this species indeed was glycosylated by deglycosylating with PNGase F, which removed all N-linked glycans. Though deglycosylation left a species 3 – 5 kDa larger than the predicted mass of deglycosylated

A



B

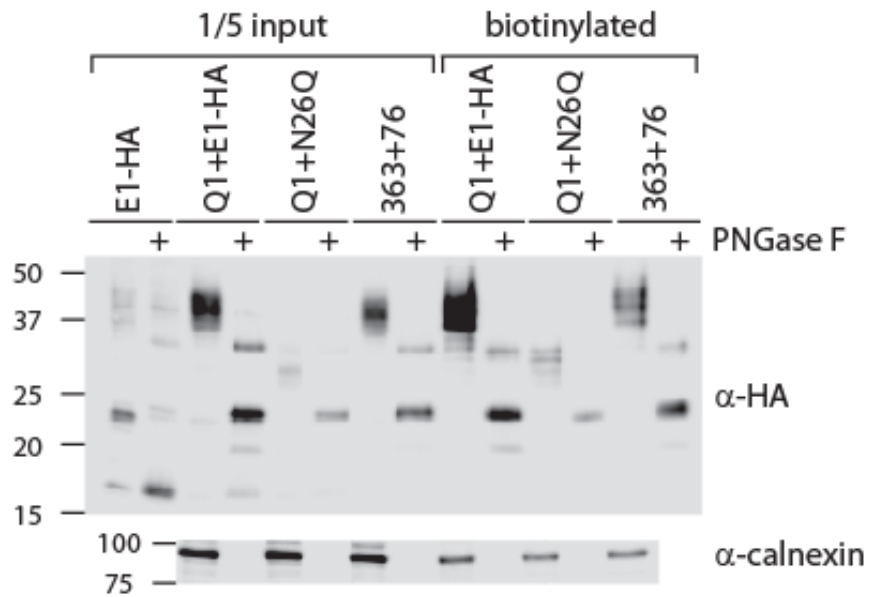


**Figure 4-5.** The ~ 150 kDa species is a Q1-E1 disulfide-bound heterodimer found on the cell surface. **A**, co-immunoprecipitation confirms the identity of the crosslinked species. Membrane proteins were oxidized with 0.1% H<sub>2</sub>O<sub>2</sub> for 10 min and subsequently immunoprecipitated by  $\alpha$ -Q1 antibodies. Proteins were then resolved on SDS-PAGE and immunoblotted with  $\alpha$ -E1. The identities of the transfected Q1 or E1 cysteine point mutants are labeled above; \_\_\_\_ denotes “cysless”, numbers denote the position of the cysteine mutation. Molecular mass markers are as indicated, while PNGase F treatment of samples is denoted by “+”. (**Left**) representative western blot of whole-cell lysates and non-immunoprecipitated supernatant proteins from non-transfected CHO cells “(-)” or transfected CHO cells resolved on non-reducing SDS-PAGE. Only the ~ 150 kDa species is depleted from the supernatant upon immunoprecipitation with  $\alpha$ -Q1 antibodies. (**Right**) representative western blot of DTT-eluted proteins immunoprecipitated with  $\alpha$ -Q1 antibodies. Upon reduction, antibodies release the heterodimeric species and the disulfide bond holding the species together is reversed. The resulting monomeric E1 peptides resolved between 37 and 50 kDa. This band possesses N-linked glycosylation because the band collapses to ~ 22 kDa upon treatment with PNGase F. **B**, cell surface biotinylation recognizes maturely glycosylated E1 peptides and the ~ 22 kDa deglycosylated species. Molecular weight markers are as indicated, antibody used for immunoblotting is labeled on the right, and the identity of the Q1/E1 pairing as well as cell surface biotinylation is labeled above. Samples treated with PNGase F subsequent to protein harvest are denoted with a “+”. (**Above**) co-expression of wild type Q1+E1; Q1-cys, H363C + E1-cys, D76C; and Q1+ E1, N26Q (E1 possessing only one N-linked



glycosylation site) gives rise to maturely glycosylated E1 peptides on the cell surface. Upon deglycosylation, the signal from these peptides collapses to a species ~ 22 kDa. The ~ 22 kDa band is distinct from immaturely glycosylated E1, the dominant species obtained from whole-cell lysates of E1 transfected alone (left-most two lanes), and appears at the exact same molecular mass in the lane containing N26Q (N26Q possesses only a single N-linked glycosylation site). (*Below*) representative experiment, run in parallel, demonstrating cell surface biotinylation for each sample modifies only ~ 5% of intracellular calnexin. Weak labeling of intracellular calnexin indicates labeled CHO cells maintained an intact cell membrane during the biotinylation procedure.

HA-tagged E1, the deglycosylated bands obtained through immunoprecipitation correspond well with species obtained by deglycosylation of cell-surface wild type HA-tagged E1 peptides (Fig. 4-5B).

These results indicate our deglycosylated species resides in the plasma membrane and is not an artifact of cysteine mutation or non-native structure. These data also implicitly demonstrate our cysteine mutant channels are correctly folded and were allowed to traffic to the cell surface. Further, we were able to dismiss the possibility that the observed mobility shift resulted from incomplete deglycosylation of immature glycans by PNGase F – E1 N27Q, which contains only one of two N-linked glycosylation sites, displays the same shift in mobility upon deglycosylation with PNGase F. The reason for this 3 – 5 kDa mobility shift has not been ascertained; we believe it results from the same post-translational modification observed by Chandrasekhar and colleagues (Chandrasekhar et al., 2006).

Once we identified the positions of cysteine mutants in Q1 and E1 able to form disulfide bound pairings in our biochemical assay, we wanted to determine how cysteine mutations at these particular positions affect  $I_{K_s}$  channel function. We returned to whole-cell perforated patch clamp with two goals in mind. 1) Mutant pairing must give rise to whole-cell currents – native-like function demonstrates we have not disrupted the native structure. 2) Oxidant-mediated current modification observed through patch clamp might reciprocate our cysteine crosslinking scan.

We began by assaying our cysteine point mutant pairing for wild type function. In Figure 4-6A – C, whole-cell currents from CHO-K1 cells were elicited by holding cells at  $-80$  mV and depolarizing with a 3-s test pulse to  $+20$  mV. The channel spends 20% of its time in the depolarized state (a 3-s test pulse performed every 15 s). Current for all disulfide bond pairings clearly exhibits the slow gating kinetics of  $I_{Ks}$  and lacks the quick rise-time or inactivation observed upon repolarization with Q1-cys expressed alone. Though current density varies by cysteine point mutant, all pairings tested give rise to  $I_{Ks}$ -like currents within 3 days of transfection.

We determined the effect of disulfide bond formation on our mutant pairings by oxidizing our cells and measuring changes in current.  $I_{Ks}$ -cys, our negative control, averaged approximately 5% current reduction after five minutes of oxidant treatment. For pairings of Q1 and E1 identified as high-impact biochemically (Fig. 4-6C), for instance H363C+H73C, we observed between 80% and 90% inhibition in current, with the reaction reaching completion within 5 minutes. In cysteine mutant pairings possessing a single cysteine point mutant, oxidant treatment also resulted in current reduction (Fig. 4-6A & B). However, the rate inhibition was far slower as compared with our *bona fide* disulfide pairings, and equilibrium current inhibition for these pairings never reached 80–90%.

We hypothesize cysteines in the S6 gate of Q1 are able to form disulfide bonds with either an endogenous aqueous protein in CHO-K1 cells or the cysteine point mutant from second gate helix within the channel complex. The fast inhibition observed between a *bona fide* crosslinking pair is indicative of both subunits being held in close

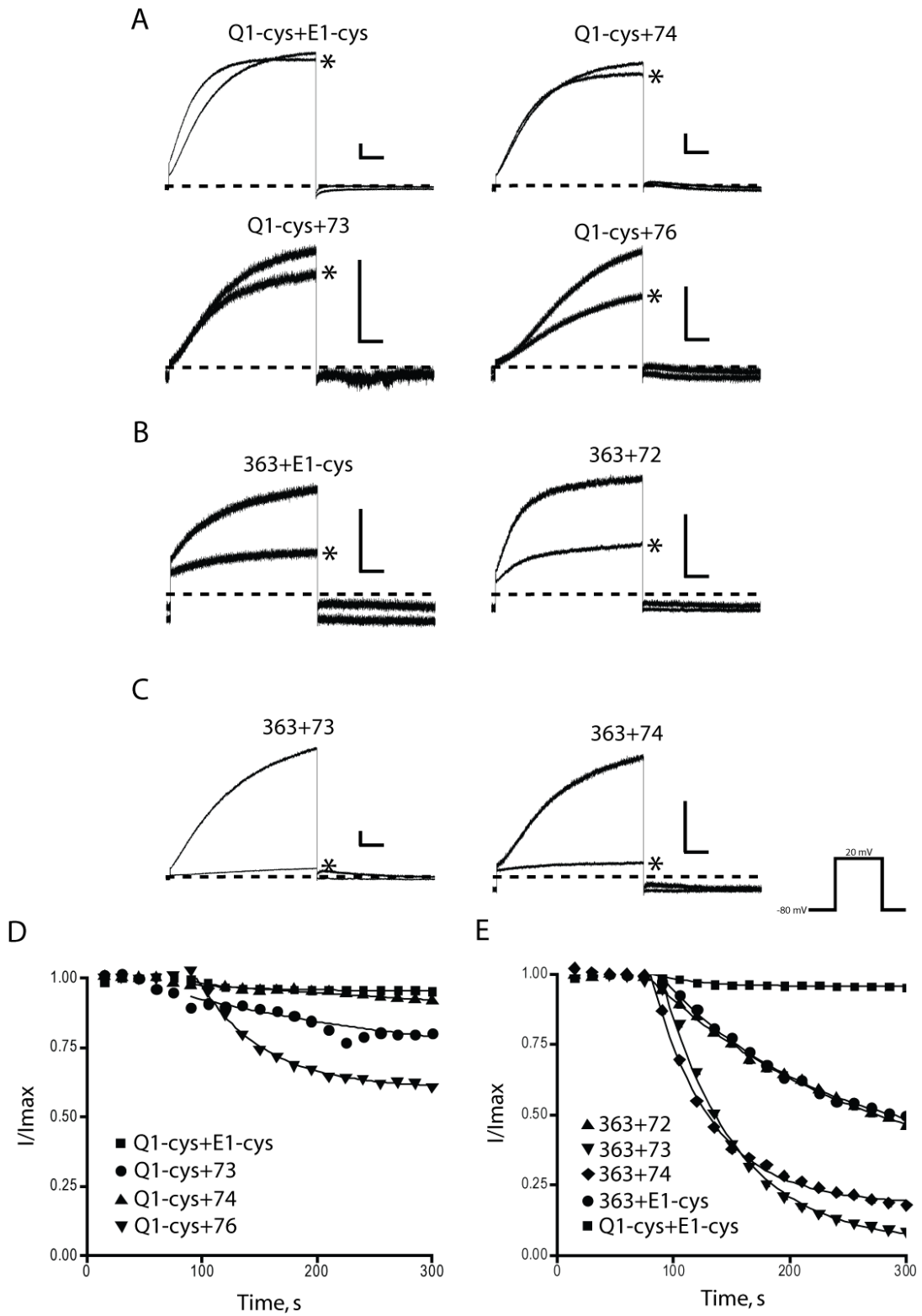


**Figure 4-6.** Whole-cell perforated patch clamp recordings of CHO cells transfected with point mutants of Q1 and E1. **A – C**, recordings of CHO cells held at  $-80$  mV and depolarized to  $+20$  mV for 3 s with a 12-s interpulse interval. This protocol holds CHO cell membranes at depolarizing potentials for 20% of the time. Once currents remain unchanged for at least a full minute (normally occurring within 5 min of seal formation), 0.1% H<sub>2</sub>O<sub>2</sub> is perfused through the external solution. Current measured at the end of oxidant treatment is marked with “\*”. Zero current is labeled by a dashed line. Scale bars denote 25 pA/pF and 0.5 s. Recordings are representative or  $n = 2 - 7$  samples per pairing. **Inset**, voltage-pulse protocol used to elicit the depicted recordings. **A**, “negative controls” for disulfide bond formation. Only E1 contains a cysteine. **B**, “negative controls” in which either a poor disulfide bond pairing is expressed, or only Q1 contains a cysteine. Currents arising from these channel subunit pairings display greater current inhibition in response to oxidation, probably as a result of H363C forming a homodimer with a second gate helix or forming a heterodimer with an endogenous, aqueous CHO-K1 protein. **C**, cysteine point mutant pairing identified as high impact through our biochemical assay. **D & E**, Representative time course of current inhibition for the data shown in **A** (**D**) or Q1-cys, H363C co-expressed with E1 cysteine point mutants (**E**). The time courses of current inhibition are overlaid with single-exponential decay. The identity of the Q1 and E1 cysteine point mutants are as labeled. The kinetics of oxidant-mediated current inhibition occur much faster compared with the “negative controls”, and steady-state inhibition of current is much greater for *bona fide* crosslink pairs compared with the “negative controls”.

proximity and juxtaposition within the native structure, increasing the effective local concentration of chemically labile sulfhydryl groups and greatly increasing the kinetics of reaction. This increase in effective local concentration can not be replicated in the absence of cysteine point mutants in both  $I_{Ks}$  subunits. We tested our hypothesis by co-expressing of H363C and E72C (a very poor disulfide binding pair), which should behave much like cysless E1. Percent inhibition of  $I_{Ks}$  current was similar in the presence or absence a cysteine residue at position 72 in E1 (Fig. 4-6B). The results from our whole-cell perforated patch clamp are summarized in Table 4-1.

Lastly, we tested the reversibility of our disulfide-mediated current inhibition by perfusing 2 – 5 mM DTT. Unfortunately, all cells treated with DTT quickly lost their gigaohm patch pipette seals within 30 s of application (data not shown). Though we were not able to reverse our crosslink formation, the observed rates of current inhibition accurately model the propensity of each crosslink pairing to form heterodimeric disulfide bonds.

Table 4-1. Oxidant-mediated current inhibition of cysteine mutant  $I_{KS}$ <sup>a</sup>

transfection	n =	% current inhibited	$\tau_{rxn}$ (s)
Q1-cys+E1-cys	5	4.5 ± 2.2	NA
Q1-cys+73	1	19.8	188
Q1-cys+74	3	15.8 ± 4.2	145 ± 19
Q1-cys+76	4	31 ± 4.1	115 ± 41
363+E1-cys	7	45.6 ± 9.8	64.4 ± 15.4
363+72	2	57.6 ± 2.5	148 ± 47
363+73	2	85.9 ± 7.8	46.5 ± 8.7
363+74	4	85.2 ± 1.5	62.4 ± 1.3

<sup>a</sup> Data was obtained from individual CHO-K1 cells transiently transfected with cysteine point mutants of Q1 and E1 as labeled. Current versus time plots were fit to single-tau exponential decay as described in Materials and Methods. Percent current inhibition and  $\tau_{rxn}$  are reported as mean ± S.E.M. NA, not applicable.

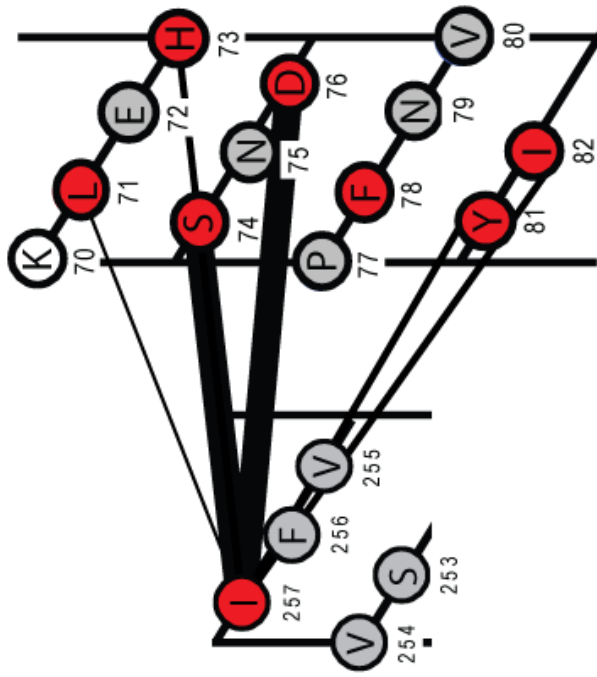
## **DISCUSSION**

Cysteine replacement of residues in the C-terminus of E1 and the cytoplasmic pore domain of Q1 has led to the identification of close contacts between these  $I_{Ks}$  subunits (Figure 4-7). Both Q1 and E1 required mutation of all endogenous cysteines in order to conduct this biochemical scan, coupled with the introduction of single, exogenous cysteines point mutations. Despite the introduction of so many cysteine point mutations, all mutant  $I_{Ks}$  channels observed electrophysiologically have given rise to currents reminiscent of native  $I_{Ks}$ . As channel function is a property of structure, we hypothesize all of the cysteine point mutations have maintained wild type-like structure. Confirmation of our high-throughput biochemical assay is also important. Demonstration that our cysteine pairings are able to associate during whole-cell perforated patch clamp experiments and maintain this association in hypotonically lysed membranes is heartening, confirming the robust nature of channel structure.

Our results may provide a relatively simple explanation for bipartite KCNE modulation of the Q1 channel complex. The permissive transmembrane modulation of E1 allows unfettered voltage sensor movement in response to changes in membrane potential. Upon depolarization, the voltage sensor reaches equilibrium with the depolarized conformation quickly in the presence or absence of E1 peptides (Rocheleau & Kobertz, 2008). Fast  $I_{Ks}$  voltage sensor movement must be uncoupled with gating motions. An association between E1 and the S6 gate of Q1 may allow a rigid E1 to sterically hinder or block S6 transition between the closed and open conformation.



**Q1, S4-5 Linker with E1**



**Q1, S6 with E1**

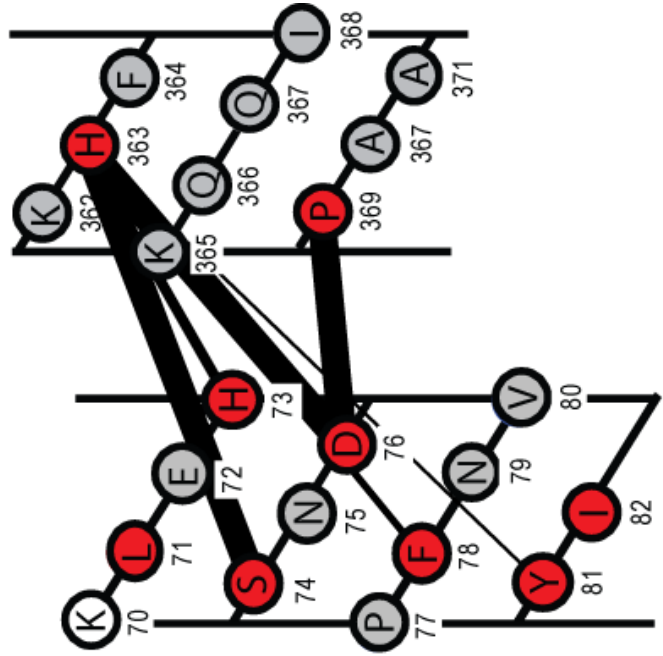


**Figure 4-7.** Close contacts within the cytoplasmic face of  $I_{Ks}$  channel complexes. Net diagrams of those regions of Q1 (outside nets) tightly associated with E1 (inside nets) are depicted. White, residues incapable of forming any disulfide bonds. Gray, positions of non-native cysteines able to form ~ 150 kDa disulfide bound heterodimer (with varying efficiency). Red, positions of non-native cysteines found to be tightly associated. Statistically significant interactions are denoted by lines connecting the interacting residues; the line width relates to the statistical significance of each crosslink (compared individually with three negative controls), with larger width indicating higher significance. *Left*, I257C, an exogenous cysteine positioned at the joint between S5 and the S4-5 linker helix of Q1, loosely associates with membrane-proximal C-terminal cysteine mutations in E1. This association required five-fold more oxidant to visualize relative to comparable “hits” between the S6 helix of Q1 and E1. Cysteines positioned at any other location within or near the S4-5 linker were not able to form heterodimers with E1 unless forced to do so through use of harsher oxidizing conditions (data not shown). *Right*, the positions of exogenous cysteines within the S6 helix of Q1 able to associate tightly with membrane-proximal C-terminal cysteine point mutants. H363C dimerizes very well with cysteines mutations previously identified as “high impact” within the E1 C-terminal tail (Chapter III).

Alternatively, a rigid, tightly bound E1 C-terminus may provide “spring-like” resistance to gate motions, thus slowing the gating of  $I_{Ks}$ .

E1 interaction with the S4-5 linker of Q1 channels may also result in  $I_{Ks}$  properties. Voltage sensor movement normally results in tension on the S4-5 linker. If E1 prevents S4-5 linker movement, voltage sensor movement will not be quickly transduced into gating motions.

The S4-5 linker helix and the gate of Q1 are able to adopt multiple conformations as part of normal channel function. Though we have definitively demonstrated an interaction between Q1 and E1, our biochemical scan does not give us insight regarding the state-dependence of the Q1-E1 association. As resting potential is a function of the electrochemical gradients of a membrane and the relative conductance of each ion, lyzed membranes would completely lack a transmembrane potential, allowing channels to rest at 0 mV; crosslinking could occur with the gate residing in the closed or open (or any heretofore unknown?) conformation. We intend to use electrophysiology in the future to distinguish between these possibilities.

Our electrophysiological results were obtained using a voltage-pulse protocol in which cysteine mutant channel complexes are depolarized 20% of the time. In order to determine a state-dependence for our disulfide bond formation, we will vary the percentage of time in the depolarized state, and observe any changes in the rate of disulfide-mediated current alteration. Changes in the rate of inhibition may be indicative of the state of channel subunits caught in a disulfide bound species.

For instance, a four-fold reduction in the dwell time at + 20 mV would only result in a modest increase in percentage of time spent at – 80 mV ( $0.75 s_{+20\text{ mV}}/15\text{ s} = 95\%$ , versus  $3 s_{+20\text{ mV}}/15\text{ s} = 80\%$ ). A more open protocol is also possible. Maintaining membrane potential at + 20 mV would completely remove any time spent at negative membrane potentials. If a particular disulfide pairing occurs within the open state, performing the reaction using a closed protocol would slow the kinetics of reaction significantly, while oxidizing in the open state would significantly speed reaction kinetics. In contrast, if disulfide bond formation occurs within the closed state, the closed protocol will not produce a significant change in reaction kinetics, but the open protocol will significantly slow the rate of reaction.

If there is no current alteration in response to disulfide bond formation, other possibilities present themselves. Disulfide bond formation may not alter the S4-5 linker or the gate in such a manner inhibiting normal function for these structures. In this case, E1 may associate with the gate or the S4-5 linker helix and move in conjunction with Q1 movements. Our biochemical assay may also find a channel state which is not electrophysiologically observable, at least not utilizing conventional methods. For instance, inactivation in Q1/E1 has never been definitively dismissed; electrophysiological recordings are not able to observe the transition to or from an inactivated state, if it does exist. Given our biochemical assay is performed in membranes which dwell at 0 mV for long periods of time, it is possible crosslink formation may occur in a heretofore unobserved inactivated state. In the unlikely event of extremely slow open to inactivated state transition, it may be possible to select for

inactivated channels by conducting oxidation experiments with long depolarizations. Alteration of current might be observable as a reduction in peak current for exceptionally long pulse (if we trap inactivated channels in a non-conducting state, fewer channel complexes could respond to subsequent membrane repolarization and depolarization).

In a parallel experimental approach for our disulfide bond scan, in which single cysteine mutations of E1 were co-expressed with a panel of Q1 cysteine point mutations, we observed a sudden drop in disulfide bond efficiency just C-terminal to P369. The binding partner for P369 also appears to be in close proximity to E1 P77, the proline residue inducing the “kink” in the C-terminal  $\alpha$ -helix of E1. Though it is clear these structures diverge from one another, the identity of any other protein contacts in this region remains to be elucidated, save a contact between the IQ domain of Q1 and calmodulin (Ghosh et al., 2006; Shamgar et al., 2006). This interaction is required for calcium sensitivity for the channel complex. Furthermore, calmodulin has been shown to be able to co-immunoprecipitate E1 with the  $I_{Ks}$  channel complex. We do not have evidence at this point, but it would be intriguing to speculate E1 may also contact calmodulin directly, perhaps forming a ternary complex on the cytoplasmic face of the channel complex.

Though the results of our disulfide crosslinking scan of the C-terminus of E1 corroborate the biochemical evidence for C-terminal E1/Q1 interaction, a recent NMR structure of E1 peptides reconstituted in lyso-myristoylphosphatidylglycerol micelles has provided an alternative structure (Kang et al., 2008). This NMR structure depicts E1 as a bent transmembrane alpha-helix which contains flexible linkers on the extra- and

intracellular sides of the transmembrane domain. The aqueous exposed  $\alpha$ -helices of this structure appear to adhere to the predicted surface of the micelle in which E1 was reconstituted. The authors then modeled the structure onto Kv1.2, a homologous structure of the Q1 channel complex. This model for Q1/E1 does agree with the experimental evidence derived from disulfide bond formation in that E1 contacts the S4-5 linker of the Q1 channel complex. However, the NMR structure for E1 does not recapitulate the interactions biochemically observed between the S6 gate and the C-terminus of E1, nor does it maintain an alpha-helical structure as demonstrated by Rocheleau et al (Tapper & George, 2000; Rocheleau *et al.*, 2006).

In this study, we used disulfide bond formation as an indicator for close juxtaposition of cysteine side chain residues between the cytoplasmic pore of Q1 and the C-terminus of E1. Though further work is required to fully understand the interaction between E1 and the cytoplasmic pore of Q1, our results supports a role for the C-terminus of E1 in giving rise to  $I_{Ks}$ -like biophysical properties, strengthening the bipartite model of KCNE modulation.

## **MATERIALS AND METHODS**

***Molecular Biology***- hKCNQ1 (Q1) and hKCNE1 containing an extracellularly exposed hemagglutinin A (HA) tag (YPYDVPDYA) (Wang & Goldstein, 1995) (E1), both residing on an expression vector containing the *Xenopus laevis* 5' and 3'  $\beta$ -globin UTRs, were mutated by Quikchange<sup>®</sup> (Stratagene) site-directed mutagenesis combined with cassette mutagenesis to remove all native cysteines. Based on hydrophobicity,

cysteines were either mutated to serine (aqueous) or alanine (membrane embedded). Mutagenesis was done iteratively in groups of three in order to check each construct for wild type-like function in *Xenopus* oocytes using TEVC (data not shown). Upon confirmation that each construct behaved like wild type, mutant constructs were then combined to produce a completely cysteine-deficient construct, which also behaved like wild type. E1 C106S was also checked and behaved like wild type. Q1, E1 and both “cysless” constructs were then subcloned into a mammalian expression vector under the CMV promoter. Individual cysteine mutations were reintroduced using the same procedure as above. All mutations were confirmed by automated PCR covering the entire mutated cassette or, in the case of the original cysless constructs, the entire open reading frame was sequenced.

**Cell Culture** - CHO-K1 cells (CHO) were grown in F-12K media (Invitrogen) supplemented with 10% Fetal Bovine Serum (Hyclone) and 1% Penicillin/Streptomycin (Invitrogen) and transiently transfected using Lipofectamine<sup>TM</sup> (Invitrogen) in Opti-MEM<sup>®</sup> (Invitrogen).

*For Biochemistry:* Each well of a six-well plate was transfected with (in  $\mu\text{g}$ ): 0.75 Q1, 1.5 E1, for  $6 \pm 0.25$  hours, then allowed to incubate in F-12K for  $\sim 42$  hours before harvest.

*For Electrophysiology:* Two different cDNA quantities were empirically determined to produce  $I_{Ks}$ -like currents. For wild type and “cysless”  $I_{Ks}$ , two wells of a six-well plate were transfected with (in  $\mu\text{g}$ ): 0.375 Q1, 3 E1, 0.25 pEGFP-C3. For

cysless point mutants as well as wild type and “cysless” Q1, two wells of a six-well plate were transfected with (in  $\mu\text{g}$ ): 0.75 Q1, 1.5 E1 or empty vector, 0.25 pEGFP-C3. Transfection media is left on cells for  $\sim 2$  hours, and then subsequently incubated in F-12K 1 – 2 days before harvest.

***Electrophysiology*** – Whole-cell perforated patch clamp was used to measure currents arising from transiently transfected CHO cells. Prior to recording, CHO cells were trypsinized and replated on glass coverslips. CHO cells on broken glass chips were used 1 – 5 hours after replating (Hamill *et al.*, 1981; Horn & Marty, 1988). Gigaohm seals were formed in a modified Tyrode’s solution (in mM): 145 NaCl, 5.4 KCl, 10 HEPES, 5 CaCl<sub>2</sub>, pH 7.5 with NaOH. Once seals were formed, the bath solution was switched for recordings to External Solution (Suh & Hille, 2002; Liu *et al.*, 2006) (in mM): 160 NaCl, 2.5 KCl, 2 CaCl<sub>2</sub>, 1 MgCl<sub>2</sub>, 10 HEPES, 8 Glucose, pH 7.5 with NaOH. Oxidant was applied to patches by adding small volumes of 30% H<sub>2</sub>O<sub>2</sub> to a final concentration of 0.1% in External Solution. Perforations were formed using amphotericin B (Horn & Marty, 1988; Rae *et al.*, 1991) (Sigma). 60 mg/ml stock solutions of amphotericin B in DMSO were made once daily, and then diluted to a final concentration of 60  $\mu\text{g}/\text{ml}$  in Inside Solution (Melman *et al.*, 2001; Liu *et al.*, 2006) (in mM): 126 KCl, 4 K<sub>2</sub>-ATP, 2 MgSO<sub>4</sub>, 5 EGTA, 0.5 CaCl<sub>2</sub>, 25 HEPES, 0.4 Na-GTP, pH 7.5 with CsOH ( $\sim 40$  mM Cs<sup>+</sup>). Once amphotericin B was added, Inside Solution was used within 20 min before being discarded. Access to the inside of the cell was



monitored by measuring peak current with 3-s test depolarizations to + 20 mV taken every 15 s from – 80 mV, and reached plateau within 5 min.

Voltage clamp was performed with an Axopatch 200B (Axon Instruments) using pClamp 10 (Molecular Devices Corporation), and measured current was digitized with Digidata 1440A (Axon Instruments). Transfected (EGFP-expressing) cells were visualized using an Axiovert 40 CFL inverted light microscope (Zeiss). Patch pipette access resistance was between 1.5 – 3.5 M $\Omega$ . Neither prediction nor correction were used in these recordings; cells with an IR drop >10 mV at 20 mV were not considered. Q1 has been shown to possess small basal activation (Gage & Kobertz, 2004), therefore recordings were not leak-subtracted. Perforated patch can lead to Donnan potential, predicted to be  $\leq$  11 mV for CHO cells (Horn & Marty, 1988; Selyanko *et al.*, 2000). Both of these factors will affect the accuracy of the voltage clamp.

Wild type and “cysless” Q1 and I<sub>Ks</sub> were assayed for native-like function using a “family” protocol, in which cells held at –80 mV were stepped every 15 s to potentials between – 100 mV and + 60 in + 20-mV increments for 3 s, followed by a 1-s command to – 30 mV. Disulfide bond formation was monitored by holding cells at – 80 mV and recording current during a 40-ms window at the end of a 20-mV, 3-s test depolarization taken every 15 s.

**Biochemistry** - Crosslinking of Q1 and E1 point mutants was mediated through disulfide bond formation (Schulteis *et al.*, 1996; Kobertz *et al.*, 2000). For scanning experiments, wells of CHO cells on a six-well plate expressing Q1 and E1 mutants were

harvested at 4 °C by thoroughly aspirating media and scraping ghosts in 250 µl/well Hypotonic Lysis solution plus Protease Inhibitors (in mM): 10 KCl, 1.5 MgCl<sub>2</sub>, 10 HEPES pH 8.0. Protease Inhibitors: 1 mM phenylmethylsulfonyl fluoride (EM Science) (from 100X stock in ethanol) and 1 µg/ml each of leupeptin (Roche), pepstatin (Roche) and aprotinin (Sigma) (from 100X stock in ethanol/acetic acid/water). After scraping, samples were pelleted (10 krpm, 10 min, 4 °C). Aqueous proteins in the supernatant were used for BCA quantitation (Pierce). Samples were then resuspended and reduced with 10 mM dithiothreitol (DTT) for 10 min. Membranes were pelleted (10 krpm, 10 min, 4 °C) and washed once in Hypotonic Lysis solution, and then resuspended again in Hypotonic Lysis solution.

Each sample was oxidized with a total of 0.01% H<sub>2</sub>O<sub>2</sub> for 10 min at RT. Oxidation was quenched at RT for 1 hour with N-ethyl maleimide to 30 mM final concentration. Membranes were pelleted (10 krpm, 10 min, 4 °C) removing the supernatant, and then solubilized by rolling for 30 min at 4 °C in 1.5% Digitonin (Calbiochem) Solution plus Protease Inhibitors (in mM): 290 NaCl, 10 KCl, 1 MgCl<sub>2</sub>, 7 Tris pH 7.5, 1.5% Digitonin. Debris were pelleted (14 krpm, 10 min, RT), the supernatant kept and diluted 1:1 with 7.2% (w/v) SDS, 100 mM Tris pH 6.8, 20% (v/v) glycerol and a trace of dye. Load volume was weighted based on BCA quantitation before resolution on non-reducing 10% SDS-PAGE.

***Co-Immunoprecipitation*** - Harvest, oxidation and quench of membrane proteins proceeded exactly as above, except that samples were oxidized with a total of 0.1% H<sub>2</sub>O<sub>2</sub>

for 10 min. Once samples were quenched, membranes were pelleted (10 krpm, 10min, 4 °C) and solubilized by rolling for 30 min at 4 °C in RIPKA plus Protease Inhibitors (in mM): 140 NaCl, 10 KCl, 1% Triton X-100, 0.1% SDS, 1% sodium deoxycholate, 10 Tris-HCl pH 7.4, 1 EDTA pH 8.0. Debris was then pelleted (14 krpm, 10 min, RT) and the supernatant collected. Before further treatment, 1/5 input samples were saved.

Samples were then split, diluted with 10% (v/v) 500 mM Na<sub>3</sub>PO<sub>4</sub> pH 7.5, and deglycosylated or mock treated with ~ 1% PNGase F (NEB) for 1 hour at 37 °C. Following deglycosylation, samples were chilled, and α-Q1 (Santa Cruz) was added directly to the reaction mixture (~ 7.1% v/v) and allowed to roll overnight at 4 °C. Antibody was then bound to Immobilized Protein G beads (Pierce) (washed three times in excess RIPKA and reconstituted as a 50:50 bead:RIPKA slurry) rolling at 4 °C overnight. Total slurry:immunoprecipitation used was ~ 14% (v/v).

Before elution, 1/5 supernatant samples were saved. Bound proteins were washed 3x in excess RIPKA and eluted from beads using Elution Solution (in mM): 140 NaCl, 10 Tris pH 7.4, 1 EDTA pH 8.0, 100 DTT, 1% SDS; rolling for a total of 30 min at 4 °C. Beads were pelleted (14 krpm, 2 min, RT) and the collected supernatant diluted 2:1 with 10.75% (w/v) SDS, 150 mM Tris pH 6.8, 30% (v/v) glycerol and a trace of dye. Load volume was weighted for samples and 1/5<sup>th</sup> inputs by BCA quantitation and dilution during deglycosylation and immunoprecipitation before resolution on non-reducing 10% SDS-PAGE (for inputs and supernatants) or 15% SDS-PAGE (for immunoprecipitations).

***Cell Surface Labeling*** - All cell surface labeling is performed in ice-cold buffers. Transfected CHO cells were washed four times with PBS<sup>2+</sup> (PBS supplemented with 1 mM MgCl<sub>2</sub> and 0.1 mM CaCl<sub>2</sub>). Cell surface proteins were then labeled with two 15 min, 1 ml/well washes of 1 mg/ml sulfo-NHS-SS-biotin (Pierce) in PBS<sup>2+</sup>. After the second labeling, the reaction was quenched by rinsing three times with and then washing twice for 15 min with PBS<sup>2+</sup> plus 100 mM glycine. Each well was then solubilized by shaking in RIPKA plus Protease Inhibitors for 30 min. Debris was pelleted (14 krpm, 10 min) and samples were quantitated by BCA. Solubilized proteins were then split and deglycosylated by PNGase F or mock treatment directly in RIPKA. Labeled proteins were bound to Immunopure<sup>®</sup> immobilized streptavidin beads (Pierce) by rolling 15 µg protein/well 1/5<sup>th</sup> inputs without beads or 75 µg protein/well labeled proteins with 25 µl of streptavidin bead slurry overnight (reconstituted 50:50 streptavidin bead:RIPKA slurry from dry streptavidin beads washed three times with excess RIPKA). The supernatants of the streptavidin-bound proteins were removed and the beads were washed three times in SDS Buffer (in mM): 150 NaCl, 10 Tris pH 7.4, 1 EDTA pH 8.0, 0.1% (w/v) SDS. Proteins bound to beads and 1/5<sup>th</sup> inputs were then eluted/mixed with 200 mM DTT, 100 mM Tris pH 6.8, 0.5% w/v SDS, 20% v/v glycerol. Beads were washed a second time with an equal volume of 200 mM DTT and combined. Eluted proteins were resolved on 15% SDS-PAGE or in duplicate on 10% SDS-PAGE for calnexin ER-labeling controls.

***Immunoblotting and Signal Quantitation*** - Proteins were transferred from SDS-PAGE to nitrocellulose for 1 hour at 0.3 A on ice. Once on nitrocellulose, proteins were

blocked and then immunoblotted with rat  $\alpha$ -HA (Roche) or rabbit  $\alpha$ -calnexin (for ER-labeling controls) (Stressgen) 1:1000 or 1:4000, respectively, overnight at 4 °C. Secondary antibodies goat  $\alpha$ -rat HRP (Santa Cruz) or goat  $\alpha$ -rabbit HRP (Cell Signalling) were applied 1:2000 or 1:8000, respectively, for 30 min at room temperature. Super Signal<sup>®</sup> (Pierce) luminol was then applied to western blots for 5 min. Fluorescence was captured using an LAS-3000 dark box (Fujifilm) using LAS-3000 Image Reader version 2.0 (Fujifilm). Luminescence from SDS-PAGE resolved proteins was quantified using MultiGauge version 3.0 (Fujifilm).

*Data analysis - for Biochemistry:* Absorbance data for each experiment was collected, corrected for background noise, and normalized using the equation:

$$y = \frac{abs_{150\text{kDa}}}{abs_{150\text{kDa}} + abs_{37-50\text{kDa}}} .$$

The resulting normalized absorbance was then plotted as a function of the position of each cysteine mutation (or lack of cysteine mutation) in KCNE1 using Origin 6 (Microcal).

Statistical significance was determined in two steps. A model of all absorbance data was calculated, and model residuals were collected. The natural logarithm of the calculated residuals fit well to a normal distribution (the Kolmogorov-Smirnov  $Z$  value was reduced two-fold by taking the natural logarithm,  $Z \approx 1.6$ ). The natural logarithm of each normalized absorbance was subsequently used in a general linear mixed model (Tukey-Kramer) to determine an adjusted  $p$ -value. Each experimental set was tested

against three negative controls (crosslink between KCNE1 cysteine point mutations and two non-labile cysteine point mutations in KCNQ1, or an internal negative control in each data set – HA-tagged KCNE1 C106S crosslinked with cysteine point mutations in KCNQ1). Only those experimental data sets displaying adjusted  $p < 0.05$  for all three negative controls are labeled. These data are binned according to the least significant  $p$ -value.

*For Electrophysiology:* Current normalized to pre-oxidant levels were plotted against time. The resultant time courses of oxidant-mediated current reduction fit well to single-tau exponential decay. Single-tau exponential time courses are overlaid on the data (Fig. 4-6D & E).

## **CHAPTER V**

### **CONCLUSIONS AND FUTURE DIRECTIONS**

#### **GENERAL DISCUSSION**

In the body of work presented in this thesis, we addressed the nature of KCNQ1-KCNE subunit interaction. Chapter II concerned the nature of KCNQ1 modulation by KCNE peptides, and reconciliation of two separate sets of observations, the function of truncated KCNE1 reported by Tapper and George, and the function of KCNE transmembrane chimeras reported by Melman and colleagues (Tapper & George, 2000; Melman *et al.*, 2001; Melman *et al.*, 2002a). Having established the importance of both the transmembrane domain and C-terminus of KCNE1 in giving rise to KCNE modulation in Chapter II, we sought to learn more about the structure and interactions of the C-terminus of KCNE1 with the KCNQ1 channel complex. Chapter III focused on determining the structure of the C-terminus of KCNE1, while Chapter IV focused on discovery of close contacts between KCNQ1 and the C-terminus of KCNE1, contacts which may prove crucial in native  $I_{Ks}$  function considering the presence of multiple Long QT mutations within this region.

In Chapter II, co-expression of KCNQ1 with partial truncation mutants of KCNE3 demonstrated the transmembrane domain was solely responsible for providing modulation of KCNQ1 channel complexes; these observations were consistent with

evidence obtained from transmembrane chimeras of KCNE peptides (Melman et al., 2001; Melman et al., 2002a). However, KCNE1 and KCNE3 are highly homologous in the juxtamembranous C-terminal domain, meaning transmembrane chimeras of each subunit will possess a nearly native KCNE C-terminus. This homology may have led to the erroneous conclusion the transmembrane domain is solely responsible for giving rise to KCNE modulation (Melman et al., 2001; Melman et al., 2002a). Our results were also in apparent conflict with the presence of known Long QT mutations in the C-terminus of KCNE1 and data obtained through partial truncation of the KCNE1 C-terminus (Tapper & George, 2000). We considered possible caveats resulting from homologous KCNE amino acid sequences, and rather than dismiss the observations from KCNE1 truncation, we considered another option: two distinguishable albeit adjacent sites within KCNE peptides give rise to modulation.

Reconciliation of all data obtained through KCNE truncation and chimera formation led to the proposal of a bipartite modulation of KCNE peptides (Figure 5-1). One KCNE modulation resides in the transmembrane domain, and the second modulation resides in the juxtamembranous, C-terminal domain. In the context of the permissive transmembrane modulation observed with KCNE1, C-terminal modulation dominates.

C-terminal modulation of KCNQ1 gives rise to the extremely slow gating kinetics (with activation half-times and deactivation kinetics on or near the seconds time scale) (Gage & Kobertz, 2004). The slow kinetics of the KCNQ1-KCNE1 channel complex do not reflect changes in the kinetics of voltage sensor movement, because voltage-sensor accessibility to chemical modification occurred at depolarizing potentials independent of



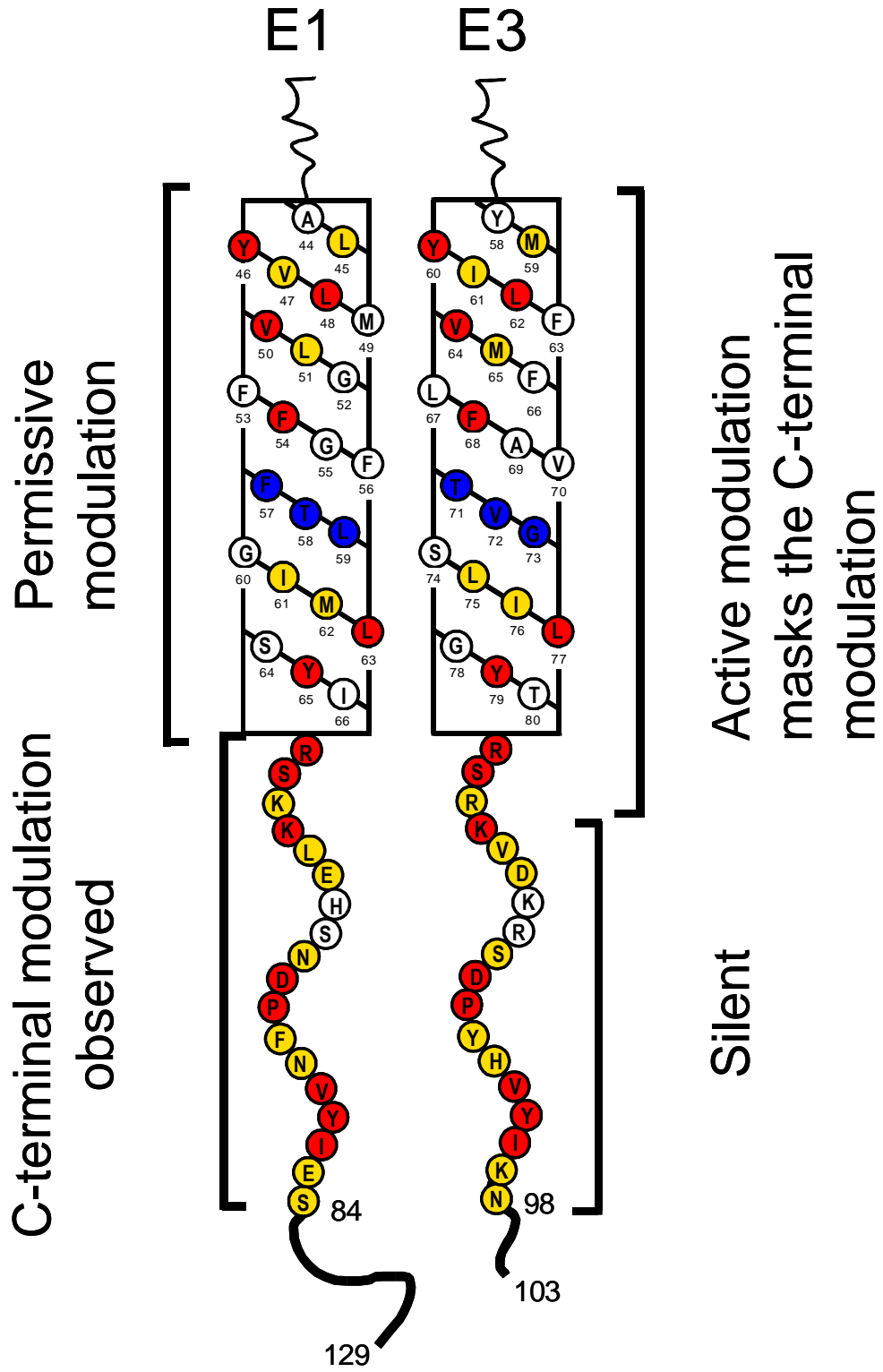


**Figure 5-1.** The bipartite model for KCNE modulation of KCNQ1 channels. Net diagrams for the transmembrane helices of both KCNE1 and KCNE3 are shown, along with the juxtamembranous C-terminal domain of each peptide. Identical amino acid residues between the two peptides are colored red. Similar amino acids are colored yellow. The KCNE triplet identified by Melman and colleagues (Melman et al., 2001) is colored blue. The bipartite model proposes that transmembrane KCNE modulation is either permissive or active. Permissive modulation allows C-terminal modulation to determine the biophysical properties of the channel complex, while active transmembrane modulation completely overrides C-terminal modulation. Notice that the juxtamembranous region in these two KCNE peptides is extremely homologous, allowing KCNE transmembrane chimeras a context that might mirror the wild type peptide, thus explaining the dramatic change in KCNE modulation observed by swapping the modulatory triplet. The bipartite model improves our understanding of KCNE peptides, as it reconciles the data obtained from partial truncations and chimeras of KCNE peptides (Tapper & George, 2000; Melman *et al.*, 2001; Melman *et al.*, 2002a).

Adapted from Gage, S.D. and W.R. Kobertz, *KCNE3 truncation mutants reveal a bipartite modulation of KCNQ1 K<sup>+</sup> channels*. *J Gen Physiol*, 2004. **124**(6): p. 759-71

measurable gating events (Rocheleau & Kobertz, 2008). Unperturbed voltage sensor movement is not surprising considering that bipartite transmembrane modulation of KCNE1 is permissive. Instead, one would expect the modulation of KCNE1 giving rise to  $I_{Ks}$  to occur away from membrane-embedded regions of KCNQ1, considering C-terminally truncated peptides possessing an unaltered KCNE1 transmembrane domain can not give rise to KCNE1-like modulation of KCNQ1 channels (Takumi *et al.*, 1988; Tapper & George, 2000). The computer model of KCNE1 modulation possesses a slow and fast gating transition for each pore-forming subunit; this fast transition may be akin to the movement of the KCNE1-modulated KCNQ1 voltage sensor, which is unimpeded perhaps because transmembrane modulation of KCNE1 is permissive (Silva & Rudy, 2005; Rocheleau & Kobertz, 2008).

The transmembrane modulation resident in KCNE3 is active and masks the modulation intrinsic to the C-terminus of KCNE3. For this reason and despite the large degree of sequence homology between the C-termini of KCNE1 and KCNE3, KCNE3 does not give rise to slow gating kinetics but instead to almost instantaneous kinetics and large basal activation. KCNE chimeras possessing the KCNE3 transmembrane domain display KCNE3-like modulation and are insensitive to mutations that disrupt the C-terminal modulation (Melman *et al.*, 2001; Melman *et al.*, 2002a; Gage & Kobertz, 2004). Though still unclear, transmembrane modulation of KCNQ1 by KCNE3 may act directly through the KCNQ1 voltage sensor, explaining the increase in KCNQ1 voltage sensor accessibility and the KCNE-like effects of point mutations within the voltage sensor (Panaghie & Abbott, 2007; Rocheleau & Kobertz, 2008).

The bipartite model of KCNE modulation supports an important role for the C-terminus of KCNE1 in producing the modulation required for native  $I_{Ks}$  function. As our experiments were performed in chimeras or in KCNE3, we wanted to test our hypothesis further through experimentation within KCNE1 itself. In Chapter III, we used perturbation mutagenesis to directly test the C-terminus of KCNE1 for secondary structure. High-impact mutations (those resulting in large changes in the free energy of gating) occurred at discrete amino acid residues. These amino mutations clustered precisely to a single face of an alpha-helix, a structure which is kinked but continues past a native proline residue, P77. Our results not only directly demonstrate a secondary structure for the C-terminus of KCNE1, but also implicitly indicate the C-terminus of KCNE1 is involved in a protein-protein interface or contact.

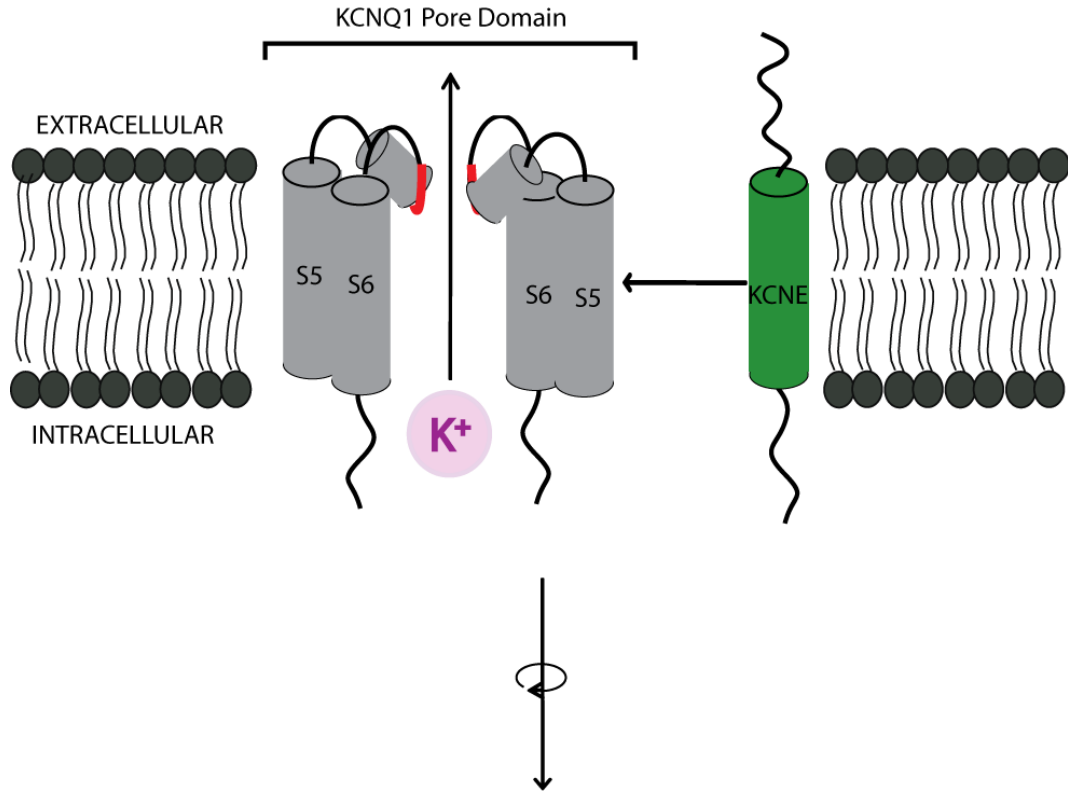
Elucidating the nature of this protein-protein contact was the focus of the work presented in Chapter IV. Knowing KCNE1 resides close to the ion conduction pathway, we attempted to form disulfide bonds between the C-terminus of KCNE1 and the aqueous-exposed intracellular face of KCNQ1 channel complexes. *A priori*, we did not know if KCNE1 actually interacted with KCNQ1 or with another aqueous protein (for instance, calmodulin) on the cytoplasmic face of the channel complex. Identification of several crosslink pairings between the two  $I_{Ks}$  subunits resolved any concerns as to the identity of the interacting protein.

All identified crosslink pairings occurred between KCNE1 and structures of KCNQ1 known to be able to adopt many conformations, implying either KCNE1 is flexible and able adjust to movement in the channel complex or KCNE1 modulation

occurs as a result of maintenance of a rigid structure. The association of KCNE1 and the gate of KCNQ1 may result in the slow gating kinetics observed in  $I_{Ks}$  through steric hindrance of normal gating transition. Alternatively, the association between the S4-5 linker helix of KCNQ1 and KCNE1 may result in uncoupling the transduction of voltage sensor movement with movement of the S6 gate.

Taken together, the work in this thesis reestablishes the importance of the C-terminus of KCNE1 in giving rise to  $I_{Ks}$  function. The modulation of KCNE1 is not only provided by the transmembrane domain, but also by the association of the C-terminus with the cytoplasmic structures within the pore domain of KCNQ1 (Figure 5-2). The thesis also proposes the bipartite model for modulation of KCNE peptides. Diverse regions of the KCNE peptide give rise to equally diverse modulations of KCNQ1 channel complexes. The hypothesis proposed does not speculate as to the nature of these distinct KCNE modulations, only to the location and juxtaposition of KCNE modulatory subdomains with the KCNQ1 channel complex. For example, it is possible tight anchoring of KCNE subunits to multiple regions of the channel complex could result in the behavior of modulated KCNQ1 channel complexes. Furthermore, evidence from KCNE3 truncation clearly raises the possibility of mixed populations giving rise to diverse macroscopic electrophysiological phenotypes even within over-expression systems.

## TRANSMEMBRANE KCNE MODULATION



## C-TERMINAL KCNE MODULATION

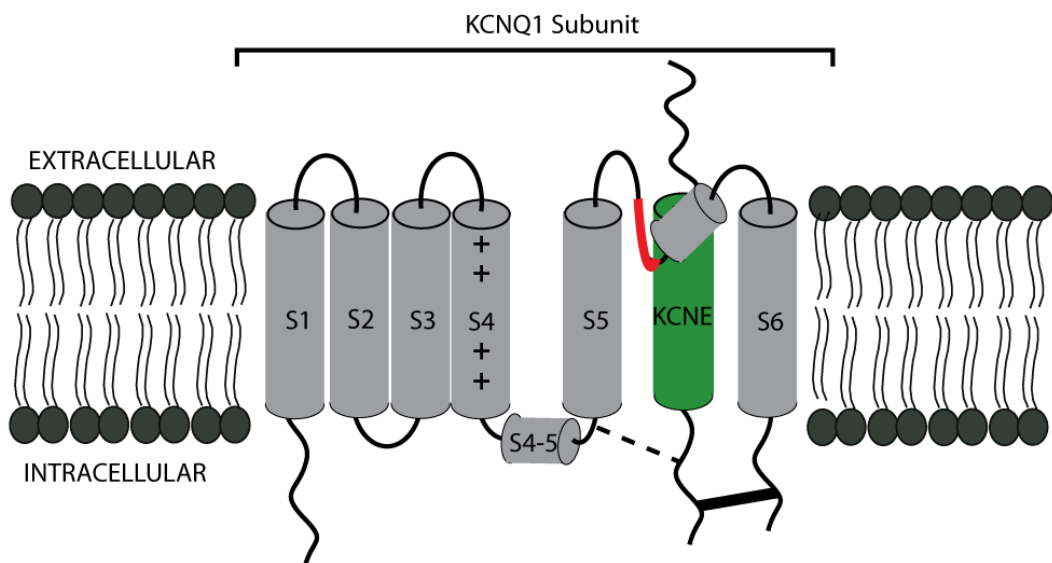


**Figure 5-2.** Bipartite KCNE modulation: transmembrane and C-terminal association. Though completely speculative, the location of each modulation implies two separate mechanisms of modulation. Red, the pore of KCNQ1; green, KCNE1 (E1); purple, a cartoon of a potassium ion ( $K^+$ ). The intracellular and extracellular faces of the membrane are labeled. *Above*, the transmembrane domain of KCNE peptides is believed to associate with the pore domain (and possibly the voltage sensor) of KCNQ1. Only the pore domains of two KCNQ1 subunits are shown for clarity. The nature of transmembranous KCNE association remains to be fully elucidated. *Below*, the C-terminal domain of KCNE1 peptide has been shown to associate tightly with the cytoplasmic face of the KCNQ1 pore domain (Chapters III and IV). As passive transmembrane modulation in KCNE1 allows the C-terminus to give rise to  $I_{Ks}$  current, tight association between the gate of KCNQ1 and KCNE1 may be responsible for giving rise to  $I_{Ks}$  current. If KCNQ1-KCNE1 association is maintained in all gate conformations, increased rigidity provided by the KCNE C-terminus may be responsible for slowed  $I_{Ks}$  gating kinetics. Alternatively, transient or state-dependent associations between KCNQ1 and KCNE1 may result in steric hindrance or excess drag, slowing motion of the S6 gate in response to changes in membrane potential.

## **FUTURE DIRECTIONS**

Several lines of research remain unexplored, and would be fitting continuations of the research present in Chapters II-IV.

*What is the state-dependence of KCNQ1-KCNE1 crosslink formation?*

Protein interactions between the C-terminus of KCNE1 and the cytoplasmic face of the KCNQ1 pore domain have been identified through disulfide bond formation in Chapter IV. Utilization of disulfide bond formation in combination with an altered voltage-pulse protocol can give us insight as to the state-dependence of crosslink formation. Crosslink formation between KCNQ1 and KCNE1 has occurred exclusively in regions of KCNQ1 which are able to adopt multiple conformations. For example, reducing the time spent in the depolarized state should decrease the reaction kinetics of crosslink formation if the crosslink occurs in the open state, but not if the reaction occurs in the closed state. Alternatively,  $I_{Ks}$  is so slow it does not reach equilibrium; current simply continues to increase. Holding membranes at depolarizing potentials (for 10-100 s) and subsequently treating cells with oxidant during this depolarization may slow activation kinetics or allow activation to reach equilibrium if crosslink occurs in the closed state; oxidant treatment would rapidly reduce currents if crosslink occurs in the open state.

Thus far, all crosslink formation results in diminished  $I_{Ks}$  conductance. Does crosslink formation always occur in such a way that there is reduction in conductance? If



disulfide bond formation can occur without a resulting change in conductance, KCNE1 may be able to move and adopt multiple conformations with the channel complex.

Another outlandish possibility presents itself: what if crosslink formation does not occur in either the closed, open or a transition state? Though unobserved using electrophysiology, an inactivated state for  $I_{Ks}$  has never been conclusively dismissed; if an inactivated state exists, then the transition to and from this state must be much slower or much faster than gating transitions between activated and deactivated (Pusch et al., 1998). During the cysteine crosslinking scan, channels dwell in membranes with no transmembrane potential (0 mV) for hours before the reaction can commence (there are simply too many steps occurring in membrane harvest to reduce this long dwell time). Even for an extremely slow transition between open and inactivated states, hours of dwell time at 0 mV may allow enough channels to become inactivated, allowing crosslinking specific to these channel complexes to occur.

*Can mixed populations of channel complexes be identified?*

Chapter II left a conundrum: is the KCNQ1-behavior observed with some of the mutant KCNE3 constructs a result of altered modulation or reduced biosynthetic efficiency? While titration of cRNA co-injection ratios produced resulted in changes in KCNE3-like character consistent with inefficient assembly, direct measurement of current arising from mutant KCNE3-assembled KCNQ1 channel complexes would be more conclusive. Direct measurement of KCNE3 modified currents could be accomplished through use of tethered channel blockers, using the method reported by Morin and

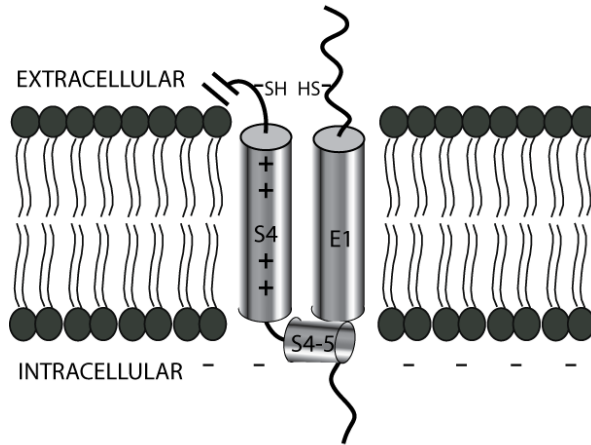
Kobertz (Morin & Kobertz, 2007, 2008). KCNQ1-like character may result from inefficient or substoichiometric assembly, either of which would be easily distinguished through use of selectively irreversible channel blockade. Resolution of channel identity (mixed populations or stoichiometries versus heteromeric channel complexes, including M-channels) could also be conclusively accomplished using this method.

*Can cysteine point mutants in the N-terminus of KCNE peptides form disulfide bonds with the extracellular side of the KCNQ1 voltage sensor? If such a pairing exists, is disulfide bond formation state-dependence between the voltage sensor of KCNQ1 and KCNE peptides?*

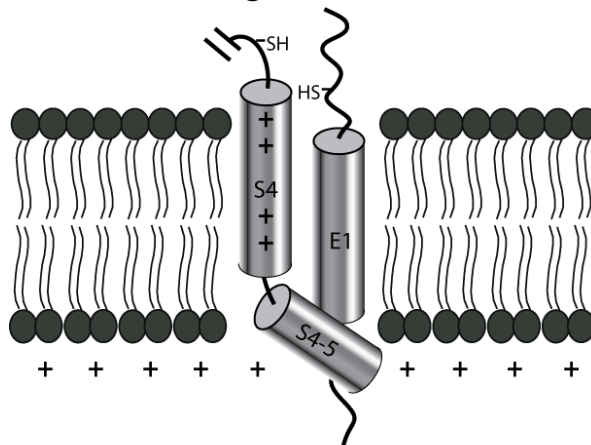
We know the C-terminus of KCNE1 is able to associate with the cytoplasmic gate of KCNQ1 (Chapter IV), but the location of the N-terminus of KCNE1 remains to be elucidated. Given the importance of the transmembrane modulation of KCNE peptides (especially KCNE3) and the close proximity of KCNE peptides to both the pore domain and the voltage sensor, one could speculate some (if not all) KCNE peptides may be able to associate directly with the voltage sensor (Figure 5-3). If KCNE peptides do associate directly with the voltage sensing domain, does this association vary depending on voltage sensor conformation?

Crosslink formation between the N-terminus of KCNE peptides and the extracellular face of the channel can be mediated through disulfide bond formation (given pretreatment of the channel complex with membrane-impermeant TCEP) and can be performed in intact CHO-K1 cells (aqueous intracellular proteins can not form disulfide

### Resting Voltage Sensor



### Activated Voltage Sensor, Immobile E1



### Resting Voltage Sensor, Mobile E1

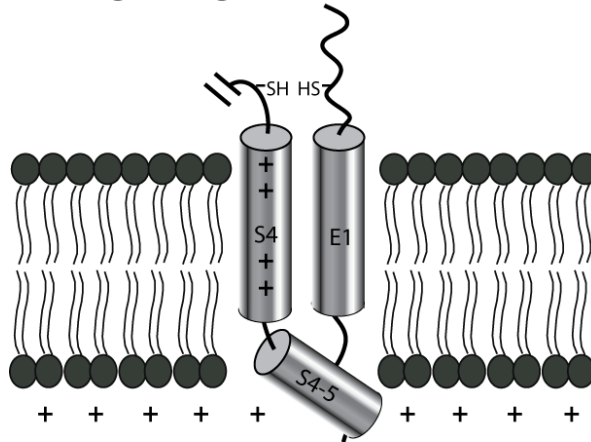


**Figure 5-3.** State-dependent crosslink formation. In this speculative example, KCNE peptides reside in close proximity to the voltage sensor of KCNQ1 channel complexes. The voltage sensor of KCNQ1 possesses an exogenous cysteine which is both close and juxtaposed to an exogenous cysteine in KCNE1 in the resting voltage sensor conformation (*above*); the proximity of these cysteine residues allows the formation of a disulfide bond in oxidizing conditions. For ease of depiction, our model assumes translational motion in the voltage sensor in response to changes in membrane potential. The intracellular and extracellular faces of the membrane are labeled, and membrane potential is indicated by “+” or “-”. If association between KCNE1 and the voltage sensor of KCNQ1 is loose or non-existent, voltage sensor motions will not transduce into movement of KCNE1, and KCNE1 will not be able to form a state-dependent disulfide bond (*middle*). If KCNE1 does associate tightly with the voltage sensor of KCNQ1, motion may occur in a concerted fashion, and disulfide bond formation may occur in either state (*below*). If the voltage sensor of KCNQ1 is free to move relative to KCNE1, transmembrane KCNE modulation may have little or no influence on voltage sensitivity.

bonds with our engineered cysteine mutants and do not need to be removed through hypotonic lysis). With identification of even one disulfide-bound pair of cysteines between KCNQ1 and the KCNE peptide in the closed state, the state-dependence of disulfide bond formation could be performed in a time-dependent manner with *Xenopus* oocytes and TEVC. The voltage sensing domain must move in response to depolarization. Any cysteine mutant on the voltage sensor must therefore also move in response to changes in membrane potential. If the KCNE peptide does not move, a rotational change in the voltage-sensor would prevent juxtaposition, while a translational movement would increase the distance between the pair of cysteines. Either change would result in a reduction in disulfide bond formation.

One could therefore ask: can the cysteine in the KCNE peptide also form a disulfide bond with this cysteine while the voltage sensor is in the depolarized state? Oocyte membranes would be held at positive membrane potentials while oxidant mediates crosslink formation. Even if disulfide bond formation between the voltage sensor and a KCNE peptide does not lead to modification of current, the membrane-bound proteins from oocytes treated with oxidant in a state-dependent manner could be harvested and resolved using SDS-PAGE. Through SDS-PAGE, disulfide bond formation could be observed as a change in apparent molecular mass.

A comparison of crosslink formation observed biochemically and electrophysiologically could provide profound insight regarding the mechanism of KCNE modulation. For instance, if current is not modified but disulfide bond formation is clearly present (as evidenced by mass shift on SDS-PAGE), KCNE peptides would have

to move with the voltage sensor and adopt multiple conformations, in a manner which does not disrupt voltage sensor response to changes in membrane potential. Voltage sensor accessibility assays, even accessibility assays involving state-dependence, have been performed often (Larsson *et al.*, 1996; Mannuzzu *et al.*, 1996; Gandhi *et al.*, 2003; Ruta *et al.*, 2005; Darman *et al.*, 2006; Nakajo & Kubo, 2007; Rocheleau & Kobertz, 2008); performing state-dependent disulfide bond formation should not prove difficult. Whether or not KCNE peptides move with the voltage sensor, the results from this project would be significant and publishable.

*With which regions of KCNQ1 does the transmembrane domain of KCNE1 interact?*

Though disulfide bond formation is not an option for crosslink formation involving membrane-embedded cysteines, cysteine-specific crosslink formation may be possible. A covalent bond between a mercurial compound and a sulfhydryl is possible in a non-aqueous environment. However, chemically crosslinking polypeptides using HgCl<sub>2</sub> or other mercury compounds require several steps and increases the number of caveats for the project. First, the membrane-embedded channel complex is covalently tethered utilizing mercury-mediated crosslink. Native structure must subsequently be completely denatured following crosslink formation. The bound polypeptides must then be covalently tethered using a second crosslinking reagent, one which is non-selective and will bind both the mercury-tethered subunits (for instance, hexamethylene diisocyanate) (Soskine *et al.*, 2002). Because the covalent bond between the cysteine

sulfhydryl and mercury is not irreversible, this type of experiment is much more likely to produce ambiguous data.

*How does the S4-5 linker helix interact with KCNE1?*

From the results of Chapter IV, KCNE1 appears to interact with the S4-5 linker helix of KCNQ1. Mutation of the S4-5 linker may therefore be able to compliment mutations within the C-terminus of KCNE1. A perturbation scan of the S4-5 linker helix may also provide evidence for a direct interaction with KCNE1 occurring within the S4-5 linker helix.

*Does the bipartite modulation of KCNE1 and KCNE3 extend to the entire gene family?*

Through utilization of KCNE chimeras as well as partial truncations, it may be possible to determine how KCNE4 and KCNE5 are able to modulate KCNQ1 channel complexes. Chimeras incorporating regions of 1) KCNE1 and KCNE3 (Melman et al., 2001; Melman et al., 2002a), 2) KCNE1 and KCNE2 or sodium channel  $\beta$ 1 subunit (Tapper & George, 2000), or 3) KCNE2 and KCNE3 (Heitzmann et al., 2007), have already been studied, leading to further understanding of how subdomains of KCNE peptides are required for modulation and pH sensitivity. Partial truncations of KCNE peptides have also provided invaluable contributions to our understanding KCNE modulation (Tapper & George, 2000; Gage & Kobertz, 2004). Extending this line of evidence to KCNE4 and KCNE5 may also lead to further understanding of KCNE

modulation. Several questions regarding how KCNE4 and KCNE5 could be addressed quickly, including:

1. Does the small size and relative lack of putative glycosylation sites on the N-terminus of KCNE4 (Figure 1-3) lead to diminished current or reduction in dwell time on the plasma membrane?
2. Does the large size of the C-terminus of KCNE4 (Figure 1-3) result in current suppression of KCNQ1 complexes, and if so, how? Does this region alter gating, stabilize an inactivated state, or encode a ball peptide which permanently inactivates KCNQ1 channels?
3. Which regions of KCNE5 are able to produce such a large apparent change in voltage sensitivity?
4. If modulation of all KCNE peptides is bi- or multipartite, can chimeras combine the modulations of two distinct KCNE peptides?

However, this line of research may prove difficult, especially with KCNE4. KCNE4 represses current from KCNQ1 channel complexes, and KCNE5 results in significant change in voltage sensitivity of  $I_{Ks}$ -like currents towards activation at very positive membrane potentials, leading to diminished macroscopic currents.



*Do all KCNE peptides interact with the gate of KCNQ1?*

Given the results of Chapter IV, this project should not be difficult. Production of cysteine-free KCNE peptides and co-expression of these peptides with our cysteine-free KCNQ1 construct would allow visualization of direct protein-protein interactions through crosslink formation dependent upon site-directed cysteine mutagenesis. Several questions present themselves:

1. Where within the KCNQ1 channel complex does the KCNE3 C-terminus interact? C-terminal mutations of KCNE3 homologous to Long QT mutations in KCNE1 impeded proper assembly of KCNE3 with KCNQ1; these results imply a direct association is required for assembly of the channel complex (Gage & Kobertz, 2004). The large degree of homology in the C-termini of KCNE1 and KCNE3 also argues KCNE peptides may interact with the same region of the channel complex.
2. Does KCNE4 suppress KCNQ1 currents by stabilizing the gate in the closed conformation? We might not be able to determine state-dependence, but protein-protein interactions between the C-terminus of KCNE4 and the gate of KCNQ1 may provide more insight concerning KCNE4 modulation. Furthermore, if KCNE4 stabilizes either the closed or inactivated states of KCNQ1 by direct protein-protein contacts, scanning cysteine mutants in KCNE4 may serendipitously lead to KCNE4 dysfunction, resulting in KCNQ1 complexes with measurable currents.
3. Does KCNE5 also interact with the gate of KCNQ1 channels (as observed with KCNE1)?

*Are there direct protein-protein interactions between KCNE1 and calmodulin within  $I_{Ks}$ ?*

Both KCNQ1 and KCNE1 appear to possess interacting alpha-helices on their cytoplasmic faces before diverging at proline residues. KCNE1 maintains an alpha helix past this divergence, but it is unclear with what (if anything) KCNE1 interacts with beyond P77 (Rocheleau et al., 2006). KCNQ1 P369, the proline which diverges in KCNQ1, is very close in space to KCNE1 P77, given P369C is able to form a strong disulfide bond with KCNE1 D76C (Chapter IV). Given Long QT point mutants just C-terminal to KCNQ1 P369 have been shown to impede KCNQ1-calmodulin association, perhaps both KCNQ1 and KCNE1 diverge from one another to interact with (different faces of...?) calmodulin (Shamgar et al., 2006). A KCNE1-calmodulin interaction has been implied by co-immunoprecipitation of KCNQ1-KCNE1-calmodulin complexes. Disruption of the KCNE1-calmodulin association may explain the Long QT phenotype exhibited by KCNE1 W87R, a Long QT point mutation in beyond P77 in the C-terminus of KCNE1 (Splawski et al., 2000).  $I_{Ks}$  channel function may be perturbed if this particular mutant is not able to interact properly with calmodulin.

Direct amino acid side chain interactions may again be detectable through disulfide bond formation (Chapter IV). However, production of cysteine-free calmodulin may prevent wild type-like function and should be assayed before the project commences.

## **CONCLUSION**

The interaction of KCNE peptides and KCNQ1 gives rise to channels displaying dramatically altered biophysical and pharmacological properties. KCNE peptides are biophysically and physiologically fascinating; a small modulatory subunit is able to intercalate into the KCNQ1 channel complex and provide modulation of the KCNQ1 channels that apparently acts through directly through the gate and voltage-sensing domains of the channel complex. The question remains, how are KCNE peptides able to alter the stability of the associated channel complex? Biophysical interest and the proven roles of both pore forming subunits and KCNE peptides in leading to disease phenotypes redouble the importance of our understanding. It has been a pleasure studying KCNE peptides, and this research will provide a foundation for understanding channel function and therapeutic discovery.

## REFERENCES

- Abbott GW, Butler MH, Bendahhou S, Dalakas MC, Ptacek LJ & Goldstein SA. (2001). MiRP2 forms potassium channels in skeletal muscle with Kv3.4 and is associated with periodic paralysis. *Cell* **104**, 217-231.
- Abbott GW, Butler MH & Goldstein SA. (2006). Phosphorylation and protonation of neighboring MiRP2 sites: function and pathophysiology of MiRP2-Kv3.4 potassium channels in periodic paralysis. *Faseb J* **20**, 293-301.
- Abbott GW & Goldstein SA. (2002). Disease-associated mutations in KCNE potassium channel subunits (MiRPs) reveal promiscuous disruption of multiple currents and conservation of mechanism. *Faseb J* **16**, 390-400.
- Abbott GW, Sesti F, Splawski I, Buck ME, Lehmann MH, Timothy KW, Keating MT & Goldstein SA. (1999). MiRP1 forms IKr potassium channels with HERG and is associated with cardiac arrhythmia. *Cell* **97**, 175-187.
- Aldrich RW, Corey DP & Stevens CF. (1983). A reinterpretation of mammalian sodium channel gating based on single channel recording. *Nature* **306**, 436-441.
- Anantharam A, Lewis A, Panaghie G, Gordon E, McCrossan ZA, Lerner DJ & Abbott GW. (2003). RNA interference reveals that endogenous *Xenopus* MinK-related peptides govern mammalian K<sup>+</sup> channel function in oocyte expression studies. *J Biol Chem* **278**, 11739-11745.
- Angelo K, Jespersen T, Grunnet M, Nielsen MS, Klaerke DA & Olesen SP. (2002). KCNE5 induces time- and voltage-dependent modulation of the KCNQ1 current. *Biophys J* **83**, 1997-2006.
- Bal M, Zaika O, Martin P & Shapiro MS. (2008). Calmodulin binding to M-type K<sup>+</sup> channels assayed by TIRF/FRET in living cells. *J Physiol* **586**, 2307-2320.
- Barhanin J, Lesage F, Guillemare E, Fink M, Lazdunski M & Romey G. (1996). K(V)LQT1 and IsK (minK) proteins associate to form the I(Ks) cardiac potassium current. *Nature* **384**, 78-80.
- Bendahhou S, Marionneau C, Haurogne K, Larroque MM, Derand R, Szuts V, Escande D, Demolombe S & Barhanin J. (2005). In vitro molecular interactions and distribution of KCNE family with KCNQ1 in the human heart. *Cardiovasc Res* **67**, 529-538.

- Bett GC, Morales MJ, Beahm DL, Duffey ME & Rasmusson RL. (2006). Ancillary subunits and stimulation frequency determine the potency of chromanol 293B block of the KCNQ1 potassium channel. *J Physiol* **576**, 755-767.
- Bianchi L, Kwok SM, Driscoll M & Sesti F. (2003). A potassium channel-MiRP complex controls neurosensory function in *Caenorhabditis elegans*. *J Biol Chem* **278**, 12415-12424.
- Bianchi L, Shen Z, Dennis AT, Priori SG, Napolitano C, Ronchetti E, Bryskin R, Schwartz PJ & Brown AM. (1999). Cellular dysfunction of LQT5-minK mutants: abnormalities of IKs, IKr and trafficking in long QT syndrome. *Hum Mol Genet* **8**, 1499-1507.
- Biervert C, Schroeder BC, Kubisch C, Berkovic SF, Propping P, Jentsch TJ & Steinlein OK. (1998). A potassium channel mutation in neonatal human epilepsy. *Science* **279**, 403-406.
- Brown DA & Adams PR. (1980). Muscarinic suppression of a novel voltage-sensitive K<sup>+</sup> current in a vertebrate neurone. *Nature* **283**, 673-676.
- Chandrasekhar KD, Bas T & Kobertz WR. (2006). KCNE1 subunits require co-assembly with K<sup>+</sup> channels for efficient trafficking and cell surface expression. *J Biol Chem* **281**, 40015-40023.
- Charlier C, Singh NA, Ryan SG, Lewis TB, Reus BE, Leach RJ & Leppert M. (1998). A pore mutation in a novel KQT-like potassium channel gene in an idiopathic epilepsy family. *Nat Genet* **18**, 53-55.
- Chen H & Goldstein SA. (2007). Serial perturbation of MinK in IKs implies an alpha-helical transmembrane span traversing the channel corpus. *Biophys J* **93**, 2332-2340.
- Chen H, Kim LA, Rajan S, Xu S & Goldstein SA. (2003). Charybdotoxin binding in the I(Ks) pore demonstrates two MinK subunits in each channel complex. *Neuron* **40**, 15-23.
- Chen L, Kurokawa J & Kass RS. (2005). Phosphorylation of the A-kinase-anchoring protein Yotiao contributes to protein kinase A regulation of a heart potassium channel. *J Biol Chem* **280**, 31347-31352.
- Chouabe C, Neyroud N, Guicheney P, Lazdunski M, Romey G & Barhanin J. (1997). Properties of KvLQT1 K<sup>+</sup> channel mutations in Romano-Ward and Jervell and Lange-Nielsen inherited cardiac arrhythmias. *Embo J* **16**, 5472-5479.

- Cooper EC, Harrington E, Jan YN & Jan LY. (2001). M channel KCNQ2 subunits are localized to key sites for control of neuronal network oscillations and synchronization in mouse brain. *J Neurosci* **21**, 9529-9540.
- Cooper EC & Jan LY. (2003). M-channels: neurological diseases, neuromodulation, and drug development. *Arch Neurol* **60**, 496-500.
- Cowley EA & Linsdell P. (2002). Characterization of basolateral K<sup>+</sup> channels underlying anion secretion in the human airway cell line Calu-3. *J Physiol* **538**, 747-757.
- Creighton TE. (1992). *Proteins: Structures and Molecular Properties*. W. H. Freeman and Company, New York, NY.
- Cuthbert AW & MacVinish LJ. (2003). Mechanisms of anion secretion in Calu-3 human airway epithelial cells by 7,8-benzoquinoline. *Br J Pharmacol* **140**, 81-90.
- Dahimene S, Alcolea S, Naud P, Jourdon P, Escande D, Brasseur R, Thomas A, Baro I & Merot J. (2006). The N-terminal juxtamembranous domain of KCNQ1 is critical for channel surface expression: implications in the Romano-Ward LQT1 syndrome. *Circ Res* **99**, 1076-1083.
- Darman RB, Ivy AA, Ketty V & Blaustein RO. (2006). Constraints on voltage sensor movement in the shaker K<sup>+</sup> channel. *J Gen Physiol* **128**, 687-699.
- Decher N, Bundis F, Vajna R & Steinmeyer K. (2003). KCNE2 modulates current amplitudes and activation kinetics of HCN4: influence of KCNE family members on HCN4 currents. *Pflugers Arch* **446**, 633-640.
- Dedek K, Kunath B, Kananura C, Reuner U, Jentsch TJ & Steinlein OK. (2001). Myokymia and neonatal epilepsy caused by a mutation in the voltage sensor of the KCNQ2 K<sup>+</sup> channel. *Proc Natl Acad Sci U S A* **98**, 12272-12277.
- Dedek K & Waldegger S. (2001). Colocalization of KCNQ1/KCNE channel subunits in the mouse gastrointestinal tract. *Pflugers Arch* **442**, 896-902.
- Deschenes I & Tomaselli GF. (2002). Modulation of Kv4.3 current by accessory subunits. *FEBS Lett* **528**, 183-188.
- Devaux JJ, Kleopa KA, Cooper EC & Scherer SS. (2004). KCNQ2 is a nodal K<sup>+</sup> channel. *J Neurosci* **24**, 1236-1244.
- Dilly KW, Kurokawa J, Terrenoire C, Reiken S, Lederer WJ, Marks AR & Kass RS. (2004). Overexpression of beta2-adrenergic receptors cAMP-dependent protein kinase phosphorylates and modulates slow delayed rectifier potassium channels

- expressed in murine heart: evidence for receptor/channel co-localization. *J Biol Chem* **279**, 40778-40787.
- Dong MQ, Lau CP, Gao Z, Tseng GN & Li GR. (2006). Characterization of recombinant human cardiac KCNQ1/KCNE1 channels (I (Ks)) stably expressed in HEK 293 cells. *J Membr Biol* **210**, 183-192.
- Doyle DA, Morais Cabral J, Pfuetzner RA, Kuo A, Gulbis JM, Cohen SL, Chait BT & MacKinnon R. (1998). The structure of the potassium channel: molecular basis of K<sup>+</sup> conduction and selectivity. *Science* **280**, 69-77.
- Ekberg J, Schuetz F, Boase NA, Conroy SJ, Manning J, Kumar S, Poronnik P & Adams DJ. (2007). Regulation of the voltage-gated K(+) channels KCNQ2/3 and KCNQ3/5 by ubiquitination. Novel role for Nedd4-2. *J Biol Chem* **282**, 12135-12142.
- Ellgaard L & Helenius A. (2003). Quality control in the endoplasmic reticulum. *Nat Rev Mol Cell Biol* **4**, 181-191.
- Engelhardt JF, Yankaskas JR, Ernst SA, Yang Y, Marino CR, Boucher RC, Cohn JA & Wilson JM. (1992). Submucosal glands are the predominant site of CFTR expression in the human bronchus. *Nat Genet* **2**, 240-248.
- Freeman LC, Lippold JJ & Mitchell KE. (2000). Glycosylation influences gating and pH sensitivity of I(sK). *J Membr Biol* **177**, 65-79.
- Gage SD & Kobertz WR. (2004). KCNE3 truncation mutants reveal a bipartite modulation of KCNQ1 K<sup>+</sup> channels. *J Gen Physiol* **124**, 759-771.
- Gandhi CS, Clark E, Loots E, Pralle A & Isacoff EY. (2003). The orientation and molecular movement of a k(+) channel voltage-sensing domain. *Neuron* **40**, 515-525.
- Gandhi CS & Isacoff EY. (2002). Molecular models of voltage sensing. *J Gen Physiol* **120**, 455-463.
- Ghosh S, Nunziato DA & Pitt GS. (2006). KCNQ1 assembly and function is blocked by long-QT syndrome mutations that disrupt interaction with calmodulin. *Circ Res* **98**, 1048-1054.
- Gonen T, Cheng Y, Sliz P, Hiroaki Y, Fujiyoshi Y, Harrison SC & Walz T. (2005). Lipid-protein interactions in double-layered two-dimensional AQP0 crystals. *Nature* **438**, 633-638.

- Grahammer F, Herling AW, Lang HJ, Schmitt-Graff A, Wittekindt OH, Nitschke R, Bleich M, Barhanin J & Warth R. (2001a). The cardiac K<sup>+</sup> channel KCNQ1 is essential for gastric acid secretion. *Gastroenterology* **120**, 1363-1371.
- Grahammer F, Warth R, Barhanin J, Bleich M & Hug MJ. (2001b). The small conductance K<sup>+</sup> channel, KCNQ1: expression, function, and subunit composition in murine trachea. *J Biol Chem* **276**, 42268-42275.
- Grunnet M, Jespersen T, Rasmussen HB, Ljungstrom T, Jorgensen NK, Olesen SP & Klaerke DA. (2002). KCNE4 is an inhibitory subunit to the KCNQ1 channel. *J Physiol* **542**, 119-130.
- Grunnet M, Olesen SP, Klaerke DA & Jespersen T. (2005). hKCNE4 inhibits the hKCNQ1 potassium current without affecting the activation kinetics. *Biochem Biophys Res Commun* **328**, 1146-1153.
- Grunnet M, Rasmussen HB, Hay-Schmidt A, Rosenstjerne M, Klaerke DA, Olesen SP & Jespersen T. (2003). KCNE4 is an inhibitory subunit to Kv1.1 and Kv1.3 potassium channels. *Biophys J* **85**, 1525-1537.
- Hackos DH, Chang TH & Swartz KJ. (2002). Scanning the intracellular S6 activation gate in the shaker K<sup>+</sup> channel. *J Gen Physiol* **119**, 521-532.
- Haitin Y & Attali B. (2008). The C-terminus of Kv7 channels: a multifunctional module. *J Physiol* **586**, 1803-1810.
- Hamill OP, Marty A, Neher E, Sakmann B & Sigworth FJ. (1981). Improved patch-clamp techniques for high-resolution current recording from cells and cell-free membrane patches. *Pflugers Arch* **391**, 85-100.
- Haws C, Finkbeiner WE, Widdicombe JH & Wine JJ. (1994). CFTR in Calu-3 human airway cells: channel properties and role in cAMP-activated Cl<sup>-</sup> conductance. *Am J Physiol* **266**, L502-512.
- Heitzmann D, Grahammer F, von Hahn T, Schmitt-Graff A, Romeo E, Nitschke R, Gerlach U, Lang HJ, Verrey F, Barhanin J & Warth R. (2004). Heteromeric KCNE2/KCNQ1 potassium channels in the luminal membrane of gastric parietal cells. *J Physiol* **561**, 547-557.
- Heitzmann D, Koren V, Wagner M, Sterner C, Reichold M, Tegtmeier I, Volk T & Warth R. (2007). KCNE beta subunits determine pH sensitivity of KCNQ1 potassium channels. *Cell Physiol Biochem* **19**, 21-32.



- Higashida H, Hoshi N, Zhang JS, Yokoyama S, Hashii M, Jin D, Noda M & Robbins J. (2005). Protein kinase C bound with A-kinase anchoring protein is involved in muscarinic receptor-activated modulation of M-type KCNQ potassium channels. *Neurosci Res* **51**, 231-234.
- Hille B. (1992). *Ionic channels of excitable membranes*. Sinauer Associates, Sunderland, Mass.
- Hong KH & Miller C. (2000). The lipid-protein interface of a Shaker K(+) channel. *J Gen Physiol* **115**, 51-58.
- Horn R & Marty A. (1988). Muscarinic activation of ionic currents measured by a new whole-cell recording method. *J Gen Physiol* **92**, 145-159.
- Hoshi N, Zhang JS, Omaki M, Takeuchi T, Yokoyama S, Wanaverbecq N, Langeberg LK, Yoneda Y, Scott JD, Brown DA & Higashida H. (2003). AKAP150 signaling complex promotes suppression of the M-current by muscarinic agonists. *Nat Neurosci* **6**, 564-571.
- Hoshi T, Zagotta WN & Aldrich RW. (1991). Two types of inactivation in Shaker K<sup>+</sup> channels: effects of alterations in the carboxy-terminal region. *Neuron* **7**, 547-556.
- Howard RJ, Clark KA, Holton JM & Minor DL, Jr. (2007). Structural insight into KCNQ (Kv7) channel assembly and channelopathy. *Neuron* **53**, 663-675.
- Jensen HS, Grunnet M & Olesen SP. (2007). Inactivation as a new regulatory mechanism for neuronal Kv7 channels. *Biophys J* **92**, 2747-2756.
- Jervell A & Lange-Nielsen F. (1957). Congenital deaf-mutism, functional heart disease with prolongation of the Q-T interval and sudden death. *Am Heart J* **54**, 59-68.
- Jespersen T, Membrez M, Nicolas CS, Pitard B, Staub O, Olesen SP, Baro I & Abriel H. (2007). The KCNQ1 potassium channel is down-regulated by ubiquitylating enzymes of the Nedd4/Nedd4-like family. *Cardiovasc Res* **74**, 64-74.
- Jiang B, Sun X, Cao K & Wang R. (2002a). Endogenous Kv channels in human embryonic kidney (HEK-293) cells. *Mol Cell Biochem* **238**, 69-79.
- Jiang Y, Lee A, Chen J, Cadene M, Chait BT & MacKinnon R. (2002b). Crystal structure and mechanism of a calcium-gated potassium channel. *Nature* **417**, 515-522.
- Jiang Y, Lee A, Chen J, Ruta V, Cadene M, Chait BT & MacKinnon R. (2003a). X-ray structure of a voltage-dependent K<sup>+</sup> channel. *Nature* **423**, 33-41.

- Jiang Y, Ruta V, Chen J, Lee A & MacKinnon R. (2003b). The principle of gating charge movement in a voltage-dependent K<sup>+</sup> channel. *Nature* **423**, 42-48.
- Kang C, Tian C, Sonnichsen FD, Smith JA, Meiler J, George AL, Jr., Vanoye CG, Kim HJ & Sanders CR. (2008). Structure of KCNE1 and implications for how it modulates the KCNQ1 potassium channel. *Biochemistry* **47**, 7999-8006.
- Kanki H, Kupersmidt S, Yang T, Wells S & Roden DM. (2004). A structural requirement for processing the cardiac K<sup>+</sup> channel KCNQ1. *J Biol Chem* **279**, 33976-33983.
- Kaufhold MA, Krabbenhoft A, Song P, Engelhardt R, Riederer B, Fahrman M, Klocker N, Beil W, Manns M, Hagen SJ & Seidler U. (2008). Localization, trafficking, and significance for acid secretion of parietal cell Kir4.1 and KCNQ1 K<sup>+</sup> channels. *Gastroenterology* **134**, 1058-1069.
- Keating MT & Sanguinetti MC. (2001). Molecular and cellular mechanisms of cardiac arrhythmias. *Cell* **104**, 569-580.
- Kharkovets T, Dedek K, Maier H, Schweizer M, Khimich D, Nouvian R, Vardanyan V, Leuwer R, Moser T & Jentsch TJ. (2006). Mice with altered KCNQ4 K<sup>+</sup> channels implicate sensory outer hair cells in human progressive deafness. *Embo J* **25**, 642-652.
- Kharkovets T, Hardelin JP, Safieddine S, Schweizer M, El-Amraoui A, Petit C & Jentsch TJ. (2000). KCNQ4, a K<sup>+</sup> channel mutated in a form of dominant deafness, is expressed in the inner ear and the central auditory pathway. *Proc Natl Acad Sci U S A* **97**, 4333-4338.
- Kobertz WR, Williams C & Miller C. (2000). Hanging gondola structure of the T1 domain in a voltage-gated K(+) channel. *Biochemistry* **39**, 10347-10352.
- Krumerman A, Gao X, Bian JS, Melman YF, Kagan A & McDonald TV. (2004). An LQT mutant minK alters KvLQT1 trafficking. *Am J Physiol Cell Physiol* **286**, C1453-1463.
- Kubisch C, Schroeder BC, Friedrich T, Lutjohann B, El-Amraoui A, Marlin S, Petit C & Jentsch TJ. (1999). KCNQ4, a novel potassium channel expressed in sensory outer hair cells, is mutated in dominant deafness. *Cell* **96**, 437-446.
- Kurokawa J, Chen L & Kass RS. (2003). Requirement of subunit expression for cAMP-mediated regulation of a heart potassium channel. *Proc Natl Acad Sci U S A* **100**, 2122-2127.

- Kurokawa J, Motoike HK, Rao J & Kass RS. (2004). Regulatory actions of the A-kinase anchoring protein Yotiao on a heart potassium channel downstream of PKA phosphorylation. *Proc Natl Acad Sci U S A* **101**, 16374-16378.
- Lai LP, Su YN, Hsieh FJ, Chiang FT, Juang JM, Liu YB, Ho YL, Chen WJ, Yeh SJ, Wang CC, Ko YL, Wu TJ, Ueng KC, Lei MH, Tsao HM, Chen SA, Lin TK, Wu MH, Lo HM, Huang SK & Lin JL. (2005). Denaturing high-performance liquid chromatography screening of the long QT syndrome-related cardiac sodium and potassium channel genes and identification of novel mutations and single nucleotide polymorphisms. *J Hum Genet* **50**, 490-496.
- Lambrecht NW, Yakubov I, Scott D & Sachs G. (2005). Identification of the K efflux channel coupled to the gastric H-K-ATPase during acid secretion. *Physiol Genomics* **21**, 81-91.
- Larsson HP, Baker OS, Dhillon DS & Isacoff EY. (1996). Transmembrane movement of the shaker K<sup>+</sup> channel S4. *Neuron* **16**, 387-397.
- Lee MP, Ravenel JD, Hu RJ, Lustig LR, Tomaselli G, Berger RD, Brandenburg SA, Litzi TJ, Bunton TE, Limb C, Francis H, Gorelikow M, Gu H, Washington K, Argani P, Goldenring JR, Coffey RJ & Feinberg AP. (2000). Targeted disruption of the *Kvlqt1* gene causes deafness and gastric hyperplasia in mice. *J Clin Invest* **106**, 1447-1455.
- Lee SY, Lee A, Chen J & MacKinnon R. (2005). Structure of the KvAP voltage-dependent K<sup>+</sup> channel and its dependence on the lipid membrane. *Proc Natl Acad Sci U S A* **102**, 15441-15446.
- Lerche C, Scherer CR, Seeböhm G, Derst C, Wei AD, Busch AE & Steinmeyer K. (2000). Molecular cloning and functional expression of KCNQ5, a potassium channel subunit that may contribute to neuronal M-current diversity. *J Biol Chem* **275**, 22395-22400.
- Letts VA, Valenzuela A, Dunbar C, Zheng QY, Johnson KR & Frankel WN. (2000). A new spontaneous mouse mutation in the *Kcne1* gene. *Mamm Genome* **11**, 831-835.
- Levy DI, Wanderling S, Biemesderfer D & Goldstein SA. (2008). MiRP3 acts as an accessory subunit with the BK potassium channel. *Am J Physiol Renal Physiol* **295**, F380-387.
- Lewis A, McCrossan ZA & Abbott GW. (2004). MinK, MiRP1, and MiRP2 diversify Kv3.1 and Kv3.2 potassium channel gating. *J Biol Chem* **279**, 7884-7892.

- Li-Smerin Y, Hackos DH & Swartz KJ. (2000a). alpha-helical structural elements within the voltage-sensing domains of a K(+) channel. *J Gen Physiol* **115**, 33-50.
- Li-Smerin Y, Hackos DH & Swartz KJ. (2000b). A localized interaction surface for voltage-sensing domains on the pore domain of a K+ channel. *Neuron* **25**, 411-423.
- Li M, Jan YN & Jan LY. (1992). Specification of subunit assembly by the hydrophilic amino-terminal domain of the Shaker potassium channel. *Science* **257**, 1225-1230.
- Liu L, Zhao R, Bai Y, Stanish LF, Evans JE, Sanderson MJ, Bonventre JV & Rittenhouse AR. (2006). M1 muscarinic receptors inhibit L-type Ca<sup>2+</sup> current and M-current by divergent signal transduction cascades. *J Neurosci* **26**, 11588-11598.
- Liu XS, Zhang M, Jiang M, Wu DM & Tseng GN. (2007). Probing the interaction between KCNE2 and KCNQ1 in their transmembrane regions. *J Membr Biol* **216**, 117-127.
- Lohrmann E, Burhoff I, Nitschke RB, Lang HJ, Mania D, Englert HC, Hropot M, Warth R, Rohm W, Bleich M & et al. (1995). A new class of inhibitors of cAMP-mediated Cl<sup>-</sup> secretion in rabbit colon, acting by the reduction of cAMP-activated K<sup>+</sup> conductance. *Pflugers Arch* **429**, 517-530.
- Long SB, Campbell EB & Mackinnon R. (2005a). Crystal structure of a mammalian voltage-dependent Shaker family K<sup>+</sup> channel. *Science* **309**, 897-903.
- Long SB, Campbell EB & Mackinnon R. (2005b). Voltage sensor of Kv1.2: structural basis of electromechanical coupling. *Science* **309**, 903-908.
- Long SB, Tao X, Campbell EB & MacKinnon R. (2007). Atomic structure of a voltage-dependent K<sup>+</sup> channel in a lipid membrane-like environment. *Nature* **450**, 376-382.
- Ludwig A, Zong X, Stieber J, Hullin R, Hofmann F & Biel M. (1999). Two pacemaker channels from human heart with profoundly different activation kinetics. *Embo J* **18**, 2323-2329.
- Lundquist AL, Manderfield LJ, Vanoye CG, Rogers CS, Donahue BS, Chang PA, Drinkwater DC, Murray KT & George AL, Jr. (2005). Expression of multiple KCNE genes in human heart may enable variable modulation of I(Ks). *J Mol Cell Cardiol* **38**, 277-287.

- Ma L, Lin C, Teng S, Chai Y, Bahring R, Vardanyan V, Li L, Pongs O & Hui R. (2003). Characterization of a novel Long QT syndrome mutation G52R-KCNE1 in a Chinese family. *Cardiovasc Res* **59**, 612-619.
- MacKinnon R. (1991). Determination of the subunit stoichiometry of a voltage-activated potassium channel. *Nature* **350**, 232-235.
- Maljevic S, Lerche C, Seeböhm G, Alekov AK, Busch AE & Lerche H. (2003). C-terminal interaction of KCNQ2 and KCNQ3 K<sup>+</sup> channels. *J Physiol* **548**, 353-360.
- Manderfield LJ & George AL, Jr. (2008). KCNE4 can co-associate with the I(Ks) (KCNQ1-KCNE1) channel complex. *FEBS J* **275**, 1336-1349.
- Mannuzzu LM, Moronne MM & Isacoff EY. (1996). Direct physical measure of conformational rearrangement underlying potassium channel gating. *Science* **271**, 213-216.
- Marcotti W & Kros CJ. (1999). Developmental expression of the potassium current I<sub>K,n</sub> contributes to maturation of mouse outer hair cells. *J Physiol* **520 Pt 3**, 653-660.
- Marrion NV. (1997). Does r-EAG contribute to the M-current? *Trends Neurosci* **20**, 243-244.
- Marx SO, Kurokawa J, Reiken S, Motoike H, D'Armiento J, Marks AR & Kass RS. (2002). Requirement of a macromolecular signaling complex for beta adrenergic receptor modulation of the KCNQ1-KCNE1 potassium channel. *Science* **295**, 496-499.
- McCrossan ZA & Abbott GW. (2004). The MinK-related peptides. *Neuropharmacology* **47**, 787-821.
- McCrossan ZA, Lewis A, Panaghie G, Jordan PN, Christini DJ, Lerner DJ & Abbott GW. (2003). MinK-related peptide 2 modulates Kv2.1 and Kv3.1 potassium channels in mammalian brain. *J Neurosci* **23**, 8077-8091.
- McDonald TV, Yu Z, Ming Z, Palma E, Meyers MB, Wang KW, Goldstein SA & Fishman GI. (1997). A minK-HERG complex regulates the cardiac potassium current I(Kr). *Nature* **388**, 289-292.
- Melman YF, Domenech A, de la Luna S & McDonald TV. (2001). Structural determinants of KvLQT1 control by the KCNE family of proteins. *J Biol Chem* **276**, 6439-6444.

- Melman YF, Krumerman A & McDonald TV. (2002a). A single transmembrane site in the KCNE-encoded proteins controls the specificity of KvLQT1 channel gating. *J Biol Chem* **277**, 25187-25194.
- Melman YF, Krummerman A & McDonald TV. (2002b). KCNE regulation of KvLQT1 channels: structure-function correlates. *Trends Cardiovasc Med* **12**, 182-187.
- Melman YF, Um SY, Krumerman A, Kagan A & McDonald TV. (2004). KCNE1 binds to the KCNQ1 pore to regulate potassium channel activity. *Neuron* **42**, 927-937.
- Meves H, Schwarz JR & Wulfsen I. (1999). Separation of M-like current and ERG current in NG108-15 cells. *Br J Pharmacol* **127**, 1213-1223.
- Moller C & Netzer R. (2006). Effects of estradiol on cardiac ion channel currents. *Eur J Pharmacol* **532**, 44-49.
- Monks SA, Needleman DJ & Miller C. (1999). Helical structure and packing orientation of the S2 segment in the Shaker K<sup>+</sup> channel. *J Gen Physiol* **113**, 415-423.
- Morais-Cabral JH, Zhou Y & MacKinnon R. (2001). Energetic optimization of ion conduction rate by the K<sup>+</sup> selectivity filter. *Nature* **414**, 37-42.
- Morin TJ & Kobertz WR. (2007). A derivatized scorpion toxin reveals the functional output of heteromeric KCNQ1-KCNE K<sup>+</sup> channel complexes. *ACS Chem Biol* **2**, 469-473.
- Morin TJ & Kobertz WR. (2008). Counting membrane-embedded KCNE beta-subunits in functioning K<sup>+</sup> channel complexes. *Proc Natl Acad Sci U S A* **105**, 1478-1482.
- Moser SL, Harron SA, Crack J, Fawcett JP & Cowley EA. (2008). Multiple KCNQ potassium channel subtypes mediate basal anion secretion from the human airway epithelial cell line Calu-3. *J Membr Biol* **221**, 153-163.
- Munoz V, Grzeda KR, Desplantez T, Pandit SV, Mironov S, Taffet SM, Rohr S, Kleber AG & Jalife J. (2007). Adenoviral expression of IKs contributes to wavebreak and fibrillatory conduction in neonatal rat ventricular cardiomyocyte monolayers. *Circ Res* **101**, 475-483.
- Murrell-Lagnado RD & Aldrich RW. (1993). Energetics of Shaker K channels block by inactivation peptides. *J Gen Physiol* **102**, 977-1003.
- Nakajo K & Kubo Y. (2007). KCNE1 and KCNE3 stabilize and/or slow voltage sensing S4 segment of KCNQ1 channel. *J Gen Physiol* **130**, 269-281.

- Napolitano C, Priori SG, Schwartz PJ, Bloise R, Ronchetti E, Nastoli J, Bottelli G, Cerrone M & Leonardi S. (2005). Genetic testing in the long QT syndrome: development and validation of an efficient approach to genotyping in clinical practice. *Jama* **294**, 2975-2980.
- Nicolas CS, Park KH, El Harchi A, Camonis J, Kass RS, Escande D, Merot J, Loussouarn G, Le Bouffant F & Baro I. (2008). IKs response to protein kinase A-dependent KCNQ1 phosphorylation requires direct interaction with microtubules. *Cardiovasc Res*.
- Nishikawa K, Toker A, Johannes FJ, Songyang Z & Cantley LC. (1997). Determination of the specific substrate sequence motifs of protein kinase C isozymes. *J Biol Chem* **272**, 952-960.
- Noda M, Obana M & Akaike N. (1998). Inhibition of M-type K<sup>+</sup> current by linopirdine, a neurotransmitter-release enhancer, in NG108-15 neuronal cells and rat cerebral neurons in culture. *Brain Res* **794**, 274-280.
- O'Mahony F, Alzamora R, Betts V, LaPaix F, Carter D, Irnaten M & Harvey BJ. (2007). Female gender-specific inhibition of KCNQ1 channels and chloride secretion by 17beta-estradiol in rat distal colonic crypts. *J Biol Chem* **282**, 24563-24573.
- O'Mahony F & Harvey BJ. (2008). Sex and estrous cycle-dependent rapid protein kinase signaling actions of estrogen in distal colonic cells. *Steroids* **73**, 889-894.
- Oliver D, Knipper M, Derst C & Fakler B. (2003). Resting potential and submembrane calcium concentration of inner hair cells in the isolated mouse cochlea are set by KCNQ-type potassium channels. *J Neurosci* **23**, 2141-2149.
- Panaghie G & Abbott GW. (2007). The role of S4 charges in voltage-dependent and voltage-independent KCNQ1 potassium channel complexes. *J Gen Physiol* **129**, 121-133.
- Pannaccione A, Boscia F, Scorziello A, Adornetto A, Castaldo P, Sirabella R, Tagliatela M, Di Renzo GF & Annunziato L. (2007). Up-regulation and increased activity of KV3.4 channels and their accessory subunit MinK-related peptide 2 induced by amyloid peptide are involved in apoptotic neuronal death. *Mol Pharmacol* **72**, 665-673.
- Papazian DM. (1999). Potassium channels: some assembly required. *Neuron* **23**, 7-10.
- Piccini M, Vitelli F, Seri M, Galletta LJ, Moran O, Bulfone A, Banfi S, Pober B & Renieri A. (1999). KCNE1-like gene is deleted in AMME contiguous gene

- syndrome: identification and characterization of the human and mouse homologs. *Genomics* **60**, 251-257.
- Posson DJ, Ge P, Miller C, Bezanilla F & Selvin PR. (2005). Small vertical movement of a K<sup>+</sup> channel voltage sensor measured with luminescence energy transfer. *Nature* **436**, 848-851.
- Potet F, Scott JD, Mohammad-Panah R, Escande D & Baro I. (2001). AKAP proteins anchor cAMP-dependent protein kinase to KvLQT1/IsK channel complex. *Am J Physiol Heart Circ Physiol* **280**, H2038-2045.
- Pusch M. (1998). Increase of the single-channel conductance of KvLQT1 potassium channels induced by the association with minK. *Pflugers Arch* **437**, 172-174.
- Pusch M, Magrassi R, Wollnik B & Conti F. (1998). Activation and inactivation of homomeric KvLQT1 potassium channels. *Biophys J* **75**, 785-792.
- Radicke S, Cotella D, Graf EM, Banse U, Jost N, Varro A, Tseng GN, Ravens U & Wettwer E. (2006). Functional modulation of the transient outward current I<sub>to</sub> by KCNE beta-subunits and regional distribution in human non-failing and failing hearts. *Cardiovasc Res* **71**, 695-703.
- Rae J, Cooper K, Gates P & Watsky M. (1991). Low access resistance perforated patch recordings using amphotericin B. *J Neurosci Methods* **37**, 15-26.
- Rees DC, Komiya H, Yeates TO, Allen JP & Feher G. (1989). The bacterial photosynthetic reaction center as a model for membrane proteins. *Annu Rev Biochem* **58**, 607-633.
- Robbins J. (2001). KCNQ potassium channels: physiology, pathophysiology, and pharmacology. *Pharmacol Ther* **90**, 1-19.
- Rocheleau JM, Gage SD & Kobertz WR. (2006). Secondary structure of a KCNE cytoplasmic domain. *J Gen Physiol* **128**, 721-729.
- Rocheleau JM & Kobertz WR. (2008). KCNE peptides differently affect voltage sensor equilibrium and equilibration rates in KCNQ1 K<sup>+</sup> channels. *J Gen Physiol* **131**, 59-68.
- Roepke TK, Anantharam A, Kirchhoff P, Busque SM, Young JB, Geibel JP, Lerner DJ & Abbott GW. (2006). The KCNE2 potassium channel ancillary subunit is essential for gastric acid secretion. *J Biol Chem* **281**, 23740-23747.



- Rohl CA, Chakrabarty A & Baldwin RL. (1996). Helix propagation and N-cap propensities of the amino acids measured in alanine-based peptides in 40 volume percent trifluoroethanol. *Protein Sci* **5**, 2623-2637.
- Ruta V, Chen J & MacKinnon R. (2005). Calibrated measurement of gating-charge arginine displacement in the KvAP voltage-dependent K<sup>+</sup> channel. *Cell* **123**, 463-475.
- Sakagami M, Fukazawa K, Matsunaga T, Fujita H, Mori N, Takumi T, Ohkubo H & Nakanishi S. (1991). Cellular localization of rat Isk protein in the stria vascularis by immunohistochemical observation. *Hear Res* **56**, 168-172.
- Sanguinetti MC, Curran ME, Zou A, Shen J, Spector PS, Atkinson DL & Keating MT. (1996). Coassembly of K(V)LQT1 and minK (IsK) proteins to form cardiac I(Ks) potassium channel. *Nature* **384**, 80-83.
- Santoro B, Liu DT, Yao H, Bartsch D, Kandel ER, Siegelbaum SA & Tibbs GR. (1998). Identification of a gene encoding a hyperpolarization-activated pacemaker channel of brain. *Cell* **93**, 717-729.
- Satoh T & Zipes DP. (1998). Cesium-induced atrial tachycardia degenerating into atrial fibrillation in dogs: atrial torsades de pointes? *J Cardiovasc Electrophysiol* **9**, 970-975.
- Schagger H & von Jagow G. (1987). Tricine-sodium dodecyl sulfate-polyacrylamide gel electrophoresis for the separation of proteins in the range from 1 to 100 kDa. *Anal Biochem* **166**, 368-379.
- Schroeder BC, Hechenberger M, Weinreich F, Kubisch C & Jentsch TJ. (2000a). KCNQ5, a novel potassium channel broadly expressed in brain, mediates M-type currents. *J Biol Chem* **275**, 24089-24095.
- Schroeder BC, Kubisch C, Stein V & Jentsch TJ. (1998). Moderate loss of function of cyclic-AMP-modulated KCNQ2/KCNQ3 K<sup>+</sup> channels causes epilepsy. *Nature* **396**, 687-690.
- Schroeder BC, Waldegger S, Fehr S, Bleich M, Warth R, Greger R & Jentsch TJ. (2000b). A constitutively open potassium channel formed by KCNQ1 and KCNE3. *Nature* **403**, 196-199.
- Schulteis CT, Nagaya N & Papazian DM. (1996). Intersubunit interaction between amino- and carboxyl-terminal cysteine residues in tetrameric shaker K<sup>+</sup> channels. *Biochemistry* **35**, 12133-12140.

- Schulze-Bahr E, Schwarz M, Hauenschild S, Wedekind H, Funke H, Haverkamp W, Breithardt G, Pongs O & Isbrandt D. (2001). A novel long-QT 5 gene mutation in the C-terminus (V109I) is associated with a mild phenotype. *J Mol Med* **79**, 504-509.
- Schwake M, Jentsch TJ & Friedrich T. (2003). A carboxy-terminal domain determines the subunit specificity of KCNQ K<sup>+</sup> channel assembly. *EMBO Rep* **4**, 76-81.
- Schwarz JR, Glassmeier G, Cooper EC, Kao TC, Nodera H, Tabuena D, Kaji R & Bostock H. (2006). KCNQ channels mediate IKs, a slow K<sup>+</sup> current regulating excitability in the rat node of Ranvier. *J Physiol* **573**, 17-34.
- Seeböhm G, Sanguinetti MC & Pusch M. (2003). Tight coupling of rubidium conductance and inactivation in human KCNQ1 potassium channels. *J Physiol* **552**, 369-378.
- Selyanko AA, Delmas P, Hadley JK, Tatulian L, Wood IC, Mistry M, London B & Brown DA. (2002). Dominant-negative subunits reveal potassium channel families that contribute to M-like potassium currents. *J Neurosci* **22**, RC212.
- Selyanko AA, Hadley JK, Wood IC, Abogadie FC, Delmas P, Buckley NJ, London B & Brown DA. (1999). Two types of K(+) channel subunit, Erg1 and KCNQ2/3, contribute to the M-like current in a mammalian neuronal cell. *J Neurosci* **19**, 7742-7756.
- Selyanko AA, Hadley JK, Wood IC, Abogadie FC, Jentsch TJ & Brown DA. (2000). Inhibition of KCNQ1-4 potassium channels expressed in mammalian cells via M1 muscarinic acetylcholine receptors. *J Physiol* **522 Pt 3**, 349-355.
- Sesti F & Goldstein SA. (1998). Single-channel characteristics of wild-type IKs channels and channels formed with two minK mutants that cause long QT syndrome. *J Gen Physiol* **112**, 651-663.
- Shamgar L, Haitin Y, Yisharel I, Malka E, Schottelndreier H, Peretz A, Paas Y & Attali B. (2008). KCNE1 constrains the voltage sensor of Kv7.1 K<sup>+</sup> channels. *PLoS ONE* **3**, e1943.
- Shamgar L, Ma L, Schmitt N, Haitin Y, Peretz A, Wiener R, Hirsch J, Pongs O & Attali B. (2006). Calmodulin is essential for cardiac IKs channel gating and assembly: impaired function in long-QT mutations. *Circ Res* **98**, 1055-1063.
- Silva J & Rudy Y. (2005). Subunit interaction determines IKs participation in cardiac repolarization and repolarization reserve. *Circulation* **112**, 1384-1391.

- Sims SM, Singer JJ & Walsh JV, Jr. (1988). Antagonistic adrenergic-muscarinic regulation of M current in smooth muscle cells. *Science* **239**, 190-193.
- Singh NA, Charlier C, Stauffer D, DuPont BR, Leach RJ, Melis R, Ronen GM, Bjerre I, Quattlebaum T, Murphy JV, McHarg ML, Gagnon D, Rosales TO, Peiffer A, Anderson VE & Leppert M. (1998). A novel potassium channel gene, KCNQ2, is mutated in an inherited epilepsy of newborns. *Nat Genet* **18**, 25-29.
- Smith PL & Frizzell RA. (1984). Chloride secretion by canine tracheal epithelium: IV. Basolateral membrane K permeability parallels secretion rate. *J Membr Biol* **77**, 187-199.
- Snyders DJ. (1999). Structure and function of cardiac potassium channels. *Cardiovasc Res* **42**, 377-390.
- Soskine M, Steiner-Mordoch S & Schuldiner S. (2002). Crosslinking of membrane-embedded cysteines reveals contact points in the EmrE oligomer. *Proc Natl Acad Sci U S A* **99**, 12043-12048.
- Splawski I, Shen J, Timothy KW, Lehmann MH, Priori S, Robinson JL, Moss AJ, Schwartz PJ, Towbin JA, Vincent GM & Keating MT. (2000). Spectrum of mutations in long-QT syndrome genes. KVLQT1, HERG, SCN5A, KCNE1, and KCNE2. *Circulation* **102**, 1178-1185.
- Splawski I, Tristani-Firouzi M, Lehmann MH, Sanguinetti MC & Keating MT. (1997). Mutations in the hminK gene cause long QT syndrome and suppress IKs function. *Nat Genet* **17**, 338-340.
- Stansfeld C, Ludwig J, Roeper J, Weseloh R, Brown D & Pongs O. (1997). A physiological role for ether-a-go-go K<sup>+</sup> channels? *Trends Neurosci* **20**, 13-14.
- Starace DM & Bezanilla F. (2001). Histidine scanning mutagenesis of basic residues of the S4 segment of the shaker k<sup>+</sup> channel. *J Gen Physiol* **117**, 469-490.
- Starace DM & Bezanilla F. (2004). A proton pore in a potassium channel voltage sensor reveals a focused electric field. *Nature* **427**, 548-553.
- Starace DM, Stefani E & Bezanilla F. (1997). Voltage-dependent proton transport by the voltage sensor of the Shaker K<sup>+</sup> channel. *Neuron* **19**, 1319-1327.
- Strutz-Seebohm N, Seebohm G, Fedorenko O, Baltaev R, Engel J, Knirsch M & Lang F. (2006). Functional coassembly of KCNQ4 with KCNE-beta- subunits in Xenopus oocytes. *Cell Physiol Biochem* **18**, 57-66.

- Sugimoto T, Tanabe Y, Shigemoto R, Iwai M, Takumi T, Ohkubo H & Nakanishi S. (1990). Immunohistochemical study of a rat membrane protein which induces a selective potassium permeation: its localization in the apical membrane portion of epithelial cells. *J Membr Biol* **113**, 39-47.
- Suh BC & Hille B. (2002). Recovery from muscarinic modulation of M current channels requires phosphatidylinositol 4,5-bisphosphate synthesis. *Neuron* **35**, 507-520.
- Tai KK & Goldstein SA. (1998). The conduction pore of a cardiac potassium channel. *Nature* **391**, 605-608.
- Takumi T, Moriyoshi K, Aramori I, Ishii T, Oiki S, Okada Y, Ohkubo H & Nakanishi S. (1991). Alteration of channel activities and gating by mutations of slow ISK potassium channel. *J Biol Chem* **266**, 22192-22198.
- Takumi T, Ohkubo H & Nakanishi S. (1988). Cloning of a membrane protein that induces a slow voltage-gated potassium current. *Science* **242**, 1042-1045.
- Tapper AR & George AL, Jr. (2000). MinK subdomains that mediate modulation of and association with KvLQT1. *J Gen Physiol* **116**, 379-390.
- Tapper AR & George AL, Jr. (2001). Location and orientation of minK within the I(Ks) potassium channel complex. *J Biol Chem* **276**, 38249-38254.
- Teng S, Ma L, Zhen Y, Lin C, Bähring R, Vardanyan V, Pongs O & Hui R. (2003). Novel gene hKCNE4 slows the activation of the KCNQ1 channel. *Biochem Biophys Res Commun* **303**, 808-813.
- Tinel N, Diochot S, Borsotto M, Lazdunski M & Barhanin J. (2000a). KCNE2 confers background current characteristics to the cardiac KCNQ1 potassium channel. *Embo J* **19**, 6326-6330.
- Tinel N, Diochot S, Lauritzen I, Barhanin J, Lazdunski M & Borsotto M. (2000b). M-type KCNQ2-KCNQ3 potassium channels are modulated by the KCNE2 subunit. *FEBS Lett* **480**, 137-141.
- Tombola F, Pathak MM & Isacoff EY. (2005). Voltage-sensing arginines in a potassium channel permeate and occlude cation-selective pores. *Neuron* **45**, 379-388.
- Toyoda F, Ueyama H, Ding WG & Matsuura H. (2006). Modulation of functional properties of KCNQ1 channel by association of KCNE1 and KCNE2. *Biochem Biophys Res Commun* **344**, 814-820.

- Vallon V, Grahammer F, Volkl H, Sandu CD, Richter K, Rexhepaj R, Gerlach U, Rong Q, Pfeifer K & Lang F. (2005). KCNQ1-dependent transport in renal and gastrointestinal epithelia. *Proc Natl Acad Sci U S A* **102**, 17864-17869.
- Vetter DE, Mann JR, Wangemann P, Liu J, McLaughlin KJ, Lesage F, Marcus DC, Lazdunski M, Heinemann SF & Barhanin J. (1996). Inner ear defects induced by null mutation of the *isk* gene. *Neuron* **17**, 1251-1264.
- Wang HS, Pan Z, Shi W, Brown BS, Wymore RS, Cohen IS, Dixon JE & McKinnon D. (1998). KCNQ2 and KCNQ3 potassium channel subunits: molecular correlates of the M-channel. *Science* **282**, 1890-1893.
- Wang KW & Goldstein SA. (1995). Subunit composition of minK potassium channels. *Neuron* **14**, 1303-1309.
- Wang KW, Tai KK & Goldstein SA. (1996). MinK residues line a potassium channel pore. *Neuron* **16**, 571-577.
- Ward OC. (1964). A New Familial Cardiac Syndrome in Children. *J Ir Med Assoc* **54**, 103-106.
- Warth R. (2003). Potassium channels in epithelial transport. *Pflugers Arch* **446**, 505-513.
- Wiener R, Haitin Y, Shamgar L, Fernandez-Alonso MC, Martos A, Chomsky-Hecht O, Rivas G, Attali B & Hirsch JA. (2008). The KCNQ1 (Kv7.1) COOH terminus, a multitiered scaffold for subunit assembly and protein interaction. *J Biol Chem* **283**, 5815-5830.
- Wine JJ, Finkbeiner WE, Haws C, Krouse ME, Moon S, Widdicombe JH & Xia Y. (1994). CFTR and other Cl<sup>-</sup> channels in human airway cells. *Jpn J Physiol* **44 Suppl 2**, S199-205.
- Wollnik B, Schroeder BC, Kubisch C, Esperer HD, Wieacker P & Jentsch TJ. (1997). Pathophysiological mechanisms of dominant and recessive KVLQT1 K<sup>+</sup> channel mutations found in inherited cardiac arrhythmias. *Hum Mol Genet* **6**, 1943-1949.
- Yang T, Kanki H & Roden DM. (2003). Phosphorylation of the IKs channel complex inhibits drug block: novel mechanism underlying variable antiarrhythmic drug actions. *Circulation* **108**, 132-134.
- Yang WP, Levesque PC, Little WA, Conder ML, Shalaby FY & Blannar MA. (1997). KvLQT1, a voltage-gated potassium channel responsible for human cardiac arrhythmias. *Proc Natl Acad Sci U S A* **94**, 4017-4021.

- Yang Y & Sigworth FJ. (1998). Single-channel properties of IKs potassium channels. *J Gen Physiol* **112**, 665-678.
- Yohannan S, Faham S, Yang D, Whitelegge JP & Bowie JU. (2004). The evolution of transmembrane helix kinks and the structural diversity of G protein-coupled receptors. *Proc Natl Acad Sci U S A* **101**, 959-963.
- Yu H, Wu J, Potapova I, Wymore RT, Holmes B, Zuckerman J, Pan Z, Wang H, Shi W, Robinson RB, El-Maghrabi MR, Benjamin W, Dixon J, McKinnon D, Cohen IS & Wymore R. (2001). MinK-related peptide 1: A beta subunit for the HCN ion channel subunit family enhances expression and speeds activation. *Circ Res* **88**, E84-87.
- Yus-Najera E, Santana-Castro I & Villarroel A. (2002). The identification and characterization of a noncontinuous calmodulin-binding site in noninactivating voltage-dependent KCNQ potassium channels. *J Biol Chem* **277**, 28545-28553.
- Zagotta WN, Hoshi T & Aldrich RW. (1990). Restoration of inactivation in mutants of Shaker potassium channels by a peptide derived from ShB. *Science* **250**, 568-571.
- Zerangue N, Schwappach B, Jan YN & Jan LY. (1999). A new ER trafficking signal regulates the subunit stoichiometry of plasma membrane K(ATP) channels. *Neuron* **22**, 537-548.
- Zhang M, Jiang M & Tseng GN. (2001). minK-related peptide 1 associates with Kv4.2 and modulates its gating function: potential role as beta subunit of cardiac transient outward channel? *Circ Res* **88**, 1012-1019.
- Zhou Y, Morais-Cabral JH, Kaufman A & MacKinnon R. (2001). Chemistry of ion coordination and hydration revealed by a K<sup>+</sup> channel-Fab complex at 2.0 Å resolution. *Nature* **414**, 43-48.